On the existence of multiple states of low flows in catchments in southeast Australia

Pallavi Goswami[1], Timothy Peterson[2], Arpita Mondal[3], and Christoph Rüdiger[4]

[1]IIT Bombay Monash Research Academy
[2]Monash University
[3]Indian Institute of Technology Bombay
[4]Bureau of Meteorology

April 4, 2023

Abstract

Hydrological variables of a catchment and their corresponding extreme characteristics have a possibility of switching regimes, particularly when a catchment undergoes protracted dry periods. This can result in a catchment experiencing a flow anomaly that is even more extreme than what was historically considered an extreme low flow event for the catchment. Catchments in southeast Australia have been shown to exhibit multiple states of mean annual flows. Given this and studies that suggest that extreme events may be changing with time, it is important to understand whether extremes in flows also have the potential to exist in multiple states. To investigate this, we studied intensity, duration, and frequency (IDF) of low flows for 161 unregulated catchments in southeast Australia. A Hidden Markov Model-based approach was used to examine shifts in the low flow characteristics. We found very strong evidence of low flow intensity exhibiting two distinct states for at least 34 (21%) catchments in the region, providing convincing reasons to believe that extremes in low flows can and have undergone regime changes. The second state of these catchments is often associated with higher values of low flow intensities. Simulation of the duration and frequency of these events, however, needs improvement with the current approach and may be better studied by accounting for climate indicators that may more suitably explain them. Impacts from a changing climate may enhance the triggering of low flows into alternate states, which calls for water managers to plan for changing regimes of extremes.

On the existence of multiple states of low flows in catchments in southeast Australia

Pallavi Goswami[1], Tim J. Peterson[2,3], Arpita Mondal[4,5], Christoph Rüdiger[2,6]

[1]IITB-Monash Research Academy, IIT Bombay, Mumbai, India
[2]Department of Civil Engineering, Monash University, Clayton, Victoria, Australia
[3]Department of Infrastructure Engineering, University of Melbourne, Parkville, Victoria, Australia
[4]Department of Civil Engineering, Indian Institute of Technology Bombay, Mumbai, India
[5]Interdisciplinary Program in Climate Studies, Indian Institute of Technology Bombay, Mumbai, India
[6]Bureau of Meteorology, Melbourne, Victoria, Australia

Key Points:

- Low flow regimes can switch states which may lead to intensification of low flow events.
- Existence of sustained warm and dry atmospheric conditions can cause the switching of catchments into an intensified low flow state.
- Information from precipitation, though useful, may not be sufficient to explain the variability in low flow extremes.

Corresponding author: Pallavi Goswami, `pallavi.goswami@monash.edu`

Abstract

Hydrological variables of a catchment and their corresponding extreme characteristics have a possibility of switching regimes, particularly when a catchment undergoes protracted dry periods. This can result in a catchment experiencing a flow anomaly that is even more extreme than what was historically considered an extreme low flow event for the catchment. Catchments in southeast Australia have been shown to exhibit multiple states of mean annual flows. Given this and studies that suggest that extreme events may be changing with time, it is important to understand whether extremes in flows also have the potential to exist in multiple states. To investigate this, we studied intensity, duration, and frequency (IDF) of low flows for 161 unregulated catchments in southeast Australia. A Hidden Markov Model-based approach was used to examine shifts in the low flow characteristics. We found very strong evidence of low flow intensity exhibiting two distinct states for at least 34 (21%) catchments in the region, providing convincing reasons to believe that extremes in low flows can and have undergone regime changes. The second state of these catchments is often associated with higher values of low flow intensities. Simulation of the duration and frequency of these events, however, needs improvement with the current approach and may be better studied by accounting for climate indicators that may more suitably explain them. Impacts from a changing climate may enhance the triggering of low flows into alternate states, which calls for water managers to plan for changing regimes of extremes.

Plain Language Summary

Recent studies have shown that the mean hydrological behavior of catchments can undergo changes. The present study explores whether extreme events, such as low flow droughts, might also be undergoing regime-switching. The term 'switching of states' or 'regime-switching' relates to a shift in the underlying probability distribution of a variable. With regards to streamflows, this may result in a catchment experiencing low flow droughts that are even more extreme than what was historically considered a drought event for the catchment. We found strong evidence of low flow intensity exhibiting two distinct states in catchments in southeast Australia, providing convincing reasons to believe that extremes in low flows can and have undergone state changes in the region. The second state of these catchments is often associated with higher values of low flow intensities. Ignoring such changes is likely to misrepresent low flow risks. This finding has profound importance in enabling hydrologists to understand the possible ways in which hydrological events can manifest themselves. Knowledge from these results supports the need to improve existing models to incorporate more dynamic realism within them, without which they might be blind to future hydrological shifts that could have a significant impact on water security.

1 Introduction

Water systems and hydrological regimes are known to be influenced by climatic perturbations, leading to irregularities in flow quantity and quality. Many studies have reported changes in rainfall-runoff relationships (Kiem & Verdon-Kidd, 2010; Van Dijk et al., 2013; Chiew et al., 2014; Miao et al., 2015; X. Liu et al., 2018). Drought flows are being observed to be drastically lower than expected for a given decline in precipitation (Alvarez-Garreton et al., 2021; Avanzi et al., 2020; Tian et al., 2020). The processes that generate runoff have been recently shown to change during (Saft et al., 2015) and after (Peterson et al., 2021) the occurrences of meteorological droughts. This results in less streamflow per unit of rainfall during and after the drought than that which occurred before the drought. Disturbances in catchments induced by changes in climate or from anthropogenic interventions have the potential to cause hydrological variables to undergo regime changes, also referred to as 'switching of states' or 'state shifts'. 'State shifts' relates to a shift in the underlying probability distribution of the variable, implying non-stationarity. This means that a forcing in the form of a disturbance can push a catchment past a fold point and into a new steady state and once the disturbance ends the catchment stays indefinitely in this new state until a disturbance pushes it back to the original state, as explained in Figure 1. In the context of regime-switching of extremes, a switching could result in a catchment experiencing a flow anomaly that is even more extreme than what was historically considered an extreme event. There is evidence suggesting that the mean behaviour of hydrologic variables can exhibit switching of states (Fowler et al., 2022; Peterson et al., 2021; Tauro, 2021; Zipper et al., 2022), i.e., they can exist in multiple states. The study by Peterson et al. (2021), for example, showed that catchments can not just exist in alternate states of streamflow regimes but can even continue to persist in such alternate states for extended periods. This suggests that low flows may also exhibit such behavior, thereby possessing far more complex form of non-stationarity than suggested by Goswami et al. (2022). However, to date, studies on extreme value analysis for streamflows have not examined this in detail. Many commonly existing streamflow models continue to discount that low flows can have temporal variability beyond their routine regime.

Southeast Australia (SEA) is known to have a hydroclimate that is among the most variable in the world (Peel et al., 2004). The hydroclimatologial extremes that the region has undergone in the past, including the Millennium Drought (Van Dijk et al., 2013), have been shown to influence the way streamflow responds (Saft et al., 2015). Many of these catchments have been shown to exhibit hydrologic non-stationarity in rainfall-runoff/climate-runoff relationships (Chiew et al., 2014), with streamflow droughts already shown to be increasing across the region (Wasko et al., 2021). Moreover, many existing studies assume catchments to have infinite resilience. Peterson et al. (2021), however, showed that annual and seasonal mean streamflow in many of these catchments exhibited switching in regimes following the Millennium Drought and that not all of them showed recovery when rainfall returned to normal. The work falsified the widely held assumption that catchments always have only a single steady state around which they fluctuate and showed that catchments could have finite resilience. The work, however, looked at mean flows, analyzed at the annual and seasonal timescales. It does not provide insights on regime-switching of extreme (low) flows, nor on the possibility of switching of such regimes at much finer (for eg., monthly) timescales. This brings forth the question of whether low flows can also undergo changes in state. With the region's susceptibility to exhibit changes in the mean behavior of streamflows, the region provides a good opportunity to study whether the behavior of extreme flows can also undergo changes in states.

Limited studies exist on the understanding and evaluation of shifts in streamflows, and none examine low flows or state change in particular. With regards to techniques for understanding changes in hydrologic extremes in general, the few most widely applied statistical approaches are the non-parametric Mann-Kendall trend analysis (Mann, 1945; Kendall, 1975), change point analysis, and the Generalized Extreme Value (GEV) theory (Coles et al., 2001). Previous studies have used the Mann-Kendall trend analysis to understand shifts in hydrologic extremes (X. Zhang et al., 2001; Miller & Piechota, 2008; Burn et al., 2010; Sagarika et al., 2014; Bennett et al., 2015). This technique, however, is not adequately tailored for the analysis of extremes per se and therefore does not offer a way to determine changes in flow magnitudes (Solander et al., 2017). The other common approach of using the GEV theory-based analysis has been used to study the extreme streamflow data in a non-stationary framework through time-dependent parameters in the GEV distribution (Katz, 2013), allowing trend (and thus regime change) detection in extremes. However, limited approaches exist that allow a comprehensive assessment of state change, entailing aspects such as time series simulation of extreme data, classification of the extreme data into different states (if they exist), and identification of the timing of state shifts.

One such technique that offers the capability to detect state-changes and breaks in persistence in a time series is the hidden Markov modeling approach. Being a doubly embedded stochastic process model, it makes for a good modeling choice for simulating data governed by complicated nonlinear hydrological phenomena. HMMs are statistical Markov models consisting of a hidden or unobservable 'parameter process' which satisfies the Markov property, and a 'state-dependent process', whose behavior depends on the underlying state (Zucchini & MacDonald, 2009). The approach provides a highly flexible modeling framework that can detect the existence of different 'states' in a variable of interest by quantifying the probability of the variable being in a given state over time. HMMs were developed during the late 1960s and early 1970s (Baum & Petrie, 1966) for speech recognition, and have since been successfully implemented in several applications, including climate and hydrologic modeling (Thyer & Kuczera, 2003; Robertson et al., 2003, 2004). Mallya et al. (2013) applied HMM to develop a drought index for probabilistic assessment of drought characteristics. Turner and Galelli (2016) applied HMM to examine the impact of regime-like behavior in streamflows on the performance of reservoir operating policy. Thyer and Kuczera (2000) used the hidden state Markov (HSM) model to simulate annual rainfall series in Australia. Rolim and de Souza Filho (2020) used it to identify shifts in low-frequency variability of streamflows. Bracken et al. (2014) used HMM along with climate indices to simulate multidecadal streamflows. More recently, Peterson et al. (2021) developed Hidden Markov Models (HMM) to statistically identify if, and when, streamflow recovers from meteorological droughts, and in doing so provide empirical evidence that catchments often have multiple hydrological states. Overall, HMMs are a useful tool for identifying state changes in a time series based on the dictating underlying process. By virtue of being a mixture model, HMM provides an unsupervised classification technique that can be applied to capture persistence and hence breaks in persistence in a time series, including low flows.

The present study aims to falsify the assumption that a single state is adequate to represent low flow events. This includes falsifying the commonly held notion that including rainfall variability is sufficient to account for non-stationarity in low flows and that low flows do not undergo long-term changes. To investigate this, the metrics used to characterize low flow events, namely, their intensity, duration, and frequency (IDF) were studied to test whether these can exist in more than one state, focusing on catchments in SEA. The study aims to provide an investigation of low flow extreme shifts along with finding when these changes are occurring for these catchments. To do this, we used the Hidden Markov modeling approach to identify state changes in the IDF of low flows. Although HMMs have been applied to investigate changes in flows and precipitation in previous studies as discussed above, these have not been specifically used to model low flow characteristics for investigating state changes in regimes of low flows. This study thus also presents a relatively less explored application of HMMs in investigating state changes in the extreme characteristics of low flows. The methodology adopted here also presents an alternative approach for examining hydrologic non-stationarity observed in the low flow IDF by examining if state-dependent distributions are required to explain the variability in the observed data.

2 Data and Methods

2.1 Study Region and Data

For the present work, 161 unimpaired catchments in southeast Australia (SEA) were studied using their monthly streamflow as flow depth (mm) and precipitation data (mm), both aggregated from daily values. The streamflow data of these catchments was sourced from Peterson et al. (2021) and pre-processed as described in Goswami et al. (2022) following the quality control of Peterson et al. (2021). The catchments were chosen based on their gauge record quality while also ensuring that all these catchments had flow records at least for 15, 7, and 5 years before, during, and after the Millennium Drought, respectively. All the catchments had at least 35 years of flow and precipitation data (Text S1 and Table S1 in Supporting Information S1). More information on the data can be found in Goswami et al. (2022). Importantly, this data provided an opportunity to investigate changes in extremes occurring in natural systems due to a changing climate and not through reservoir operations or land use practices. The 161 catchments and their corresponding gauging stations are

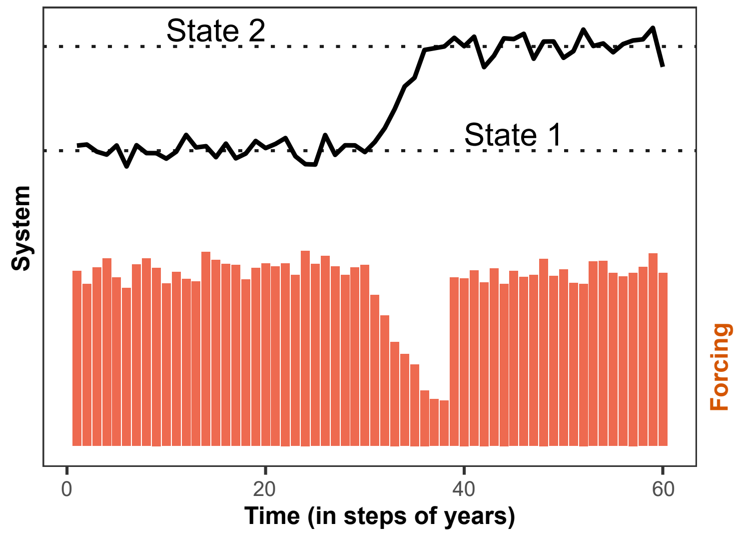

Figure 1: Illustration of regime-switching of a system (for eg., a hydrologic variable of interest) from State 1 to State 2 under the influence of a forcing (hydrologic disturbance). (Adopted from Peterson & Western, 2014.)

shown in Figure 2a, with the colored circles denoting the mean annual streamflow depth. Figure 2b shows the mean annual precipitation for the respective gauges. While this study is focused on the SEA region, the analysis and the understanding from it are relevant to all catchments where hydrological droughts are likely to become more extreme.

2.2 Deriving IDF of Low Flows

In this study, low flows were defined as representative of streamflow droughts describing a catchment's condition when streamflows are anomalously low relative to long-term monthly means. The term 'low flow' as used in this work can be understood as a type of hydrological drought. By common definition, a hydrological drought denotes a deficit in surface water and groundwater (Wilhite & Glantz, 1985). Thus, often the term hydrological drought takes on a broader hydrological definition and can refer to situations of low flows, low snowmelt, low spring flow, low groundwater levels, etc., relative to normal conditions. However, the present study focuses primarily on conditions where streamflows are anomalously low relative to their expected normal flow conditions. The study here thus uses the term 'low flows' (or 'low flow droughts') for the sake of being specific to the domain being investigated.

For identifying low flow spells and deriving their associated characteristics, an approach similar to that used in Goswami et al. (2022) was applied here. First, the monthly flow depths at any given catchment (Figure 3a) were transformed by applying a Box-Cox (BC) power transformation (Box & Cox, 1964), using catchment-specific lambda values, to reduce the skew and for better identification of flow values which were very low (Text S2 and Figure S1 in Supporting Information S1). The transformed flows were then standardized using the mean and standard deviation of the transformed flow series at that catchment. The sign of the obtained series was then reversed such that values above zero pointed to below-average streamflows. The resultant series was termed as the Streamflow Drought Index (SDI) (Figure 3b).

From the SDI series, monthly low flows were defined by using a threshold following the Peak-Over-Threshold (POT) approach (Coles et al., 2001). In the identification of low flow

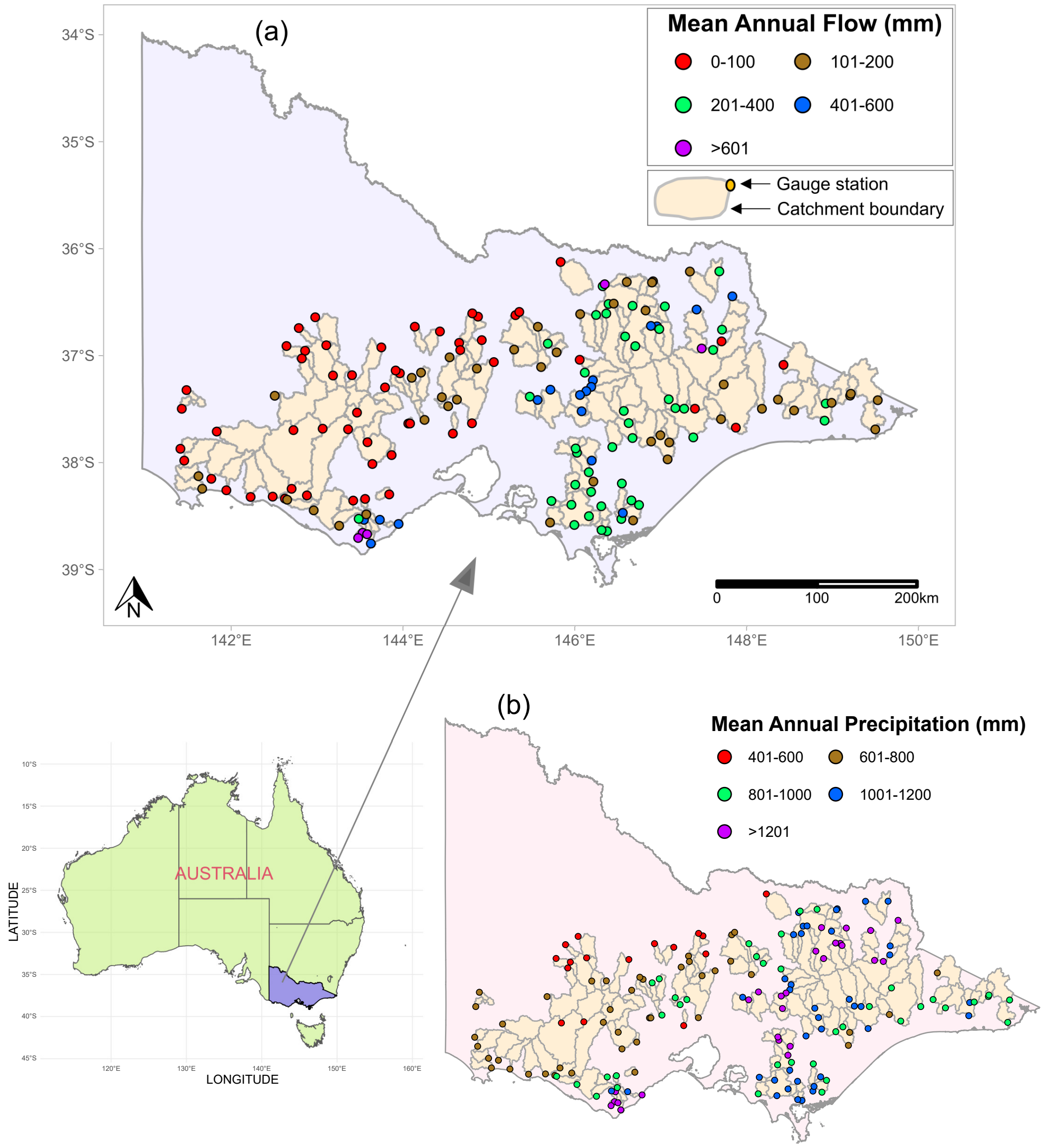

Figure 2: (a) Location of the study region and the 161 catchments (boundary shown in gray) along with their corresponding gauging stations (colored circles). The color of the gauge stations in (a) and (b) shows the mean annual flow depth and the mean annual precipitation, respectively.

periods, the choice of a low flow threshold is often subjective (Pushpalatha et al., 2012). For the current work, the threshold for defining the low flows was chosen to be the 65th percentile value of the SDI series. This ensured that most of the catchments had at least more than 40 values of intensity of low flows required for the model to perform satisfactory simulations. Higher thresholds corresponding to the 75th, 85th, and 95th percentiles resulted in significantly reduced sample sizes (Figure S2 in Supporting Information S1). This is a significant aspect as the capability of a Markovian model to simulate data improves when more data is available. Further, it was found that for the number of points lying above the threshold of 65th percentile, more than half of these lied above the 85th percentile for most of these catchments.

For this work, we focus on three important characteristics of low flows, namely, their intensity, duration, and annual frequency. These were derived from the SDI time series following their respective definitions in Goswami et al. (2022), as shown in Figure 3c. The duration of a low flow event was defined as the number of months for which the monthly SDI series remained above the threshold. The peak value that the SDI takes over the low flow spell was regarded as the intensity of the event. The more positive the peak value in a spell, the more intense the low flow event. The total number of such low flow events occurring in a streamflow water year was regarded as the annual frequency of the low flow events. The water year for computing frequency was taken from March of the current year, running for 12 months until February of the next year, following the definition as in X. S. Zhang et al. (2016). The March-February water year is typical in parts of SE Australia (particularly Victoria), where minimum flows are usually observed at the end of the Boreal summer.

2.3 Modeling IDF Using Hidden Markov Models (HMMs)

2.3.1 Hidden Markov Models for Low Flow IDF

HMM is a statistical Markov model consisting of two parts: an unobservable (or hidden) 'parameter process', C, which satisfies the Markov property, and a 'state-dependent process', X, in such a way that when $C^{(t)}$ is known, the distribution of X depends only on the present state of C and not on the previous states or observations (Zucchini & MacDonald, 2009). HMM assumes that the behavior of the process X depends on C. A simple HMM can be summarized by the following two equations:

$$Pr\ (C^{(t)} \mid \boldsymbol{C}^{(t-1)}) = Pr\ (C^{(t)} \mid C^{(t-1)}) \qquad t = 2, 3, ... \tag{1}$$

$$Pr\ (X^{(t)} \mid \boldsymbol{X}^{(t-1)}, \boldsymbol{C}^{(t)}) = Pr\ (X^{(t)} \mid C^{(t)}) \quad t \in \mathbb{N} \tag{2}$$

where, $C^{(t)}$ represents the value of C at a given time t, $\boldsymbol{C}^{(t)}$ is the Markov chain of probabilities and denotes the vector $[C_1,\ C_2,\ C_3, ..., C_t]$. $X^{(t)}$ represents the value of X at a given time t, and $\boldsymbol{X}^{(t)}$ denotes the vector $[X_1,\ X_2,\ X_3, ..., X_t]$. If the Markov chain $\boldsymbol{C}^{(t)}$ has m states, the HMM of X is called an m-state HMM, where each state has a different distribution. The model provides a Markov chain, i.e. the probability of X being in each state over time which involves maximization of the following probability (Zucchini & MacDonald, 2009):

$$Pr\ (\boldsymbol{C}^{(T)} = \boldsymbol{c}^{(T)} \mid \boldsymbol{X}^{(T)} = {}_{obs}x_t{}^{(T)}) \tag{3}$$

In the above expression, $\boldsymbol{c}$ is a sequence of possible states over the time steps and x is the vector of observed data. For an m-state HMM there are m^T possible sequences, T being the length of the time series.

Using this background of HMMs, we built temporal HMMs were built for each of the three low flow characteristics (i.e. low flow IDF) that examined for one and two states in these. The hidden states were the states of the existing climatic conditions. The model learnt about the state of extremes (C) by observing the low flow characteristic being modeled (x). Since the actual number of hydrological states for a given low flow characteristic is unknown, it was assumed that the low flow characteristics of a catchment can cycle through two states. A given low flow characteristic was thus simulated as being in one of the two distinct states. At each time point, t, the observed low flow characteristic was considered a random variable defined by a parametric distribution for each state. The state distribution at any time t depended upon the Markov chain of states at the preceding time step. For state, i, and at time, t, the conditional mean for the distribution of the given low flow characteristic under consideration was simulated as:

$$\widehat{{}_tx_i} = a_{0,i} + a_1.(sAPI_t) \qquad : for\ intensity\ and\ duration \tag{4a}$$

$$\widehat{{}_tx_i} = a_{0,i} + a_1.(mean\ annual\ sAPI_t) \qquad : for\ frequency \tag{4b}$$

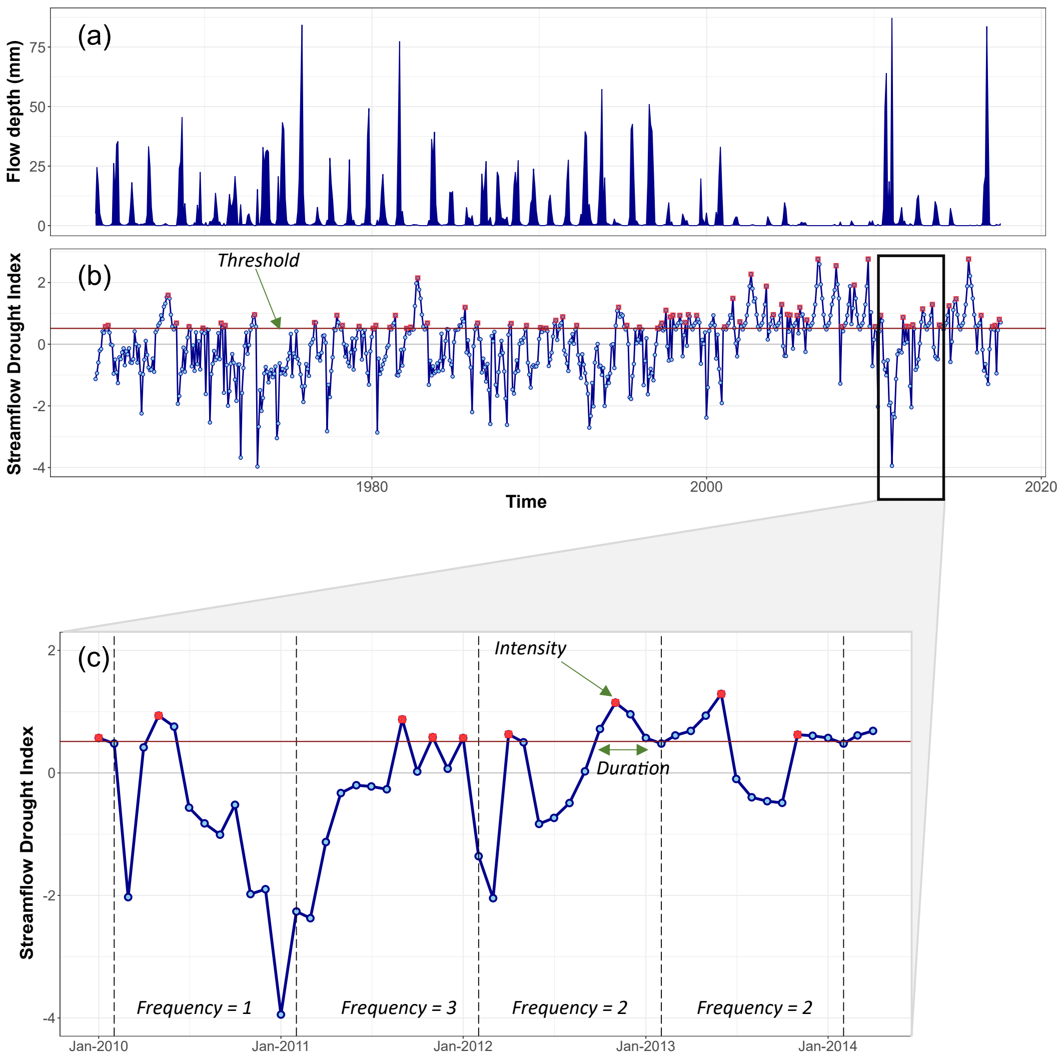

Figure 3: Deriving the intensity, duration, and frequency of low flows. (a) Flow depth (mm) time series for Station ID 407230. (b) Times series of the de-seasonalized (and reversed in sign) flow, termed as the Streamflow Drought Index (SDI), derived from the flow values for the catchment. The threshold is shown by the brown horizontal line at SDI = 0.51 which represents the 65th percentile of the SDI time series for this catchment. Values of SDI lying above the threshold represent low flows. (c) A zoomed window of the SDI series for the years 2010–2013 to illustrate how the IDF are derived from the SDI time series.

where $a_{0,i}$ was a state-dependent parameter allowing for a shift in the catchment's hydrological response, a_1 was a state-independent parameter that links a suitable model covariate to x. In this study, the standardized antecedent precipitation index, sAPI (or the mean annual sAPI for modeling frequency) was used as the covariate responsible for the observed variability in the low flow characteristic (sAPI is discussed in detail in Section 2.3.2). In Equations 4a and 4b, the $sAPI_t$ (or mean annual $sAPI_t$) was taken at the corresponding time instance when the low flow characteristic was observed. The error in this model was defined as a time-invariant state-dependent variance, ${\sigma_i}^2$.

The Markov state $C^{(t)}$ at time t was simulated as:

$$C^{(t)} = Markov\ (\mathbf{\Gamma}) \tag{5}$$

where Γ is the transition matrix. Since the number of extreme states was assumed as two, we, therefore, investigated one- (Γ_1) and two- (Γ_2) state Markov models. The transitioning between any two consecutive states is explained using the schematic in Figure 4a. The two-state matrix Γ_2 can be written as:

$$\Gamma_2 = \begin{vmatrix} p_{11} & p_{12} \\ p_{21} & p_{22} \end{vmatrix} = \begin{vmatrix} p_{11} & 1 - p_{11} \\ 1 - p_{22} & p_{22} \end{vmatrix} \tag{6}$$

Here, p_{ij} (terms shown in Figure 4a), denotes the probability of the state at t transitioning from $C_i^{(t-1)}$ to $C_j^{(t)}$ (where $i, j \leq 2$), i.e.,:

$$p_{ij} = Pr({C_j}^{(t)} \mid {C_i}^{(t-1)}) \tag{7}$$

Further assuming the HMM is homogeneous (i.e. transition probabilities are time-invariant), $\mathbf{\Gamma}_1$ and $\mathbf{\Gamma}_2$ required the estimation of zero and two transition probabilities, respectively. Additionally, the initial probability of being in each state was defined as follows:

$$\boldsymbol{\delta}_1 = 1 \boldsymbol{\delta}_2 = \begin{vmatrix} \boldsymbol{\delta}_1 \\ \boldsymbol{\delta}_2 \end{vmatrix} = \begin{vmatrix} \boldsymbol{\delta}_1 \\ 1 - \boldsymbol{\delta}_1 \end{vmatrix} \tag{8}$$

where $\boldsymbol{\delta}_1$ and $\boldsymbol{\delta}_2$ were the initial probabilities of being in states 1 and 2, respectively.

The probability density in the error model of the HMM was derived using a two-parameter gamma distribution, a log-normal distribution, and a Poisson distribution for the intensity, duration, and frequency of low flows, respectively (Table 1). This was done after testing the capabilities of these respective distributions to satisfactorily represent these characteristics.

The gamma distribution, f_{Gam}, as used for building the HMM for modeling intensity, can be represented as:

$$f_{Gam}\left(x = {}_{obs}x_t;\ k = \frac{{}_t{x_i}^2}{{\sigma_i}^2},\ \theta = \frac{{\sigma_i}^2}{{}_t x_i}\right) = \frac{x^{k-1} e^{-\frac{x}{\theta}}}{\theta^k G(k)} \qquad for\ x, \theta, k > 0 \tag{9}$$

where θ is the scale parameter, k is the shape parameter and $G(k)$ is the gamma function on k. The parameters k and θ were derived to ensure that the mean of the gamma distribution was as defined by Equation 4a, and were obtained by rearrangement of the $Markov\ Mean$, $E[x] = k\theta = {}_t x_i$ and the $Markov\ Variance$, $Var[x] = k\theta^2 = {\sigma_i}^2$. In simple form,

$$k = \frac{(Markov\ Mean)^2}{Markov\ Variance} \tag{10}$$

$$\theta = \frac{Markov\ Variance}{Markov\ Mean} \tag{11}$$

The log-normal distribution, $f_{LogNorm}$, as used for modeling duration can be represented as:

$$f_{LogNorm}\left(x = {}_{obs}x_t; \mu = log\frac{{}_t{x_i}^2}{\sqrt{{\sigma_i}^2 + {}_t{x_i}^2}}; \sigma = \sqrt{log\left\{\frac{{\sigma_i}^2}{{}_t{x_i}^2} + 1\right\}}\right) =$$

$$\frac{1}{x\sigma\sqrt{2\pi}} exp\frac{-(log\ x - \mu)^2}{2\sigma^2}, \qquad for\ x > 0 \tag{12}$$

where μ and σ are the mean and standard deviation of logarithmic values of x and were related to the $Markov\ Mean$, $E[x]$, and $Markov\ Variance$, $Var[x]$, as:

$$\mu = log\frac{(Markov\ Mean)^2}{\sqrt{Markov\ Variance + (Markov\ Mean)^2}} \tag{13}$$

$$\sigma = \sqrt{log\left\{\frac{Markov\ Variance}{(Markov\ Mean)^2} + 1\right\}} \tag{14}$$

The Poisson distribution, f_{Pois}, as used for modeling frequency can be represented as

$$f_{Pois}\left(x = {}_{obs}x_t;\ \lambda = \sigma_i^2\right) = \frac{\lambda^x e^{-\lambda}}{x!} \qquad for\ x \geq 0\ and\ \lambda > 0 \tag{15}$$

where λ, the mean parameter of the Poisson distribution, was arrived at using

$$\lambda = Markov\ Mean \tag{16}$$

The parameters of the HMM were arrived at using a constrained maximum likelihood estimation. The details of the calibration process are presented in Text S3 in Supporting Information S1. To arrive at the most probable sequence of states from all possible combinations of sequences for the given observation sequence of intensity/duration/frequency (I/D/F), an efficient dynamic programming method, called the Viterbi algorithm (Forney, 1973; Zucchini & MacDonald, 2009) was used. This algorithm identifies the most probable sequence of states from the Markov Chain of probabilities. The states of I/D/F obtained through this were also referred to as the Viterbi states (named after the algorithm). The algorithm was applied over the entire observation record to identify the most probable sequence of I/D/F states, thereby also identifying any switching, if at all, in the states of the I/D/F.

2.3.2 Covariate Used in the IDF HMMs

For this study, the HMMs of IDF were built using a linear relationship between these low flow characteristics and the available water through precipitation. To represent the available water through precipitation at a catchment, a form of the Antecedent Precipitation Index (API) was used. This serves as a covariate in the HMMs. Similar to the Standardized Precipitation Index (SPI), the API is an empirical index for indirectly estimating how much water is available in the catchment (soil) from precipitation. While SPI is calculated based on a fitted distribution of a moving average of the precipitation time series, API provides a current precipitation water availability indicator employing a constant rate of water depletion from the soil. API estimates the current water available in the soil by multiplying API at the previous time step by a depletion factor and adding the previous time step's precipitation. The definition of API as used in the present work is partly adapted from studies like Kohler and Linsley (1951); Crow et al. (2005); Y. Y. Liu et al. (2011); Holmes et al. (2017), where this index has been used for determining drought conditions and for other watershed analysis. API is a simplified water balance model built on the assumption that the amount of available water in a catchment is related to its antecedent precipitation conditions.

We computed the API at monthly time steps, multiplying the index from the previous month by the depletion rate (γ) and adding the current monthly precipitation as shown below:

$$API_t = min\left(\gamma_n API_{t-1} + 0.75P_t,\ API_{max,n}\right) \tag{17}$$

with the API at the first time step calculated as:

$$API_{(t=1)} = 0.75P_{(t=1)} \tag{18}$$

API_t and $API_{(t-1)}$ are the current and previous month's API, with γ modulating API_{t-1}, and P_t is the current month's precipitation depth. The multiplicative factor of 0.75 to P_t was used to account for the loss of precipitation water while reaching the soil (interception). Since API is representative of the amount of available water in the soil, it was capped to a maximum value ($API_{max,n}$) to indicate full saturation (Dharssi et al., 2017; Holmes et al., 2017) at a given catchment n. The value of $API_{max,n}$ was varied in proportion to the mean of all monthly precipitation values at that catchment, $\overline{P_n}$, as shown in Equation 19. The value of the multiplicative factor ϕ_n in Equation 19 indicates the proportion of maximum monthly water that the soil can hold to the average precipitation at the station.

$$API_{max,n} = \phi_n.\overline{P_n} \qquad \phi_n \in [4, 10] \tag{19}$$

The parameters γ and ϕ as used in Equations 17 and 19, respectively, are meant to simplify the complex mechanisms controlling water availability from precipitation at a catchment. They incorporate the dynamic range and variability of the actual daily API values that get reflected as monthly aggregated values. The values of ϕ and that of γ at a given catchment were chosen by running a simple optimization experiment for each catchment individually instead of assuming a single constant value for them uniformly across the study region. This was done as these parameters have a considerably large spatial variation due to several factors, including soil type, soil density, vegetation, exposure, hill slope, etc.

The optimization was aimed at yielding such values of these parameters that maximized the correlation between the low flow intensities at a catchment and the standardized time series of the catchment's API (sAPI). This allowed a maximum transfer of information in form of linear dependence from precipitation (through sAPI) to low flow intensity, assuming the latter was a response of the former. The range of the multiplicative factor ϕ was set to vary from 4 to 10 with increments of 1 while that of γ was varied from 0 to 0.99 with increments of 0.01. Since API as defined above is a measure of dryness or wetness of the soil in response to the monthly precipitation totals, the API is the soil water memory and is a proxy for the amount of water available from precipitation to contribute to flows. It takes into consideration the concurrent and lagged transfer of information from precipitation to flows (as represented by Equation 17). Further, it was also found that API as used here yielded a more direct relationship with low flow intensities than precipitation or SPI did with low flow intensities (Figure S3, Supporting Information S1). Since the API time series was derived with an inherent assumption that $API = 0$ at $t = 0$, the first twelve values of monthly sAPI were discarded considering those months to be the warming-up period of the API series. In the HMM models of intensity and duration, sAPI was used as a covariate, while for the annual frequency HMM, the mean of annual sAPI was used as the model covariate to be consistent with the timescales. Figure S5a shows the sAPI as obtained for a sample station through the process explained above. Figure S5b shows the established (inverse) relation between SDI and sAPI over time for a sample station. The sAPI closely mimics the SDI, thus supporting the use of sAPI as a predictor in the HMM.

2.3.3 Configurations of One-state and Two-state IDF Models

For modeling low flow intensity, a monthly HMM was built with gamma distribution as the error distribution model. The intensity data at a catchment was modeled using the corresponding value of the sAPI occurring at the same point in time. For any given catchment, two models were built — a one-state model and a two-state model. The mean and standard deviation of the two-state model were allowed to vary as shown in Table 1. While the mean was a function of the covariate as well as the state, the variance was varied only with the state and not with time. Similarly, for modeling duration, a monthly HMM was built with a log-normal distribution as the error distribution model. The duration data at a catchment was modeled using the corresponding value of the sAPI occurring at the same point of time as the intensity (peak) of the low flow spell. For modeling low flow frequency, the total count of all low flow events that took place in a streamflow water year was used. Annual HMMs were built with Poisson distribution as the error distribution model and the mean annual sAPI was used as a covariate.

Table 1 shows the model configurations for the one-state and two-state HMMs of the IDF. By employing such a framework, the cumulative probability of IDF was time-varying because of the non-stationary mean and standard deviation. Note that in the interests of parsimony, HMMs built here did not consider state changes for the parameter a_1 (Equations 4a and 4b).

Table 1: Configurations of the IDF HMMs

Low flow characteristic	**Covariate used**	**Error distribution model** (ε)	**Model configuration**
Intensity (I)	sAPI	Gamma	$\widehat{{}_tI_i} = a_{0,i} + a_1.(sAPI)_t$ ${}_tI_i \sim Gam(\widehat{{}_tI_i}, {\sigma_i}^2 \mid i)$
Duration (D)	sAPI	Log-normal	$\widehat{{}_tD_i} = a_{0,i} + a_1.(sAPI)_t$ ${}_tD_i \sim LogNorm(\widehat{{}_tD_i}, {\sigma_i}^2 \mid i)$
Frequency (F)	Mean Annual sAPI	Poisson	$\widehat{{}_tF_i} = a_{0,i} + a_1.(Mean\ Annual\ sAPI)_t$ ${}_tF_i \sim Pois(\widehat{{}_tF_i}, {\sigma_i}^2 \mid i)$

Ranges: $a_0 \in [-50,\ 50]$; $a_1 \in [-5,\ 5]$; $\sigma \in [1e-7,\ 35]$
The subscript i denotes the state index and can take values 1 or 2.
σ_i denotes the standard deviation of the error model in state i

2.3.4 Assigning of Viterbi States

Figure 4 depicts the possible Markov state transitions considered for the analysis here. As mentioned before in Section 2.3.1, it was assumed that the maximum number of states a given low flow characteristic's time series can take are only two, viz., normal and non-normal (Figure 4a). For illustration, Figure 4b shows the possible model outcomes of applying the framework on the intensities of low flows, where the three panels represent the time sequence of the Viterbi states taken under each of the outcomes. It may be noted that since we are modeling extreme characteristics of low flows, both states represent regimes of extremes. Thus, the normal state of the regime of an extreme implies a state when values of I/D/F of low flow droughts given the history of the region may be considered usual or not unexpected. In simple words, the normal state of low flow I/D/F as defined in the study here corresponds to low flow droughts that could be an outcome of a seasonal fluctuation resulting in flow conditions that, while still considered extreme, are within the statistical likelihood of an expected low flow drought condition for the region. The non-normal state, on the other hand, can either be less extreme than normal low flows or more extreme than normal low flows. However, both cannot co-occur for the time series of I/D/F for a given catchment, following the assumption that the maximum number of states allowed is 2. While modeling each of the IDF, we assigned states by assuming that the time stamp that had the value of the covariate (sAPI for intensity and duration; mean annual sAPI for frequency) closest to the median value of the covariate for a catchment was the time when the given I/D/F value was in a normal state. A two-state model of HMM would have either 'high' and 'normal' states or 'low' and 'normal' states (Figure 4a). The HMM built here classified an observation to be in a high state if the 50th percentile of the Viterbi I/D/F value simulated at a given point in time was more/higher than the 50th percentile of the normal state I/D/F value. An observation was classified to be in a low state if the 50th percentile of the Viterbi I/D/F value simulated at a given point in time was less than the 50th percentile of the normal state I/D/F value.

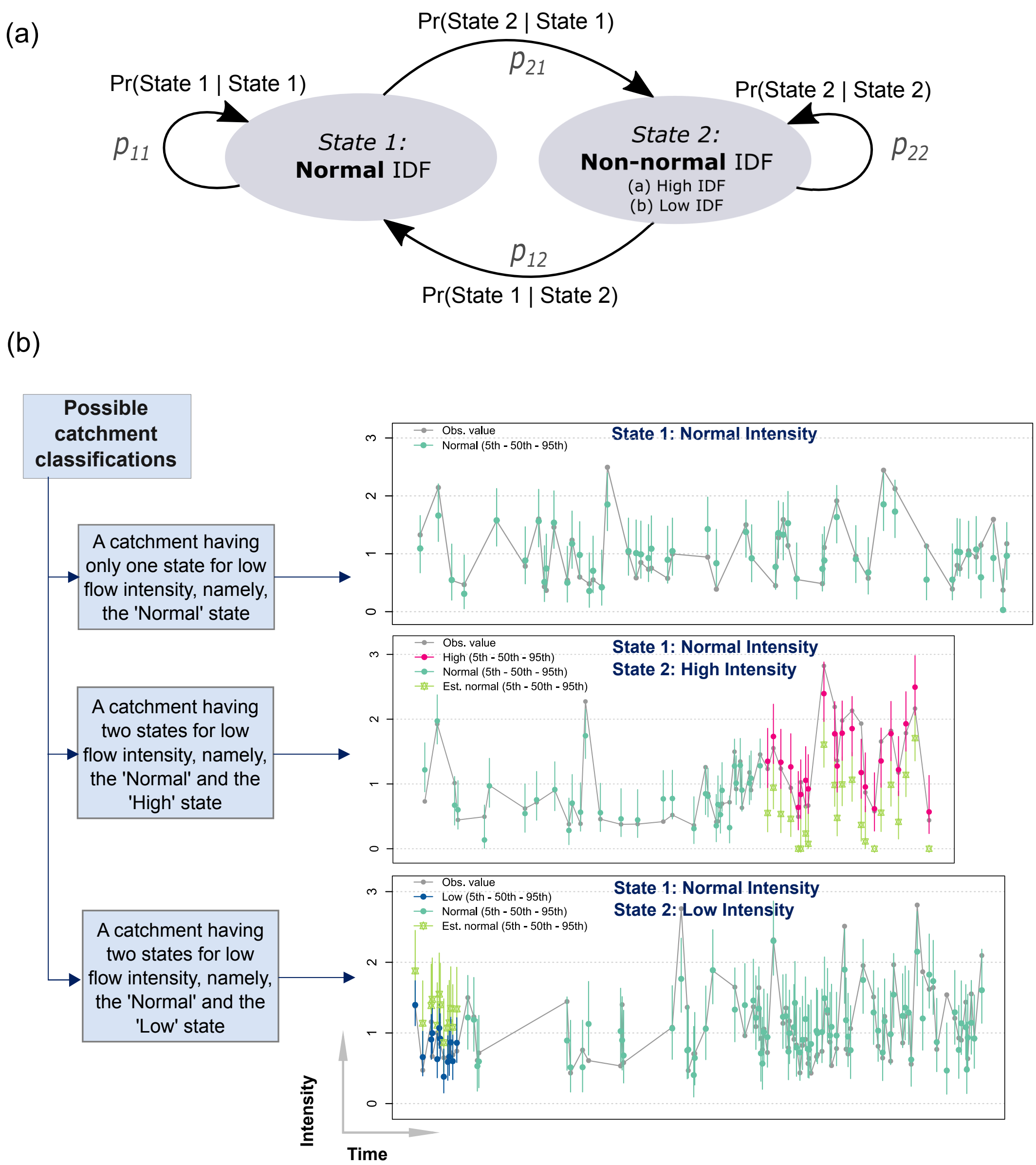

Figure 4: (a) Depiction of Markov state transitions in the applied HMM framework. Each state can either continue to sustain or switch to the other state. (b) The three possible outcomes from applying the proposed HMM to a low flow characteristic. For illustration, the time series of the intensity of low flows is used to demonstrate the possible results from applying the model. The top panel shows a catchment where the intensity only has one state. The middle panel shows a catchment where the intensity has two states, with the second state (the high state) representing more intense low flows. The bottom panel shows a catchment where the intensity has two states, with the second state (the low state) representing less intense low flows.

2.4 Identifying Catchments With Two States in IDF

The flowchart in Figure 5 summarizes the overall flow of the methodology pertaining to the analysis carried out. Following the steps as laid out in Figure 5, to decide the best model for a given characteristic at a catchment, the Akaike Information Criterion (AIC) was used. This is expressed as

$$AIC = -2ln(\mathscr{L}) + 2N \tag{20}$$

where N is the number of model parameters being estimated and $\mathscr{L}$ is the maximized likelihood of the model (expressed in Equation 3 in Supporting Information S1). Among the two models tested, i.e., the best one-state and the best two-state model, the one that had the lowest AIC was chosen for the catchment. Following the use of the AIC criterion, a catchment was identified as having two states in I/D/F if the best model at the catchment had: (a) observations belonging to a normal state and some to a low I/D/F state or (b) observations belonging to a normal state and some to a high I/D/F state as depicted in Figure 4b and as stated in the steps in Figure 5. In the present context of low flows, higher values of a low flow characteristic indicate a more extreme low flow event.

At catchments where, for a given low flow characteristic, the two-state model was the better model, the strength of simulation of the two-state model over the one-state model was established using the evidence ratio (ER) (Burnham & Anderson, 2002). The evidence ratio offers a way to quantify the strength of the evidence that the selected model (the two-state HMM in this case) is convincingly superior to the alternative model (the one-state HMM). It was computed by comparing the Akaike weights, w, of the two competing models, namely, the two-state model (2SM) and the one-state model (1SM), as expressed below:

$$ER = \frac{w_{2SM}}{w_{1SM}} \tag{21}$$

Here w_{1SM} and w_{2SM} are the Akaike weights for the one-state and two-state models, respectively, and are defined as:

$$w_{2SM} = \frac{1}{1 + exp(-\frac{1}{2}\Delta)} \tag{22}$$

$$w_{1SM} = \frac{exp(-\frac{1}{2}\Delta)}{1 + exp(-\frac{1}{2}\Delta)} \tag{23}$$

where Δ in this case is the AIC difference between the best one-state model and the best two-state model:

$$\Delta = AIC_{1SM} - AIC_{2SM} \tag{24}$$

The ER value serves to establish confidence in the two-state model relative to the one-state model, and hence the strength of evidence for the existence of two states. Any ER value > 10 suggests that the observations are more likely to be explained by the two-state model than the one-state model. The higher this value, the stronger the evidence. For the current work, we considered ER values greater than 10 (or its logarithmic values greater than 1) as denoting sufficient evidence to believe that a two-state model is convincingly better in performance over the one-state model, following Burnham and Anderson (2002); Goswami et al. (2022). The ER, however, only denotes how good the two-state model is relative to the one-state model and does not provide sufficient information on how qualified the two-state model is to represent the low flow characteristic being modeled. To address the later aspect, the model residuals were tested for their normality using the Shapiro-Wilk's test ($alpha$ = 0.05) (Shapiro & Wilk, 1965) and were retained for further analysis only if their Shapiro-Wilk's test p-value was greater than 0.05. In addition, the aim was also to have a 2SM with at least a predefined minimum number of I/D/F values in each state to ensure that a meaningful state does indeed exists. For this, catchments that had less than five I/D/F data points in any state were removed for further analysis. To make sure the

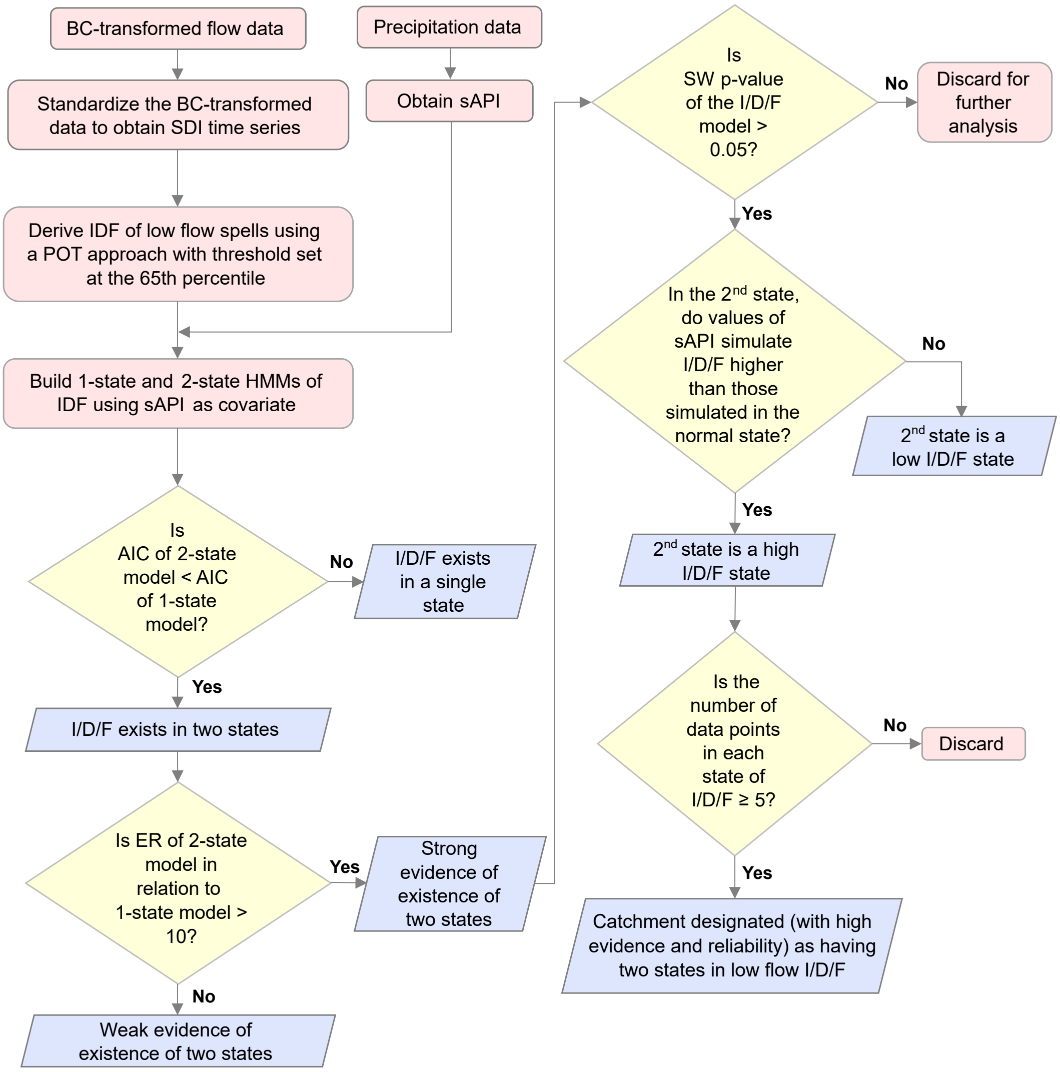

BC: Box-Cox; SDI: Streamflow Drought Index; I/D/F: Intensity/ Duration/ Frequency; POT: Peak Over Threshold; SW: Shapiro Wilk; sAPI: Standardized Antecedent Precipitation Index; HMMs: Hidden Markov Models; AIC: Akaike Information Criterion; ER: Evidence Ratio

Figure 5: Flowchart illustrating the main steps followed to identify if a catchment has two states in low flow I/D/F.

best model performed adequately, we also inspected the number of significant lags in the Auto-Correlation Function (ACF) of the normal pseudo-residuals, the histogram, and the Q-Q plot of the normal pseudo-residuals (Zucchini & MacDonald, 2009). The ACF serves as a visual check to confirm whether the model residuals are serially correlated or not. Serially correlated errors indicate that the model is not adequately built and there is loss of some information, thereby indicating that the model could be improved further.

3 Results and Discussion

3.1 States of Low Flow IDF

Figure 6 shows the low flow intensity Viterbi states over time for an example catchment, with Figure 6a showing the variation of the model covariate, i.e., sAPI. The results in Figure 6b shows that two states were identified, whereby the catchment was in a normal state until 1999, after which it switched to and persisted in a high intensity state. Furthermore, the conditional state probabilities (in Figure 6c) show that there is a very high probability of the aforementioned states. Practically, this indicates that low flow periods become more intense (i.e. drier) after 1999. This is illustrated in Figure 6b by the estimated normal values of intensity (points in lime green). These are the model-estimated values that indicate what would have been the intensity had the catchment been in the normal state at that epoch. These are the model-estimated values that indicate what would have been the intensity had the catchment been in the normal state at that epoch. These are determined using the relationship of intensity with the covariate as in the normal state (Equation 4a, with $i = 1$). For the epochs when the catchment is found to have switched into the second state, the results from Figure 6 suggest that the intensity for a given value of covariate is much higher than what it would have been expected had the catchment been in the normal state. Here the intensity HMM not only distinguishes the two states of low flow intensity but also informs the timing of the shifts in its states. Importantly, Figure 6 demonstrates that despite the inclusion of a covariate, the observed low flow intensity is best explained using more than one distribution. That is, the catchment not only displays non-stationarity arising from the precipitation (Figure 6a) but also from the state shifting. This provides preliminary evidence toward falsifying that one state is sufficient to explain low flow intensities.

Figure 6c shows the conditional probability of being in a given state at any given time for the catchment. It reflects the switching of the catchment between the two states. The catchment is believed to have switched to the other state when the state probability of the other state becomes greater than that of the state in which the catchment is currently in. Such a behavior as shown in Figure 6 suggests that hydrological droughts are becoming more extreme in the catchment, with the catchment continuing to be in an amplified extreme state until the end of the observation period. The two states as seen in Figure 6b are defined by two different distributions, supporting the notion of the need for state-dependent distributions. Thus, the observed intensity can lie in two states, shown by the green and pink color points. The second state represents more extreme low flow intensity than those represented by the normal low flow state. It must be noted here that the data represented by both states are extreme values, i.e. values pertaining to low flow droughts. The second state here refers to a more intensified extreme state, suggesting an amplification of extremes (low flow events here) in such catchments. The existence of mixture distribution as emerging from the outcomes in Figure 6 could mean that the observations in the two states are generated from separate flow processes or flow dynamics unique to the states and which are not explained by the variability in water availability from precipitation alone. These dynamics may be arising from real physical attributes, such as changes in baseflow. It is thus likely that the more intense low flows may be caused by less baseflow during such periods. Another factor that could be in play is systematic changes in groundwater levels. However, all these need further investigation.

For intensity data, it was found that the model satisfactorily simulates the values except for only a few instances in time where it misses estimating very high values of intensity accurately. However, most of the observations lie within the 95% confidence interval of the model. Considering this and the fact that modeling extreme values adequately is a challenge for any modeling framework, for the primary question being addressed in this work, the HMM framework proved to be a suitable technique for investigating changing regimes of extremes. Corresponding to Figure 6, Figure S4 in Supporting Information S1 provides an assessment of the model performance for the intensity HMM of the catchment in terms of the distribution of the normal pseudo-residuals and their autocorrelation. With the present ability of the HMM, the framework performs well in simulating low flow intensity data. The model residuals were found to be normally distributed along with the Shapiro-Wilk p-value being more than 0.05. This implies that the model residuals have very little information contained in them and they can be considered to be nearly random, suggesting a good match between the modeled values and the observations. A model having Shapiro-

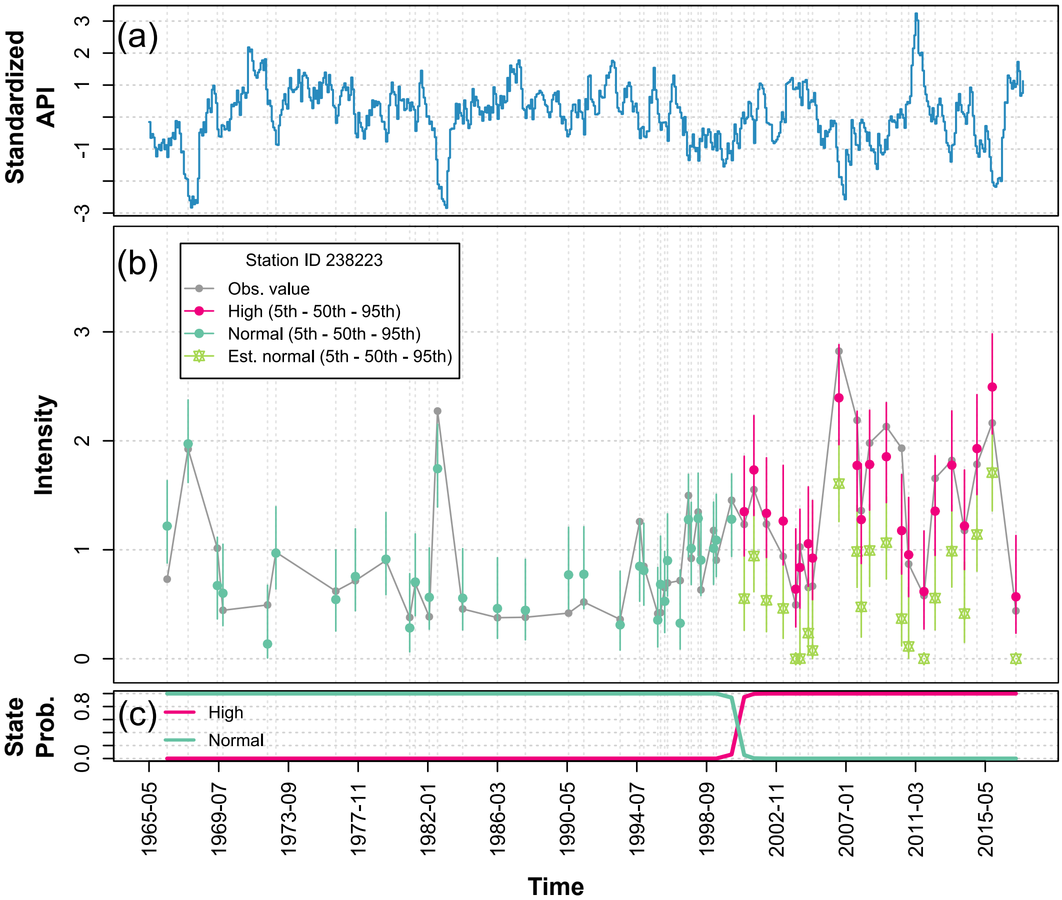

Figure 6: Viterbi states taken by the low flow intensity over time for station ID 238223. (a) The catchment's monthly variation of the sAPI, which is used as a covariate in the intensity model. (b) Time series of low flow intensity of the catchment. The green-colored circles indicate modeled values that belong to the normal state. Pink-colored circles indicate values belonging to the second state (more extreme than normal state). The lime green stars occurring in the same vertical spaces as that of the pink circles indicate the model-established value of intensity in the normal state at that time step. At any given time, the colored circles (or stars) represent the median value of the intensity. The colored vertical lines associated with each of these represent the error bar covering the 5th to the 95th percentile of the estimates. The gray-colored circles denote the observed intensities. (c) Variation of state conditional probability depicting the probability of intensity being in a given state at any given time. Clearly, a single state is not sufficient to describe the intensity data at this catchment.

Wilk's p-value greater than 0.05 suggests A similar inference holds for the ACF plot where there are not many lags that are significant, indicating that the model errors have very low predictive power.

Figure 7 shows the low flow duration results for a different example catchment. Although the outcomes from AIC showed that the duration data was better described by a 2SM than a 1SM, Figure 7b suggests that the duration modeling as undertaken in the current framework has a scope for improvement. As can be seen in Figure 7b, the median duration in a given state at each time point shows very little variability, which casts doubt on sAPI being an appropriate covariate for duration. Figure 8 shows the model simulation of annual frequency for a sample catchment. Figure 8a shows the corresponding time series of mean annual sAPI, which is the covariate to the frequency model. For the sample catchment, all the values lie in a single state (the normal state) as can be seen from Figure 8b. Hence a single state does a better job of explaining the frequency data than two states in this case. However, the simulated frequency values following the modeling as done here resulted in large error bars associated with the modeled values, implying that the frequency model too, like the duration model, may be further improved. Figures S5 and S6 in Supporting Information S1 provide assessments of model residual behavior corresponding to the duration and frequency HMM results discussed in Figures 7 and 8, respectively.

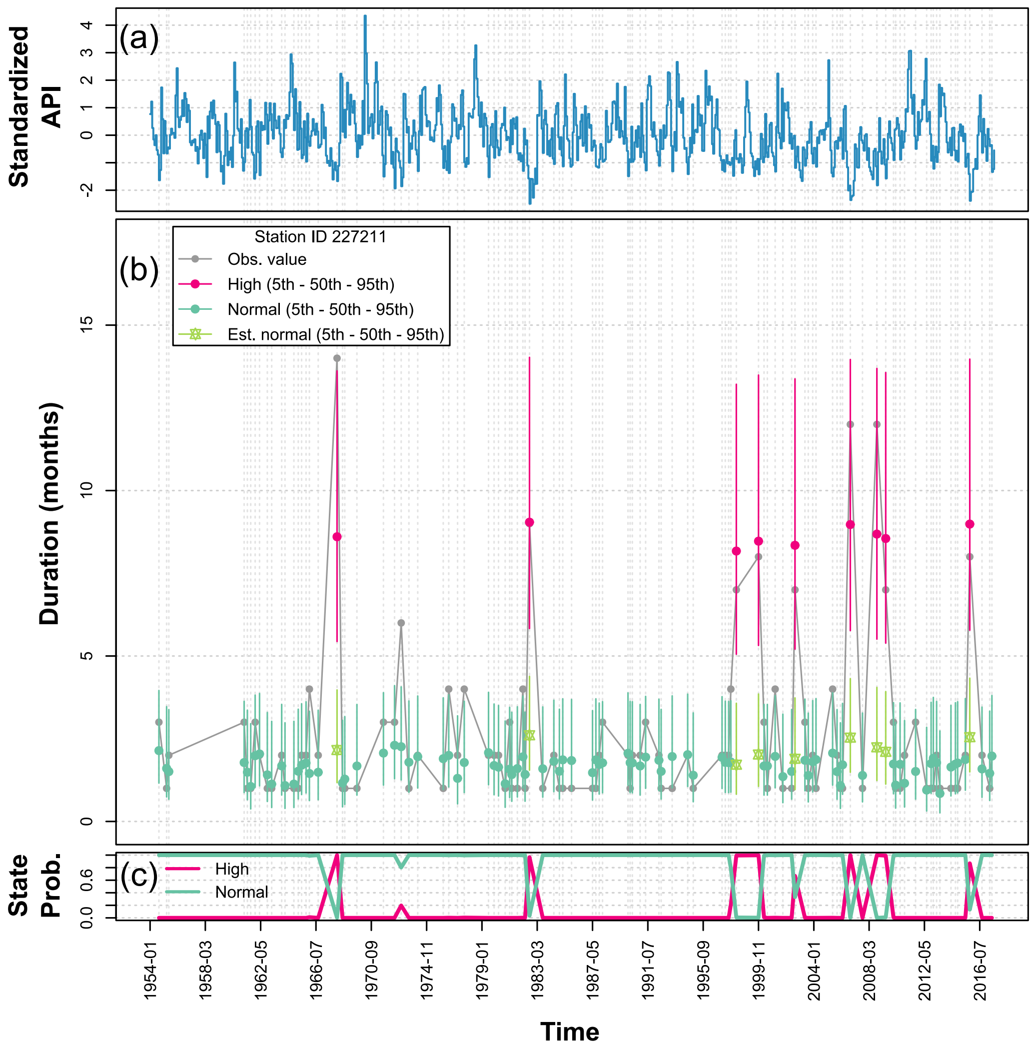

Figure 7: Viterbi states taken by the low flow duration over time for station ID 227211. See Figure 6 for a description of the figure elements.

As pointed out above, the current approach for modeling duration and frequency in the HMM framework needs improvement. Time series simulation of duration and frequency thus remains a challenge. The IDF HMMs as used here are built upon the linear dependence between sAPI and the low flow characteristic being modeled (Equation 4a and 4b). Thus, the results suggest that the sAPI's relation with duration and frequency is either non-linear, or an alternate covariate should be sought. For example, sAPI at a fortnightly or daily scale

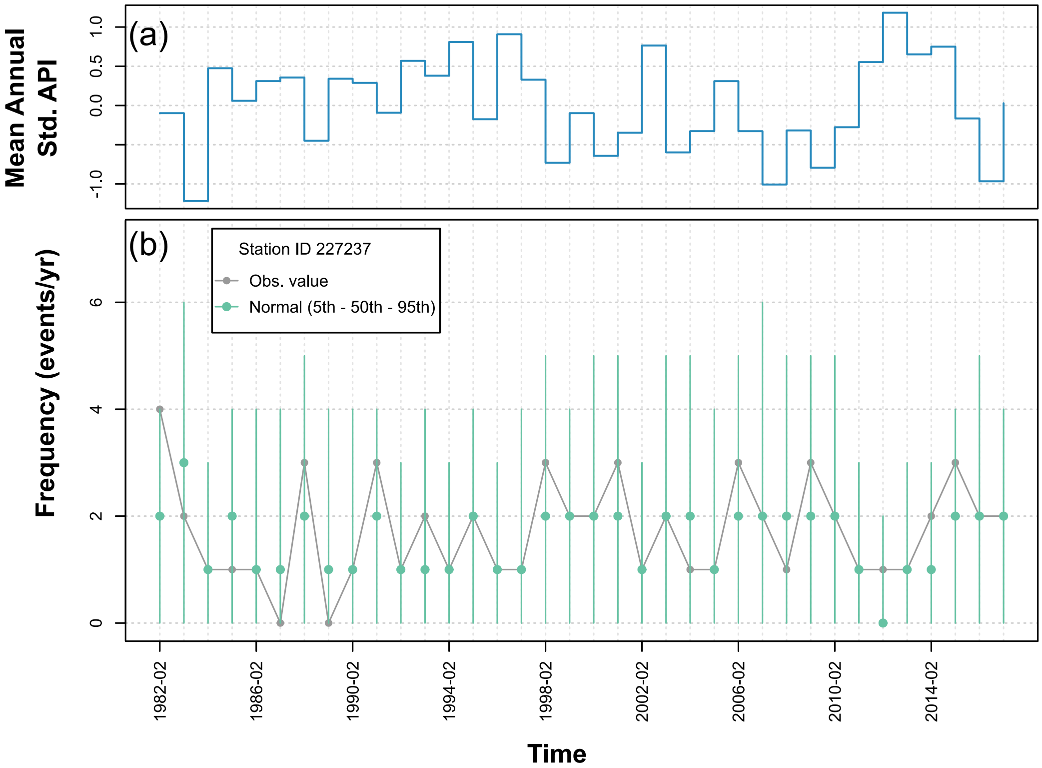

Figure 8: Variation of low flow annual frequency values with time for station ID 227237. (a) Catchment's mean annual sAPI which is used as a covariate in the frequency model. (b) Time series of the observed and simulated frequency. Only a single state was sufficient to describe the frequency data at this catchment.

than monthly may be a better predictor for duration, and seasonal mean sAPI instead of annual mean sAPI may work better for modeling low flow frequency. Another possibility could be understanding and establishing which physical covariate, if not sAPI, governs the variability in these characteristics and may potentially replace sAPI in these models.

For the reasons stated above, following this section, we focus primarily on presenting and discussing the results for low flow intensities, with only a brief discussion about duration and frequency.

3.2 Catchments with Two States in IDF

As depicted in the steps in Figure 5 and as discussed under Section 2.4, the candidate models at a catchment were screened for AIC and ER. Figure 9a shows the spatial distribution of catchments obtained after screening for AIC of 2SM < AIC of 1SM, and log(ER) > 1 for the intensity model over the study region. A total of 115 (71%) catchments (purple-colored) showed strong evidence of the existence of two states in the intensity of low flows. This suggests that low flow intensity extremes are a mixed process and hence warrant a mixture of distributions to represent them. Such results provide formal strength of evidence for the hypotheses that extremes can quantitatively shift to different states if perturbed and hence a single state cannot adequately explain them.

The 115 catchments as identified in Figure 9a were further screened for model performance based on the Shapiro-Wilk p-value for normality of the residuals. The number of catchments

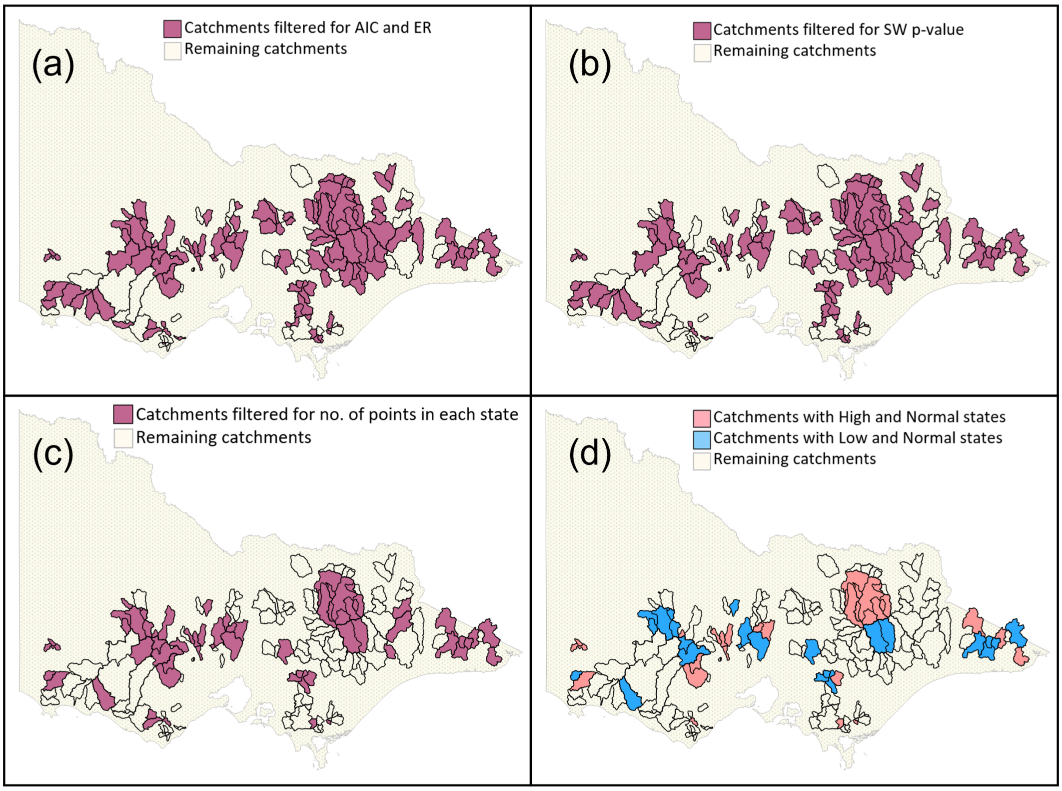

Figure 9: Spatial distribution of catchments having two states in low flow intensities. Figures a–d show the two-state catchments retained on subsequent steps of filtering. (a) The 115 catchments (colored in purple) having AIC of 2SM < AIC of 1SM and log(ER)>1 for 2SM over 1SM. (b) The 101 catchments (colored in purple) having Shapiro-Wilk p-value>0.05. (c) The 34 catchments (colored in purple) which had at least 5 intensity data points in each state (and hence at least 5 unique low flow spells in each regime). (d) Of the 34 catchments, the 21 catchments that have normal and high intensity states shown in a shade of red. For these catchments, the second state is a high intensity state. Of the 34 catchments, the 13 catchments that have normal and low intensity states shown in blue. The second state for these 13 catchments is a low intensity state.

that indicate high evidence for 2SM over 1SM provides provides support for the hypothesis that low flow extremes might switch states. 101 of these 115 satisfied the condition of Shapiro-Wilk p-value>0.05. These are shown further in Figure 9b (colored in purple). Further, to ensure a meaningful state exists, these 101 catchments were also checked for having the number of data points in each state more than or equal to 5. This condition ensured that such a catchment will have at least 5 unique low flow spells in both, normal and non-normal, regimes. Figure 9c shows the final 34 catchments meeting these criteria. Of these 34 catchments, there were catchments where the second state (the non-normal state) pointed to a low intensity state (shown in blue in Figure 9d) and catchments where the second state was a high intensity state (shown in a shade of red in Figure 9d).

The high spatial variability shown in Figure 9d is unexpected. It may be due to catchment-specific biophysical factors (combination of one or more of the slope, mean elevation, soil types, climate, vegetation, etc.) and hydrologic response to extremes emerging from the complex interactions of vegetation and soil hydraulics, making low flows, at least in the case of the SEA region, somewhat heterogeneous in space. The tendency to switch or to exhibit resilience against switching may thus possibly be controlled by a combination of topography, climatic factors, soils, and vegetation. Catchments having the second state as high state are likely to switch from a normal low flow state to a more extreme low flow state characterized by higher than usual values of low flow intensities, entailing a magnification of low flows. Further, since proxy information from precipitation and soil moisture was already provided in the form of sAPI for modeling the low flow intensities, the emergence of a two-state model with very high evidence and model reliability at as many as 34 catchments (Figure 9) suggests that not all observations can be explained by the precipitation data. Thus, extremes in low flows may not be sufficiently explained by changes in precipitation.

Figure 10 follows a similar basis as Figure 9, showing the catchments retained at every stage of filtering. Using AIC and ER values as the filtering criteria, a total of 112 (Figure 10a) out of 161 catchments showed a 2SM to be superior to 1SM in modeling low flow duration data. The 5 red shaded catchments in Figure 10d represent catchments as obtained after all the steps of performance filtering. For these, the second state of low flow duration was associated with higher values of duration. There is a good overlap of catchments having high evidence for exhibiting two states in intensity as well as in duration as can be seen from Figures 9a and 10a. The spatial differences, however, grow as one moves from subplots a–d in these figures. As per the AIC and ER criteria, of the 161 catchments, the number of catchments having two states in (1) only intensity (but not duration) were 30, (2) only duration (but not intensity) were 27, and (3) both intensity and duration were 85.

Unlike intensity and duration, annual frequency of the low flow events, on the other hand, did not exhibit switching of states for the way the framework models this characteristic. Of the catchments studied, only one catchment emerged where the 2SM was better than 1SM. Since for frequency of low flows, the number of catchments satisfying the AIC and ER criteria was not sufficient, the figure for the spatial distribution of 2SM catchments of frequency is not included here.

For several of the SEA catchments, the existence of multiple states of extremes is a recent phenomenon. The exact reasons that drive the switching of states of low flows still need to be explored. The answer may come with improved knowledge of the underlying systemic processes governing these and their complex feedbacks to one another. The results here provide evidence for low flow state transitions in these catchments and the changing regimes of hydrological extremes (low flow droughts). The intensities in the 'high' state represent unusual low flow droughts induced possibly from a hydrological disturbance which sets a positive feedback for the catchment's extreme characteristics to slip into the second state, as has been concluded to be the case for total flows by Peterson et al. (2021). Such a hydrological disturbance could be from catchment-wide changes, which control the runoff, changing the partitioning of the incoming precipitation at the surface between infiltration and surface runoff. This disturbance may be brought about by prolonged meteorological droughts and natural factors. Studies have also suggested groundwater storage (Fowler et al., 2020; Hughes et al., 2012; Kinal & Stoneman, 2012) and plant water use (Peterson et al., 2021; Ukkola et al., 2016) as causal factors, with the latter producing a positive feedback and hence persistent alternate states. Long hydrological memory linked with stored groundwater may also be an important facet (Alvarez-Garreton et al., 2021), which makes the current flow volumes to be governed more strongly by antecedent conditions. In such cases, the subsurface storages carried forward in time are often capable of equalizing the deficiencies in precipitation during the onset of a drought (Avanzi et al., 2020). Anomalously low streamflows have also been implicated in changes in the seasonality of climate conditions (both atmospheric and precipitation demands) (Williams et al., 2022). However, all this demands further research to draw more detailed conclusions around the drivers for the switch, including how feedbacks from the catchment's biophysical components may be affecting water partitioning (e.g., Peterson, Western, & Argent, 2014) and the triggers from global climate shifts.

Apart from natural controls on flows, low flows can vary as a response to human controls on flows as well (Gebremicael et al., 2013; Guzha et al., 2018). Studies have shown that

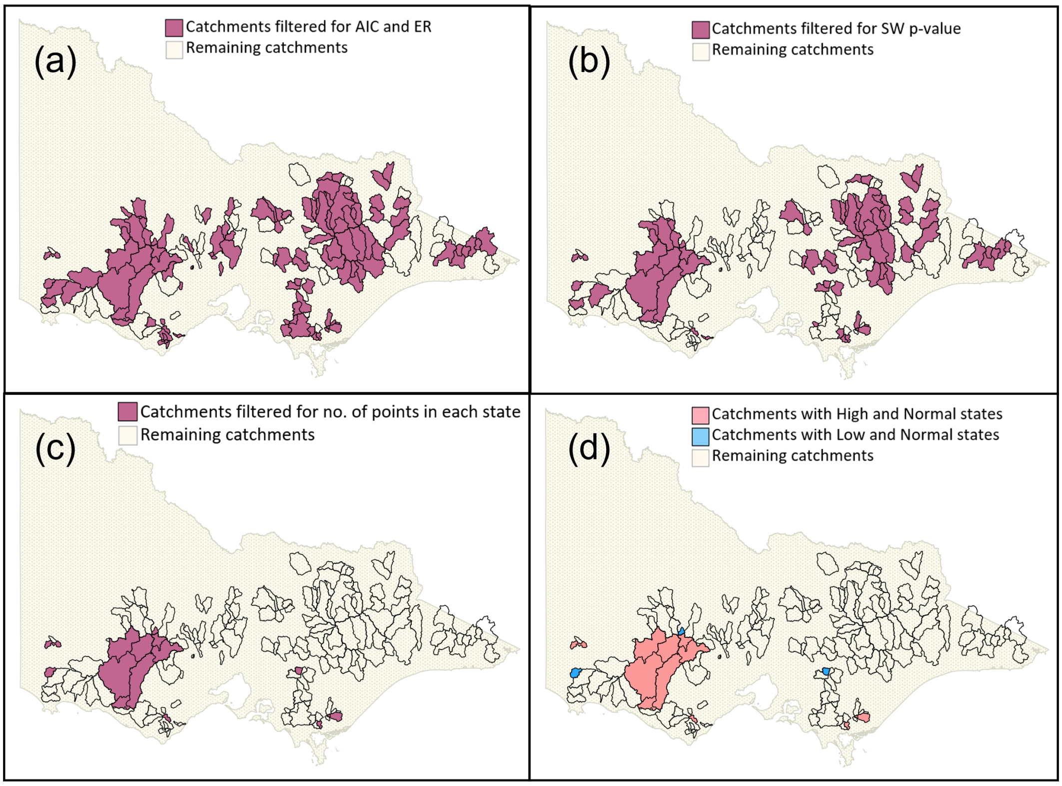

Figure 10: Same as Figure 9 but for duration of low flows. Figures a–d show the two-state catchments retained on subsequent steps of filtering. (a) The 112 catchments (colored in purple) having AIC of 2SM < AIC of 1SM and log(ER)>1 for 2SM over 1SM. (b) The 63 catchments (colored in purple) having Shapiro-Wilk p-value>0.05. (c) The 34 catchments (colored in purple) which had at least 5 duration data points in each state. (d) Of the 8 catchments, the 5 catchments that have normal and high duration states shown in a shade of red. For these catchments, the second state is a high duration state. Of the 34 catchments, the 3 catchments that have normal and low duration states shown in blue. The second state for these 3 catchments is a low duration state.

human activities such as water abstraction interventions and land use/cover change, such as fire/non-fire induced vegetation changes, can modify low flows in a catchment (Li et al., 2007; Chang et al., 2016; Gebremicael et al., 2020) as these activities may change the partitioning of the incoming precipitation on the land surface (Gates et al., 2011). In the case of the present study, the 161 SEA catchments were unregulated and had water extractions <10% of the mean annual runoff. Effects from land use change may be a driver responsible for switching of states of extremes. However, for these catchments, Peterson et al. (2021) (in their Supplementary Material) show that land use change (1985-2019) did not explain the observed runoff state shifts. The switching of states of low flows as found in this study is thus more likely an outcome of changes in the hydroclimate of the region or the response of a catchment to these or both.

3.3 Low Flow Intensity State Changes and Atmospheric Conditions

Extreme dry and warm conditions of the atmosphere may be one of the drivers of low flow switching. To examine this, a timeline of the 21 catchments identified to be switching between a normal intensity state and a high intensity state was studied. Figure 11a shows the number of catchments, of the 21 catchments, existing in their second state of low flow intensity for the time period 1950–2016. The height of the vertical black-colored bars indicates the number of catchments experiencing a low flow intensity lying in the second state at a given time. The gaps in between the bars represent a time instance when either none of those catchments had a low flow intensity (peak) occurrence or when there is a low flow intensity (peak) occurrence, but it belongs to the normal state. The height of the yellow bar at each month depicts the number of catchments that had gauge flow data available. The recent meteorological drought periods in the state of Victoria (Australian Bureau of Statistics, Year Book Australia 1998) were: (i) 1967–1968, (ii) 1972–1973, and (iii) 1982–1983. Combined with the Millennium Drought (1997-2009), these 4 periods denote abnormally dry periods over SEA on record. These are shown as gray-colored vertical strips in Figure 11a. These periods appear to coincide with peaks in the number of catchments in the second state of low flow intensity.

Also shown in Figure 11 are the periods of abnormally high sea surface temperature anomalies of the Niño3.4 region, characteristic of an El Niño event (orange vertical bars). These were derived from the Ocean Niño Index (ONI) obtained from the United States National Oceanic and Atmospheric Administration (NOAA) Climate Prediction Centre (CPC) (`www.cpc.ncep.noaa.gov`) (Refer Text S5 and Table S3 in Supporting Information S1 for details). It was also seen that many catchments switched to the second state during the warm episodes of the El Niño Southern Oscillation. However, the number of these catchments is comparable to those belonging to neither the meteorological drought nor the El Niño periods for the present study (Figure 11b and c). Figure 11 suggests that warm and dry atmospheric conditions such as those prevailing during sustained meteorological drought spells may create conditions conducive for catchments to switch states of low flows.

The boxplots in the lower panel of Figure 11 show the number of catchments in the second state for various periods, namely, periods of meteorological droughts (b), periods of warm ENSO (c), and periods that were neither meteorological droughts nor warm ENSO periods (d). The figure suggests that meteorological droughts have the potential to change low flow spells, adding to the existing literature on how severe and protracted meteorological droughts can potentially destabilize the hydrological behavior and resilience of catchments. With the projected increase (Xu et al., 2019) and changes in future meteorological droughts and the complex interactions between meteorological and hydrological droughts, low flow regimes are more likely to be dynamic and subject to modifications. Importantly, Figure 11 highlights the changing regimes of hydrological extremes in a changing climate. The results in the figure also suggest that the phenomenon of switching of low flow regimes can neither be considered exceptional nor rare any longer. With low flow droughts exhibiting regime-switching, the risks associated with them are also expected to vary in time. As the risk changes, water managers will have to understand how resilient are the catchments to changes in extremes.

4 Conclusions

Catchments can undergo complex changes in their behavior which can change how low flows respond to such changes. The study here examined whether low flow characteristics can exist in more than one state. This was done using HMMs with antecedent precipitation index as a covariate, applied to examine low flow IDF in 161 catchments in SEA. It was found that for the majority of the catchments ($\approx 70\%$), a two-state model explained the low flow intensity and duration data better than a one-state model, thereby suggesting that low flows exhibit multiple states. Very strong evidence of low flow intensity exhibiting two distinct states was found for at least 34 (21%) catchments in the region. For most catchments exhibiting switching of states of low flow intensity, the second state entailed an intensification of low flows. The regime-switching behavior can cause low flows to manifest in very different ways at two different epochs for the same catchment. Such a temporal behavior also points to changing risks associated with hydrological droughts. The two states are possibly governed

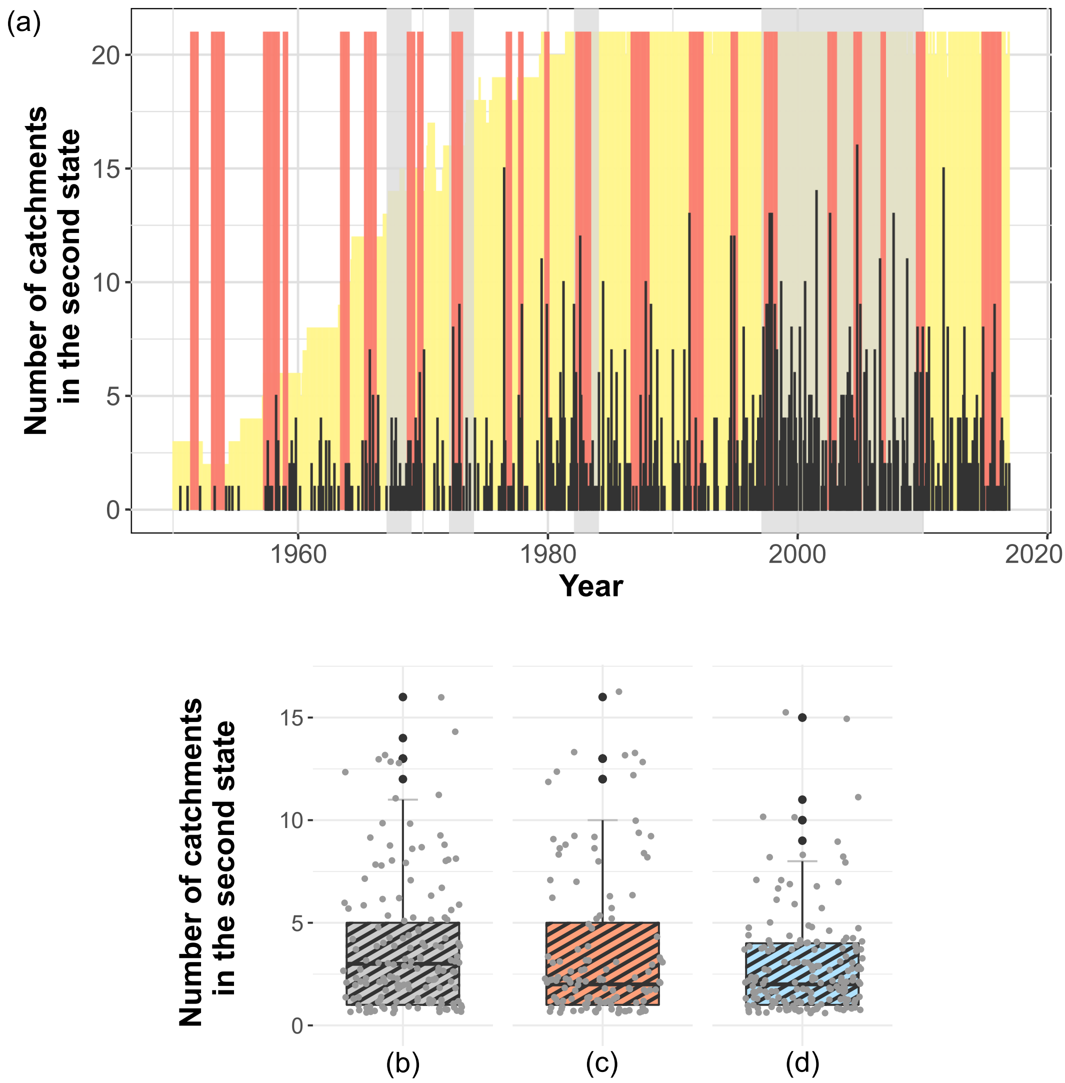

Figure 11: (a) Timeline (1950–2016) of the switching of states of low flow intensity for the 21 catchments. The height of the black-colored bars represents the number of catchments in the second state at a given time. The height of the yellow-colored bars at each month represents how many of these 21 catchments had flow data available for that month. The four gray-colored vertical strips shown in the background represent the four recent severe meteorological drought spells for the Victoria region, which are (i) 1967–1968, (ii) 1972–1973, (iii) 1982–1983, and (iv) 1997-2009, respectively, from left to right. The red-colored vertical strips represent time instances when the ONI indicates the occurrence of a warm ENSO episode. The three boxplots shown in the lower panel depict the number of catchments in the second state during (b) meteorological drought periods, (c) warm ENSO periods, (d) periods that were neither b nor c.

by unique processes generating the observations in the two states. Importantly this indicates that the use of one distribution is inadequate to explain the observed data, as is widely done. The work demonstrates the capability and reliability of HMMs to simulate extreme low flow intensities as well as the capability to capture temporal shifts in states.

Further, since the information from the catchment's antecedent conditions and precipitation was intrinsic to the model, the emergence of a two-state model at a catchment implies that information from precipitation, though useful in simulating low flow behavior, may not be sufficient to explain changes in low flow extremes. Low flow intensities in the second state are not explained by the corresponding variability in precipitation. The duration and frequency HMM have a scope for improvement in the current framework. For frequency of low flows, the current capability of the model framework was not satisfactory for establishing the strength of the 2SM over 1SM. These models may be improved by either incorporating non-linear relation with sAPI or by using covariates (for eg., climate indices) that may explain the variability in them better.

Switching of catchments into an intensified low flow state may be strongly influenced by sustained dry atmospheric conditions such as those during protracted meteorological droughts as well as the changes in them. The study also helps to understand how future extreme hydrological characteristics may behave in response to such meteo-climatological disturbances triggered naturally or due to climate change. This points to possible changes that catchments can undergo during and after a meteorological drought and how that impacts extreme hydrological behavior and response. As dry conditions and meteorological droughts change and become more frequent in a changing climate, their impact on hydrological cycle and on extreme flows can be very significant.

More research needs to be undertaken to understand the underlying physical processes and the driving mechanisms in play to explain the existence of more than one low flow regime, thereby reducing uncertainty about future low flow dynamics in watersheds. The results here demonstrate the potential of catchments to exhibit shifts in regimes of low flow extremes. A crucial aspect of enhancing future water security lies in understanding how these shifts might translate into impacts on streamflow services and how to manage these periods. Identification of shifts may enable system planners to consider solutions such as supply augmentation, demand management, inter-basin water transfers, managed groundwater aquifer recharge, conjunctive use, etc., thereby augmenting system resilience during low flow shifts in the future.

Conflict of Interest

The authors declare no conflicts of interest relevant to this study.

Acknowledgments

The authors acknowledge the IITB-Monash Research Academy for funding P. Goswami with a PhD scholarship to support this research. The authors are thankful to Christopher Pickett-Heaps from the Bureau of Meteorology, Australia, for his constructive comments on the manuscript, adding to its improvement. The authors also thank and acknowledge the developers and contributors of all the R packages that were used for this analysis.

Data Availability Statement

The implementation of the Hidden Markov modeling was carried out in the software environment R (R Core Team, 2021) using the R package "*HydroState*" available at `https://github.com/peterson-tim-j/HydroState`. The streamflow and precipitation data used for this study are available at `https://doi.org/10.5281/zenodo.6412694`. The ONI data was sourced from `https://origin.cpc.ncep.noaa.gov/products/analysis_monitoring/ensostuff/ONI_v5.php`. To aid in the analysis of the current work, R packages such as DEoptim, MASS, extRemes, ggplot2, ggpattern, ggpubr, zoo, dplyr, rgdal, sf, RColorBrewer, ggsn, cowplot, and ggspatial were also used. Developers and contributors of all these packages are acknowledged.

References

Alvarez-Garreton, C., Boisier, J. P., Garreaud, R., Seibert, J., & Vis, M. (2021). Progressive water deficits during multiyear droughts in basins with long hydrological memory in Chile. *Hydrology and Earth System Sciences*, *25*(1), 429–446.

Australian Bureau of Statistics. (Year Book Australia 1998). Canberra, Australia: Australian Government Publishing Service, 1998. *Australia*.

Avanzi, F., Rungee, J., Maurer, T., Bales, R., Ma, Q., Glaser, S., & Conklin, M. (2020). Climate elasticity of evapotranspiration shifts the water balance of Mediterranean climates during multi-year droughts. *Hydrology and Earth System Sciences*, *24*(9), 4317–4337.

Baum, L. E., & Petrie, T. (1966). Statistical inference for probabilistic functions of finite state Markov chains. *The annals of mathematical statistics*, *37*(6), 1554–1563.

Bennett, K. E., Cannon, A. J., & Hinzman, L. (2015). Historical trends and extremes in boreal Alaska river basins. *Journal of Hydrology*, *527*, 590–607.

Box, G. E. P., & Cox, D. R. (1964). An Analysis of Transformations. *Journal of the Royal Statistical Society: Series B (Methodological)*, *26*(2), 211–243. doi: 10.1111/j.2517-6161.1964.tb00553.x

Bracken, C., Rajagopalan, B., & Zagona, E. (2014). A hidden Markov model combined with climate indices for multidecadal streamflow simulation. *Water Resources Research*, *50*(10), 7836–7846.

Burn, D. H., Sharif, M., & Zhang, K. (2010). Detection of trends in hydrological extremes for Canadian watersheds. *Hydrological Processes*, *24*(13), 1781–1790.

Burnham, K. P., & Anderson, D. R. (2002). *A practical information-theoretic approach* (Vol. 2). Springer New York.

Chang, J., Zhang, H., Wang, Y., & Zhu, Y. (2016). Assessing the impact of climate variability and human activities on streamflow variation. *Hydrology and Earth System Sciences*, *20*(4), 1547–1560.

Chiew, F. H. S., Potter, N., Vaze, J., Petheram, C., Zhang, L., Teng, J., & Post, D. (2014). Observed hydrologic non-stationarity in far south-eastern Australia: implications for modelling and prediction. *Stochastic Environmental Research and Risk Assessment*, *28*(1), 3–15.

Coles, S., Bawa, J., Trenner, L., & Dorazio, P. (2001). *An introduction to statistical modeling of extreme values* (Vol. 208). Springer.

Crow, W. T., Bindlish, R., & Jackson, T. J. (2005). The added value of spaceborne passive microwave soil moisture retrievals for forecasting rainfall-runoff partitioning. *Geophysical Research Letters*, *32*(18).

Dharssi, I., Bally, J., Steinle, P., McJannet, D., & Walker, J. (2017). Comparison of soil wetness from multiple models over Australia with observations. *Water Resources Research*, *53*(1), 633–646.

Forney, G. D. (1973). The viterbi algorithm. *Proceedings of the IEEE*, *61*(3), 268–278.

Fowler, K., Knoben, W., Peel, M., Peterson, T. J., Ryu, D., Saft, M., … Western, A. (2020). Many commonly used rainfall-runoff models lack long, slow dynamics: Implications for runoff projections. *Water Resources Research*, e2019WR025286.

Fowler, K., Peel, M., Saft, M., Nathan, R., Horne, A., Wilby, R., … Peterson, T. (2022). Hydrological shifts threaten water resources. *Water Resources Research*, e2021WR031210.

Gates, J. B., Scanlon, B. R., Mu, X., & Zhang, L. (2011). Impacts of soil conservation on groundwater recharge in the semi-arid Loess Plateau, China. *Hydrogeology Journal*, *19*(4), 865–875.

Gebremicael, T. G., Mohamed, Y., Betrie, G., Van der Zaag, P., & Teferi, E. (2013). Trend analysis of runoff and sediment fluxes in the Upper Blue Nile basin: A combined

analysis of statistical tests, physically-based models and landuse maps. *Journal of Hydrology*, *482*, 57–68.
Gebremicael, T. G., Mohamed, Y. A., van der Zaag, P., Hassaballah, K., & Hagos, E. Y. (2020). Change in low flows due to catchment management dynamics—Application of a comparative modelling approach. *Hydrological Processes*, *34*(9), 2101–2116.
Goswami, P., Peterson, T. J., Mondal, A., & Rüdiger, C. (2022). Non-stationary Influences of Large-scale Climate Drivers on Low Flow Extremes in Southeast Australia. *Water Resources Research*, e2021WR031508.
Guzha, A., Rufino, M. C., Okoth, S., Jacobs, S., & Nóbrega, R. (2018). Impacts of land use and land cover change on surface runoff, discharge and low flows: Evidence from East Africa. *Journal of Hydrology: Regional Studies*, *15*, 49–67.
Holmes, A., Rüdiger, C., Mueller, B., Hirschi, M., & Tapper, N. (2017). Variability of soil moisture proxies and hot days across the climate regimes of Australia. *Geophysical Research Letters*, *44*(14), 7265–7275.
Hughes, J., Petrone, K., & Silberstein, R. (2012). Drought, groundwater storage and stream flow decline in southwestern Australia. *Geophysical Research Letters*, *39*(3).
Katz, R. W. (2013). Statistical methods for nonstationary extremes. In *Extremes in a changing climate* (pp. 15–37). Springer.
Kendall, M. G. (1975). *Rank correlation methods.* (4th ed. 2d impression). Griffin.
Kiem, A. S., & Verdon-Kidd, D. C. (2010). Towards understanding hydroclimatic change in Victoria, Australia–preliminary insights into the "Big Dry". *Hydrology and Earth System Sciences*, *14*(3), 433–445. doi: 10.5194/hess-14-433-2010
Kinal, J., & Stoneman, G. (2012). Disconnection of groundwater from surface water causes a fundamental change in hydrology in a forested catchment in south-western Australia. *Journal of Hydrology*, *472*, 14–24.
Kohler, M. A., & Linsley, R. K. (1951). *Predicting the runoff from storm rainfall* (Vol. 30). US Department of Commerce, Weather Bureau.
Li, L.-J., Zhang, L., Wang, H., Wang, J., Yang, J.-W., Jiang, D.-J., ... Qin, D.-Y. (2007). Assessing the impact of climate variability and human activities on streamflow from the Wuding River basin in China. *Hydrological Processes: An International Journal*, *21*(25), 3485–3491.
Liu, X., Liu, C., & Brutsaert, W. (2018). Investigation of a generalized nonlinear form of the complementary principle for evaporation estimation. *Journal of Geophysical Research: Atmospheres*, *123*(8), 3933–3942.
Liu, Y. Y., Parinussa, R., Dorigo, W. A., De Jeu, R. A., Wagner, W., Van Dijk, A., ... Evans, J. (2011). Developing an improved soil moisture dataset by blending passive and active microwave satellite-based retrievals. *Hydrology and Earth System Sciences*, *15*(2), 425–436.
Mallya, G., Tripathi, S., Kirshner, S., & Govindaraju, R. S. (2013). Probabilistic Assessment of Drought Characteristics Using Hidden Markov Model. *Journal of Hydrologic Engineering*, *18*(7), 834–845. doi: 10.1061/(asce)he.1943-5584.0000699
Mann, H. B. (1945). Nonparametric tests against trend. *Econometrica: Journal of the econometric society*, 245–259.
Miao, C., Ashouri, H., Hsu, K.-L., Sorooshian, S., & Duan, Q. (2015). Evaluation of the PERSIANN-CDR daily rainfall estimates in capturing the behavior of extreme precipitation events over China. *Journal of Hydrometeorology*, *16*(3), 1387–1396.
Miller, W. P., & Piechota, T. C. (2008). Regional analysis of trend and step changes observed in hydroclimatic variables around the Colorado River Basin. *Journal of Hydrometeorology*, *9*(5), 1020–1034.
Peel, M. C., McMahon, T. A., & Finlayson, B. L. (2004). Continental differences in the variability of annual runoff-update and reassessment. *Journal of Hydrology*, *295*(1-4), 185–197.
Peterson, T. J., Saft, M., Peel, M. C., & John, A. (2021). Watersheds may not recover from drought. *Science*, *372*(6543), 745–749. doi: 10.1126/science.abd5085
Peterson, T. J., & Western, A. (2014). Multiple hydrological attractors under stochastic

daily forcing: 1. Can multiple attractors exist? *Water Resources Research*, *50*(4), 2993–3009.
Peterson, T. J., Western, A., & Argent, R. (2014). Multiple hydrological attractors under stochastic daily forcing: 2. Can multiple attractors emerge? *Water Resources Research*, *50*(4), 3010–3029.
Pushpalatha, R., Perrin, C., Le Moine, N., & Andréassian, V. (2012). A review of efficiency criteria suitable for evaluating low-flow simulations. *Journal of Hydrology*, *420*, 171–182.
R Core Team. (2021). R: A Language and Environment for Statistical Computing [Computer software manual]. R Foundation for Statistical Computing, Vienna, Austria. Retrieved from `https://www.R-project.org/`
Robertson, A. W., Kirshner, S., & Smyth, P. (2003). Hidden Markov models for modeling daily rainfall occurrence over Brazil. *Information and Computer Science, University of California*.
Robertson, A. W., Kirshner, S., & Smyth, P. (2004). Downscaling of daily rainfall occurrence over northeast Brazil using a hidden Markov model. *Journal of climate*, *17*(22), 4407–4424.
Rolim, L. Z. R., & de Souza Filho, F. d. A. (2020). Shift detection in hydrological regimes and pluriannual low-frequency streamflow forecasting using the hidden markov model. *Water*, *12*(7), 2058.
Saft, M., Western, A. W., Zhang, L., Peel, M. C., & Potter, N. J. (2015). The influence of multiyear drought on the annual rainfall-runoff relationship: An Australian perspective. *Water Resources Research*, *51*(4), 2444–2463. doi: 10.1002/2014WR015348
Sagarika, S., Kalra, A., & Ahmad, S. (2014). Evaluating the effect of persistence on long-term trends and analyzing step changes in streamflows of the continental United States. *Journal of Hydrology*, *517*, 36–53.
Shapiro, S. S., & Wilk, M. B. (1965). An analysis of variance test for normality (complete samples). *Biometrika*, *52*(3/4), 591–611.
Solander, K. C., Bennett, K. E., & Middleton, R. S. (2017). Shifts in historical streamflow extremes in the Colorado River Basin. *Journal of Hydrology: Regional Studies*, *12*, 363–377.
Tauro, F. (2021). River basins on the edge of change. *Science*, *372*(6543), 680–681.
Thyer, M., & Kuczera, G. (2000). Modeling long-term persistence in hydroclimatic time series using a hidden state Markov model. *Water resources research*, *36*(11), 3301–3310.
Thyer, M., & Kuczera, G. (2003). A hidden Markov model for modelling long-term persistence in multi-site rainfall time series 1. Model calibration using a Bayesian approach. *Journal of Hydrology*, *275*(1-2), 12–26.
Tian, W., Bai, P., Wang, K., Liang, K., & Liu, C. (2020). Simulating the change of precipitation-runoff relationship during drought years in the eastern monsoon region of China. *Science of the Total Environment*, *723*, 138172.
Turner, S., & Galelli, S. (2016). Regime-shifting streamflow processes: Implications for water supply reservoir operations. *Water Resources Research*, *52*(5), 3984–4002.
Ukkola, A. M., Prentice, I. C., Keenan, T. F., Van Dijk, A. I., Viney, N. R., Myneni, R. B., & Bi, J. (2016). Reduced streamflow in water-stressed climates consistent with CO2 effects on vegetation. *Nature Climate Change*, *6*(1), 75–78.
Van Dijk, A. I., Beck, H. E., Crosbie, R. S., De Jeu, R. A., Liu, Y. Y., Podger, G. M., ... Viney, N. R. (2013). The Millennium Drought in southeast Australia (2001-2009): Natural and human causes and implications for water resources, ecosystems, economy, and society. *Water Resources Research*, *49*(2), 1040–1057. doi: 10.1002/wrcr.20123
Wasko, C., Shao, Y., Vogel, E., Wilson, L., Wang, Q. J., Frost, A., & Donnelly, C. (2021). Understanding trends in hydrologic extremes across Australia. *Journal of Hydrology*, *593*, 125877. doi: 10.1016/j.jhydrol.2020.125877
Wilhite, D. A., & Glantz, M. H. (1985). Understanding: the drought phenomenon: the role of definitions. *Water international*, *10*(3), 111–120.

Williams, A. P., Cook, B. I., & Smerdon, J. E. (2022). Rapid intensification of the emerging southwestern North American megadrought in 2020–2021. *Nature Climate Change*, *12*(3), 232–234.
Xu, L., Chen, N., & Zhang, X. (2019). Global drought trends under 1.5 and 2 C warming. *International Journal of Climatology*, *39*(4), 2375–2385. doi: 10.1002/joc.5958
Zhang, X., Harvey, K. D., Hogg, W., & Yuzyk, T. R. (2001). Trends in Canadian streamflow. *Water Resources Research*, *37*(4), 987–998.
Zhang, X. S., Amirthanathan, G. E., Bari, M. A., Laugesen, R. M., Shin, D., Kent, D. M., ... Tuteja, N. K. (2016). How streamflow has changed across Australia since the 1950s: evidence from the network of hydrologic reference stations. *Hydrology and Earth System Sciences*, *20*(9), 3947–3965.
Zipper, S., Popescu, I., Compare, K., Zhang, C., & Seybold, E. C. (2022). Alternative stable states and hydrological regime shifts in a large intermittent river. *Environmental Research Letters*, *17*(7), 074005.
Zucchini, W., & MacDonald, I. L. (2009). *Hidden Markov models for time series: an introduction using R.* Chapman and Hall/CRC.

On the existence of multiple states of low flows in catchments in southeast Australia

Pallavi Goswami[1], Tim J. Peterson[2,3], Arpita Mondal[4,5], Christoph Rüdiger[2,6]

[1]IITB-Monash Research Academy, IIT Bombay, Mumbai, India
[2]Department of Civil Engineering, Monash University, Clayton, Victoria, Australia
[3]Department of Infrastructure Engineering, University of Melbourne, Parkville, Victoria, Australia
[4]Department of Civil Engineering, Indian Institute of Technology Bombay, Mumbai, India
[5]Interdisciplinary Program in Climate Studies, Indian Institute of Technology Bombay, Mumbai, India
[6]Bureau of Meteorology, Melbourne, Victoria, Australia

Key Points:

- Low flow regimes can switch states which may lead to intensification of low flow events.
- Existence of sustained warm and dry atmospheric conditions can cause the switching of catchments into an intensified low flow state.
- Information from precipitation, though useful, may not be sufficient to explain the variability in low flow extremes.

Corresponding author: Pallavi Goswami, pallavi.goswami@monash.edu

Abstract

Hydrological variables of a catchment and their corresponding extreme characteristics have a possibility of switching regimes, particularly when a catchment undergoes protracted dry periods. This can result in a catchment experiencing a flow anomaly that is even more extreme than what was historically considered an extreme low flow event for the catchment. Catchments in southeast Australia have been shown to exhibit multiple states of mean annual flows. Given this and studies that suggest that extreme events may be changing with time, it is important to understand whether extremes in flows also have the potential to exist in multiple states. To investigate this, we studied intensity, duration, and frequency (IDF) of low flows for 161 unregulated catchments in southeast Australia. A Hidden Markov Model-based approach was used to examine shifts in the low flow characteristics. We found very strong evidence of low flow intensity exhibiting two distinct states for at least 34 (21%) catchments in the region, providing convincing reasons to believe that extremes in low flows can and have undergone regime changes. The second state of these catchments is often associated with higher values of low flow intensities. Simulation of the duration and frequency of these events, however, needs improvement with the current approach and may be better studied by accounting for climate indicators that may more suitably explain them. Impacts from a changing climate may enhance the triggering of low flows into alternate states, which calls for water managers to plan for changing regimes of extremes.

Plain Language Summary

Recent studies have shown that the mean hydrological behavior of catchments can undergo changes. The present study explores whether extreme events, such as low flow droughts, might also be undergoing regime-switching. The term 'switching of states' or 'regime-switching' relates to a shift in the underlying probability distribution of a variable. With regards to streamflows, this may result in a catchment experiencing low flow droughts that are even more extreme than what was historically considered a drought event for the catchment. We found strong evidence of low flow intensity exhibiting two distinct states in catchments in southeast Australia, providing convincing reasons to believe that extremes in low flows can and have undergone state changes in the region. The second state of these catchments is often associated with higher values of low flow intensities. Ignoring such changes is likely to misrepresent low flow risks. This finding has profound importance in enabling hydrologists to understand the possible ways in which hydrological events can manifest themselves. Knowledge from these results supports the need to improve existing models to incorporate more dynamic realism within them, without which they might be blind to future hydrological shifts that could have a significant impact on water security.

1 Introduction

Water systems and hydrological regimes are known to be influenced by climatic perturbations, leading to irregularities in flow quantity and quality. Many studies have reported changes in rainfall-runoff relationships (Kiem & Verdon-Kidd, 2010; Van Dijk et al., 2013; Chiew et al., 2014; Miao et al., 2015; X. Liu et al., 2018). Drought flows are being observed to be drastically lower than expected for a given decline in precipitation (Alvarez-Garreton et al., 2021; Avanzi et al., 2020; Tian et al., 2020). The processes that generate runoff have been recently shown to change during (Saft et al., 2015) and after (Peterson et al., 2021) the occurrences of meteorological droughts. This results in less streamflow per unit of rainfall during and after the drought than that which occurred before the drought. Disturbances in catchments induced by changes in climate or from anthropogenic interventions have the potential to cause hydrological variables to undergo regime changes, also referred to as 'switching of states' or 'state shifts'. 'State shifts' relates to a shift in the underlying probability distribution of the variable, implying non-stationarity. This means that a forcing in the form of a disturbance can push a catchment past a fold point and into a new steady state and once the disturbance ends the catchment stays indefinitely in this new state until a disturbance pushes it back to the original state, as explained in Figure 1. In the context of regime-switching of extremes, a switching could result in a catchment experiencing a flow anomaly that is even more extreme than what was historically considered an extreme event. There is evidence suggesting that the mean behaviour of hydrologic variables can exhibit switching of states (Fowler et al., 2022; Peterson et al., 2021; Tauro, 2021; Zipper et al., 2022), i.e., they can exist in multiple states. The study by Peterson et al. (2021), for example, showed that catchments can not just exist in alternate states of streamflow regimes but can even continue to persist in such alternate states for extended periods. This suggests that low flows may also exhibit such behavior, thereby possessing far more complex form of non-stationarity than suggested by Goswami et al. (2022). However, to date, studies on extreme value analysis for streamflows have not examined this in detail. Many commonly existing streamflow models continue to discount that low flows can have temporal variability beyond their routine regime.

Southeast Australia (SEA) is known to have a hydroclimate that is among the most variable in the world (Peel et al., 2004). The hydroclimatologial extremes that the region has undergone in the past, including the Millennium Drought (Van Dijk et al., 2013), have been shown to influence the way streamflow responds (Saft et al., 2015). Many of these catchments have been shown to exhibit hydrologic non-stationarity in rainfall-runoff/climate-runoff relationships (Chiew et al., 2014), with streamflow droughts already shown to be increasing across the region (Wasko et al., 2021). Moreover, many existing studies assume catchments to have infinite resilience. Peterson et al. (2021), however, showed that annual and seasonal mean streamflow in many of these catchments exhibited switching in regimes following the Millennium Drought and that not all of them showed recovery when rainfall returned to normal. The work falsified the widely held assumption that catchments always have only a single steady state around which they fluctuate and showed that catchments could have finite resilience. The work, however, looked at mean flows, analyzed at the annual and seasonal timescales. It does not provide insights on regime-switching of extreme (low) flows, nor on the possibility of switching of such regimes at much finer (for eg., monthly) timescales. This brings forth the question of whether low flows can also undergo changes in state. With the region's susceptibility to exhibit changes in the mean behavior of streamflows, the region provides a good opportunity to study whether the behavior of extreme flows can also undergo changes in states.

Limited studies exist on the understanding and evaluation of shifts in streamflows, and none examine low flows or state change in particular. With regards to techniques for understanding changes in hydrologic extremes in general, the few most widely applied statistical approaches are the non-parametric Mann-Kendall trend analysis (Mann, 1945; Kendall, 1975), change point analysis, and the Generalized Extreme Value (GEV) theory (Coles et al., 2001). Previous studies have used the Mann-Kendall trend analysis to understand shifts in hydrologic extremes (X. Zhang et al., 2001; Miller & Piechota, 2008; Burn et al., 2010; Sagarika et al., 2014; Bennett et al., 2015). This technique, however, is not adequately tailored for the analysis of extremes per se and therefore does not offer a way to determine changes in flow magnitudes (Solander et al., 2017). The other common approach of using the GEV theory-based analysis has been used to study the extreme streamflow data in a non-stationary framework through time-dependent parameters in the GEV distribution (Katz, 2013), allowing trend (and thus regime change) detection in extremes. However, limited approaches exist that allow a comprehensive assessment of state change, entailing aspects such as time series simulation of extreme data, classification of the extreme data into different states (if they exist), and identification of the timing of state shifts.

One such technique that offers the capability to detect state-changes and breaks in persistence in a time series is the hidden Markov modeling approach. Being a doubly embedded stochastic process model, it makes for a good modeling choice for simulating data governed by complicated nonlinear hydrological phenomena. HMMs are statistical Markov models consisting of a hidden or unobservable 'parameter process' which satisfies the Markov property, and a 'state-dependent process', whose behavior depends on the underlying state (Zucchini & MacDonald, 2009). The approach provides a highly flexible modeling framework that can detect the existence of different 'states' in a variable of interest by quantifying the probability of the variable being in a given state over time. HMMs were developed during the late 1960s and early 1970s (Baum & Petrie, 1966) for speech recognition, and have since been successfully implemented in several applications, including climate and hydrologic modeling (Thyer & Kuczera, 2003; Robertson et al., 2003, 2004). Mallya et al. (2013) applied HMM to develop a drought index for probabilistic assessment of drought characteristics. Turner and Galelli (2016) applied HMM to examine the impact of regime-like behavior in streamflows on the performance of reservoir operating policy. Thyer and Kuczera (2000) used the hidden state Markov (HSM) model to simulate annual rainfall series in Australia. Rolim and de Souza Filho (2020) used it to identify shifts in low-frequency variability of streamflows. Bracken et al. (2014) used HMM along with climate indices to simulate multidecadal streamflows. More recently, Peterson et al. (2021) developed Hidden Markov Models (HMM) to statistically identify if, and when, streamflow recovers from meteorological droughts, and in doing so provide empirical evidence that catchments often have multiple hydrological states. Overall, HMMs are a useful tool for identifying state changes in a time series based on the dictating underlying process. By virtue of being a mixture model, HMM provides an unsupervised classification technique that can be applied to capture persistence and hence breaks in persistence in a time series, including low flows.

The present study aims to falsify the assumption that a single state is adequate to represent low flow events. This includes falsifying the commonly held notion that including rainfall variability is sufficient to account for non-stationarity in low flows and that low flows do not undergo long-term changes. To investigate this, the metrics used to characterize low flow events, namely, their intensity, duration, and frequency (IDF) were studied to test whether these can exist in more than one state, focusing on catchments in SEA. The study aims to provide an investigation of low flow extreme shifts along with finding when these changes are occurring for these catchments. To do this, we used the Hidden Markov modeling approach to identify state changes in the IDF of low flows. Although HMMs have been applied to investigate changes in flows and precipitation in previous studies as discussed above, these have not been specifically used to model low flow characteristics for investigating state changes in regimes of low flows. This study thus also presents a relatively less explored application of HMMs in investigating state changes in the extreme characteristics of low flows. The methodology adopted here also presents an alternative approach for examining hydrologic non-stationarity observed in the low flow IDF by examining if state-dependent distributions are required to explain the variability in the observed data.

2 Data and Methods

2.1 Study Region and Data

For the present work, 161 unimpaired catchments in southeast Australia (SEA) were studied using their monthly streamflow as flow depth (mm) and precipitation data (mm), both aggregated from daily values. The streamflow data of these catchments was sourced from Peterson et al. (2021) and pre-processed as described in Goswami et al. (2022) following the quality control of Peterson et al. (2021). The catchments were chosen based on their gauge record quality while also ensuring that all these catchments had flow records at least for 15, 7, and 5 years before, during, and after the Millennium Drought, respectively. All the catchments had at least 35 years of flow and precipitation data (Text S1 and Table S1 in Supporting Information S1). More information on the data can be found in Goswami et al. (2022). Importantly, this data provided an opportunity to investigate changes in extremes occurring in natural systems due to a changing climate and not through reservoir operations or land use practices. The 161 catchments and their corresponding gauging stations are

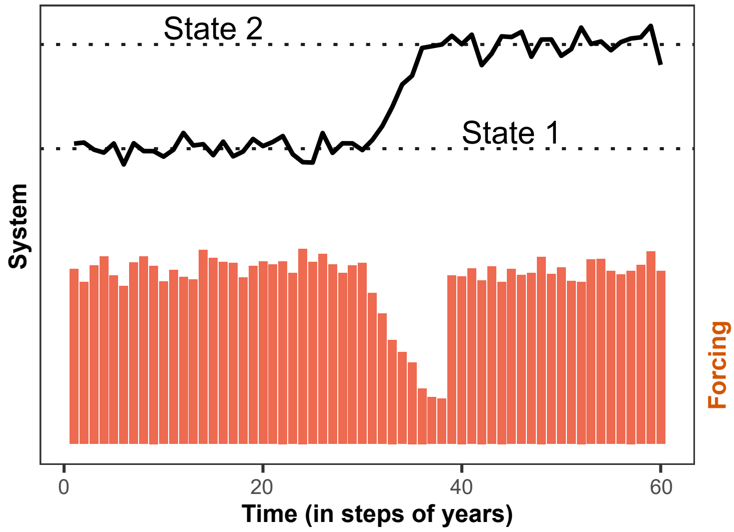

Figure 1: Illustration of regime-switching of a system (for eg., a hydrologic variable of interest) from State 1 to State 2 under the influence of a forcing (hydrologic disturbance). (Adopted from Peterson & Western, 2014.)

shown in Figure 2a, with the colored circles denoting the mean annual streamflow depth. Figure 2b shows the mean annual precipitation for the respective gauges. While this study is focused on the SEA region, the analysis and the understanding from it are relevant to all catchments where hydrological droughts are likely to become more extreme.

2.2 Deriving IDF of Low Flows

In this study, low flows were defined as representative of streamflow droughts describing a catchment's condition when streamflows are anomalously low relative to long-term monthly means. The term 'low flow' as used in this work can be understood as a type of hydrological drought. By common definition, a hydrological drought denotes a deficit in surface water and groundwater (Wilhite & Glantz, 1985). Thus, often the term hydrological drought takes on a broader hydrological definition and can refer to situations of low flows, low snowmelt, low spring flow, low groundwater levels, etc., relative to normal conditions. However, the present study focuses primarily on conditions where streamflows are anomalously low relative to their expected normal flow conditions. The study here thus uses the term 'low flows' (or 'low flow droughts') for the sake of being specific to the domain being investigated.

For identifying low flow spells and deriving their associated characteristics, an approach similar to that used in Goswami et al. (2022) was applied here. First, the monthly flow depths at any given catchment (Figure 3a) were transformed by applying a Box-Cox (BC) power transformation (Box & Cox, 1964), using catchment-specific lambda values, to reduce the skew and for better identification of flow values which were very low (Text S2 and Figure S1 in Supporting Information S1). The transformed flows were then standardized using the mean and standard deviation of the transformed flow series at that catchment. The sign of the obtained series was then reversed such that values above zero pointed to below-average streamflows. The resultant series was termed as the Streamflow Drought Index (SDI) (Figure 3b).

From the SDI series, monthly low flows were defined by using a threshold following the Peak-Over-Threshold (POT) approach (Coles et al., 2001). In the identification of low flow

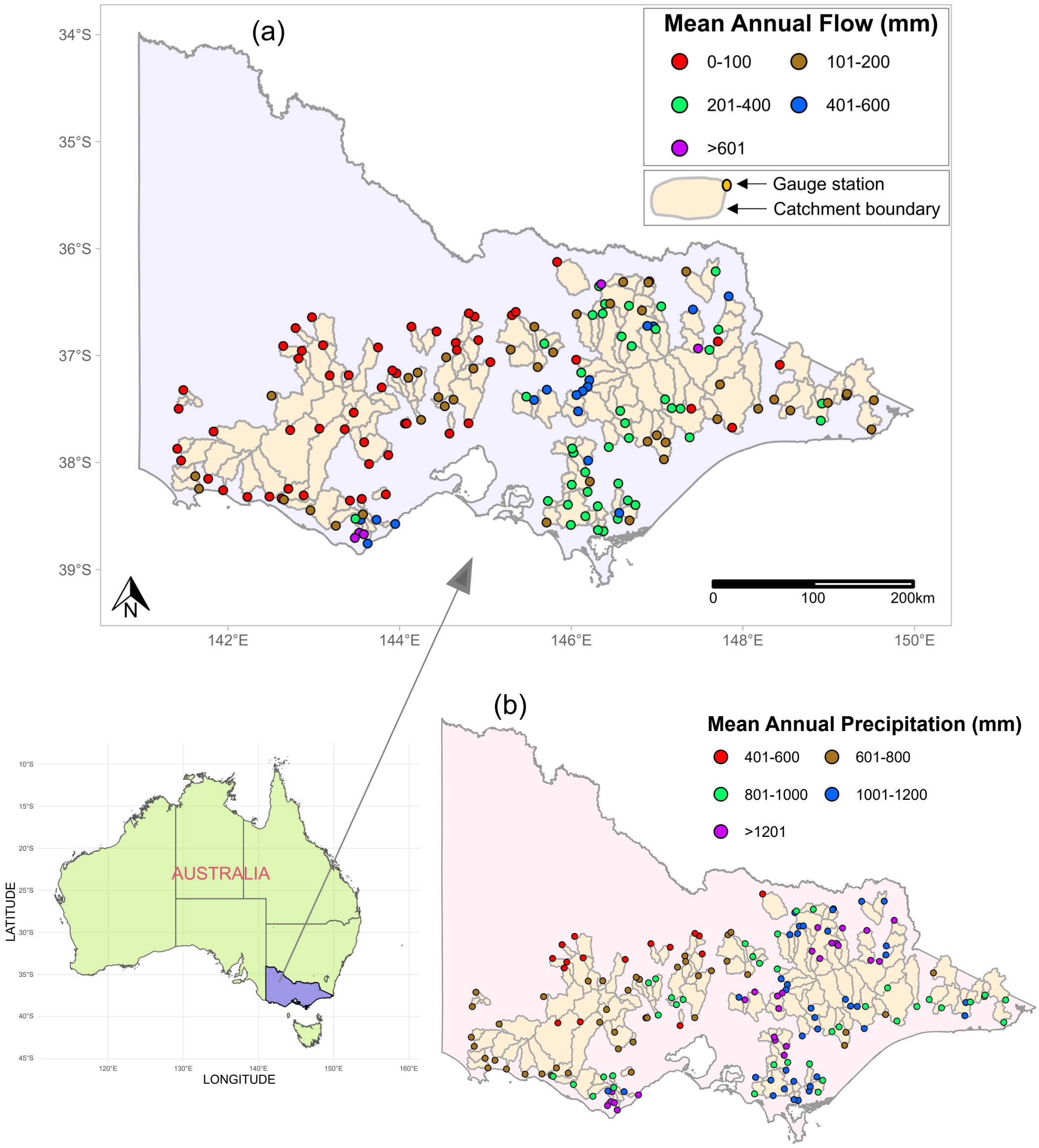

Figure 2: (a) Location of the study region and the 161 catchments (boundary shown in gray) along with their corresponding gauging stations (colored circles). The color of the gauge stations in (a) and (b) shows the mean annual flow depth and the mean annual precipitation, respectively.

periods, the choice of a low flow threshold is often subjective (Pushpalatha et al., 2012). For the current work, the threshold for defining the low flows was chosen to be the 65th percentile value of the SDI series. This ensured that most of the catchments had at least more than 40 values of intensity of low flows required for the model to perform satisfactory simulations. Higher thresholds corresponding to the 75th, 85th, and 95th percentiles resulted in significantly reduced sample sizes (Figure S2 in Supporting Information S1). This is a significant aspect as the capability of a Markovian model to simulate data improves when more data is available. Further, it was found that for the number of points lying above the threshold of 65th percentile, more than half of these lied above the 85th percentile for most of these catchments.

For this work, we focus on three important characteristics of low flows, namely, their intensity, duration, and annual frequency. These were derived from the SDI time series following their respective definitions in Goswami et al. (2022), as shown in Figure 3c. The duration of a low flow event was defined as the number of months for which the monthly SDI series remained above the threshold. The peak value that the SDI takes over the low flow spell was regarded as the intensity of the event. The more positive the peak value in a spell, the more intense the low flow event. The total number of such low flow events occurring in a streamflow water year was regarded as the annual frequency of the low flow events. The water year for computing frequency was taken from March of the current year, running for 12 months until February of the next year, following the definition as in X. S. Zhang et al. (2016). The March-February water year is typical in parts of SE Australia (particularly Victoria), where minimum flows are usually observed at the end of the Boreal summer.

2.3 Modeling IDF Using Hidden Markov Models (HMMs)

2.3.1 Hidden Markov Models for Low Flow IDF

HMM is a statistical Markov model consisting of two parts: an unobservable (or hidden) 'parameter process', C, which satisfies the Markov property, and a 'state-dependent process', X, in such a way that when $C^{(t)}$ is known, the distribution of X depends only on the present state of C and not on the previous states or observations (Zucchini & MacDonald, 2009). HMM assumes that the behavior of the process X depends on C. A simple HMM can be summarized by the following two equations:

$$Pr\ (C^{(t)} \mid \boldsymbol{C}^{(t-1)}) = Pr\ (C^{(t)} \mid C^{(t-1)}) \qquad t = 2, 3, ... \tag{1}$$

$$Pr\ (X^{(t)} \mid \boldsymbol{X}^{(t-1)}, \boldsymbol{C}^{(t)}) = Pr\ (X^{(t)} \mid C^{(t)}) \quad t \in \mathbb{N} \tag{2}$$

where, $C^{(t)}$ represents the value of C at a given time t, $\boldsymbol{C}^{(t)}$ is the Markov chain of probabilities and denotes the vector $[C_1,\ C_2,\ C_3, ..., C_t]$. $X^{(t)}$ represents the value of X at a given time t, and $\boldsymbol{X}^{(t)}$ denotes the vector $[X_1,\ X_2,\ X_3, ..., X_t]$. If the Markov chain $\boldsymbol{C}^{(t)}$ has m states, the HMM of X is called an m-state HMM, where each state has a different distribution. The model provides a Markov chain, i.e. the probability of X being in each state over time which involves maximization of the following probability (Zucchini & MacDonald, 2009):

$$Pr\ (\boldsymbol{C}^{(T)} = \boldsymbol{c}^{(T)} \mid \boldsymbol{X}^{(T)} = {}_{obs}x_t{}^{(T)}) \tag{3}$$

In the above expression, $\boldsymbol{c}$ is a sequence of possible states over the time steps and x is the vector of observed data. For an m-state HMM there are m^T possible sequences, T being the length of the time series.

Using this background of HMMs, we built temporal HMMs were built for each of the three low flow characteristics (i.e. low flow IDF) that examined for one and two states in these. The hidden states were the states of the existing climatic conditions. The model learnt about the state of extremes (C) by observing the low flow characteristic being modeled (x). Since the actual number of hydrological states for a given low flow characteristic is unknown, it was assumed that the low flow characteristics of a catchment can cycle through two states. A given low flow characteristic was thus simulated as being in one of the two distinct states. At each time point, t, the observed low flow characteristic was considered a random variable defined by a parametric distribution for each state. The state distribution at any time t depended upon the Markov chain of states at the preceding time step. For state, i, and at time, t, the conditional mean for the distribution of the given low flow characteristic under consideration was simulated as:

$$\widehat{{}_tx_i} = a_{0,i} + a_1.(sAPI_t) \qquad : for\ intensity\ and\ duration \tag{4a}$$
$$\widehat{{}_tx_i} = a_{0,i} + a_1.(mean\ annual\ sAPI_t) \qquad : for\ frequency \tag{4b}$$

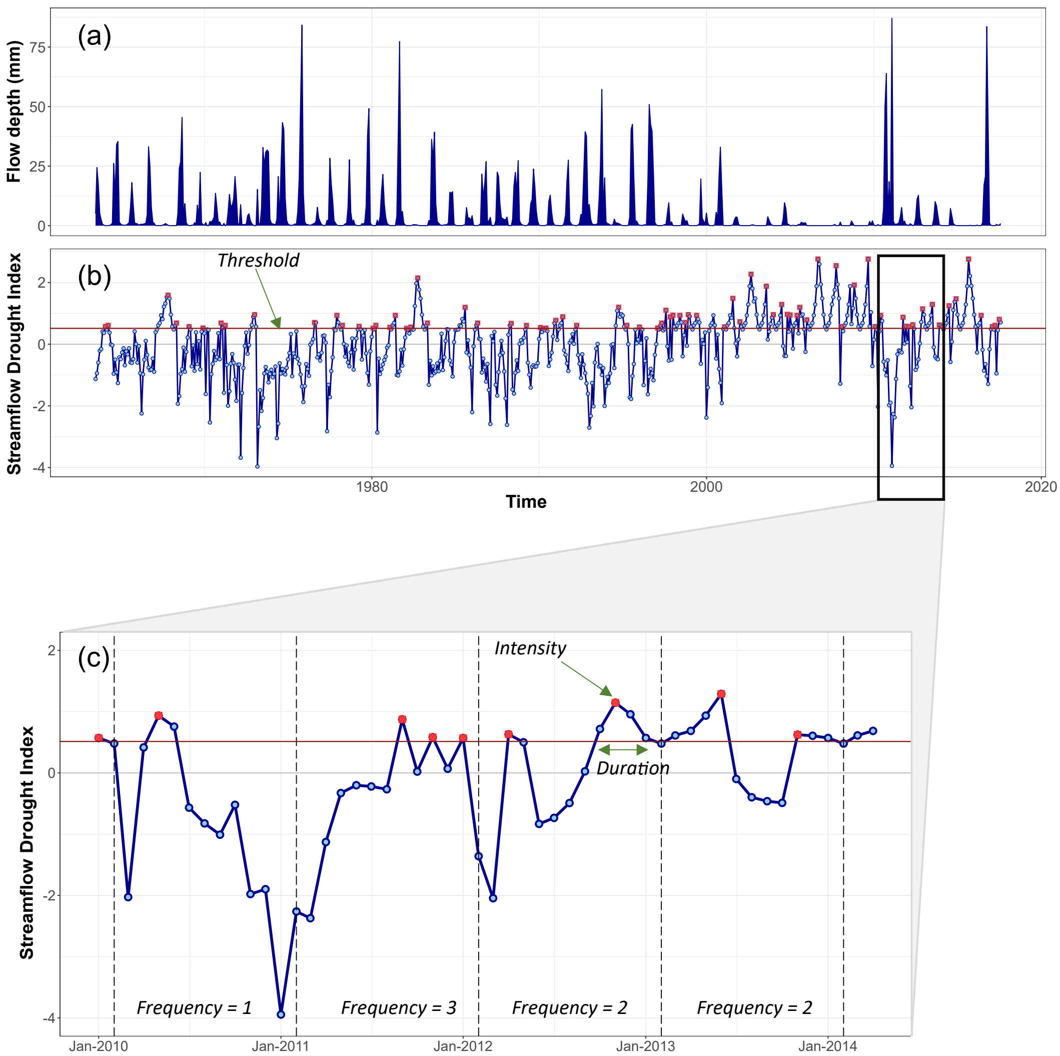

Figure 3: Deriving the intensity, duration, and frequency of low flows. (a) Flow depth (mm) time series for Station ID 407230. (b) Times series of the de-seasonalized (and reversed in sign) flow, termed as the Streamflow Drought Index (SDI), derived from the flow values for the catchment. The threshold is shown by the brown horizontal line at SDI = 0.51 which represents the 65th percentile of the SDI time series for this catchment. Values of SDI lying above the threshold represent low flows. (c) A zoomed window of the SDI series for the years 2010–2013 to illustrate how the IDF are derived from the SDI time series.

where $a_{0,i}$ was a state-dependent parameter allowing for a shift in the catchment's hydrological response, a_1 was a state-independent parameter that links a suitable model covariate to x. In this study, the standardized antecedent precipitation index, sAPI (or the mean annual sAPI for modeling frequency) was used as the covariate responsible for the observed variability in the low flow characteristic (sAPI is discussed in detail in Section 2.3.2). In Equations 4a and 4b, the $sAPI_t$ (or mean annual $sAPI_t$) was taken at the corresponding time instance when the low flow characteristic was observed. The error in this model was defined as a time-invariant state-dependent variance, ${\sigma_i}^2$.

The Markov state $C^{(t)}$ at time t was simulated as:

$$C^{(t)} = Markov\ (\mathbf{\Gamma}) \tag{5}$$

where Γ is the transition matrix. Since the number of extreme states was assumed as two, we, therefore, investigated one- (Γ_1) and two- (Γ_2) state Markov models. The transitioning between any two consecutive states is explained using the schematic in Figure 4a. The two-state matrix Γ_2 can be written as:

$$\Gamma_2 = \begin{vmatrix} p_{11} & p_{12} \\ p_{21} & p_{22} \end{vmatrix} = \begin{vmatrix} p_{11} & 1-p_{11} \\ 1-p_{22} & p_{22} \end{vmatrix} \tag{6}$$

Here, p_{ij} (terms shown in Figure 4a), denotes the probability of the state at t transitioning from $C_i^{(t-1)}$ to $C_j^{(t)}$ (where $i,j \leq 2$), i.e.,:

$$p_{ij} = Pr({C_j}^{(t)} \mid {C_i}^{(t-1)}) \tag{7}$$

Further assuming the HMM is homogeneous (i.e. transition probabilities are time-invariant), $\mathbf{\Gamma}_1$ and $\mathbf{\Gamma}_2$ required the estimation of zero and two transition probabilities, respectively. Additionally, the initial probability of being in each state was defined as follows:

$$\boldsymbol{\delta}_1 = 1 \boldsymbol{\delta}_2 = \begin{vmatrix} \boldsymbol{\delta}_1 \\ \boldsymbol{\delta}_2 \end{vmatrix} = \begin{vmatrix} \boldsymbol{\delta}_1 \\ 1-\boldsymbol{\delta}_1 \end{vmatrix} \tag{8}$$

where $\boldsymbol{\delta}_1$ and $\boldsymbol{\delta}_2$ were the initial probabilities of being in states 1 and 2, respectively.

The probability density in the error model of the HMM was derived using a two-parameter gamma distribution, a log-normal distribution, and a Poisson distribution for the intensity, duration, and frequency of low flows, respectively (Table 1). This was done after testing the capabilities of these respective distributions to satisfactorily represent these characteristics.

The gamma distribution, f_{Gam}, as used for building the HMM for modeling intensity, can be represented as:

$$f_{Gam}\left(x = {}_{obs}x_t;\ k = \frac{{}_t{x_i}^2}{{\sigma_i}^2},\ \theta = \frac{{\sigma_i}^2}{{}_t x_i}\right) = \frac{x^{k-1}e^{-\frac{x}{\theta}}}{\theta^k G(k)} \qquad for\ x, \theta, k > 0 \tag{9}$$

where θ is the scale parameter, k is the shape parameter and $G(k)$ is the gamma function on k. The parameters k and θ were derived to ensure that the mean of the gamma distribution was as defined by Equation 4a, and were obtained by rearrangement of the $Markov\ Mean$, $E[x] = k\theta = {}_t x_i$ and the $Markov\ Variance$, $Var[x] = k\theta^2 = {\sigma_i}^2$. In simple form,

$$k = \frac{(Markov\ Mean)^2}{Markov\ Variance} \tag{10}$$

$$\theta = \frac{Markov\ Variance}{Markov\ Mean} \tag{11}$$

The log-normal distribution, $f_{LogNorm}$, as used for modeling duration can be represented as:

$$f_{LogNorm}\left(x = {}_{obs}x_t; \mu = log\frac{{}_t{x_i}^2}{\sqrt{{\sigma_i}^2 + {}_t{x_i}^2}}; \sigma = \sqrt{log\left\{\frac{{\sigma_i}^2}{{}_t{x_i}^2} + 1\right\}}\ \right) =$$

$$\frac{1}{x\sigma\sqrt{2\pi}} exp\frac{-(log\ x - \mu)^2}{2\sigma^2}, \qquad for\ x > 0 \tag{12}$$

where μ and σ are the mean and standard deviation of logarithmic values of x and were related to the $Markov\ Mean$, $E[x]$, and $Markov\ Variance$, $Var[x]$, as:

$$\mu = log\frac{(Markov\ Mean)^2}{\sqrt{Markov\ Variance + (Markov\ Mean)^2}} \tag{13}$$

$$\sigma = \sqrt{log\left\{\frac{Markov\ Variance}{(Markov\ Mean)^2} + 1\right\}} \tag{14}$$

The Poisson distribution, f_{Pois}, as used for modeling frequency can be represented as

$$f_{Pois}\left(x = {}_{obs}x_t;\ \lambda = \sigma_i^2\right) = \frac{\lambda^x e^{-\lambda}}{x!} \qquad for\ x \geq 0\ and\ \lambda > 0 \tag{15}$$

where λ, the mean parameter of the Poisson distribution, was arrived at using

$$\lambda = Markov\ Mean \tag{16}$$

The parameters of the HMM were arrived at using a constrained maximum likelihood estimation. The details of the calibration process are presented in Text S3 in Supporting Information S1. To arrive at the most probable sequence of states from all possible combinations of sequences for the given observation sequence of intensity/duration/frequency (I/D/F), an efficient dynamic programming method, called the Viterbi algorithm (Forney, 1973; Zucchini & MacDonald, 2009) was used. This algorithm identifies the most probable sequence of states from the Markov Chain of probabilities. The states of I/D/F obtained through this were also referred to as the Viterbi states (named after the algorithm). The algorithm was applied over the entire observation record to identify the most probable sequence of I/D/F states, thereby also identifying any switching, if at all, in the states of the I/D/F.

2.3.2 Covariate Used in the IDF HMMs

For this study, the HMMs of IDF were built using a linear relationship between these low flow characteristics and the available water through precipitation. To represent the available water through precipitation at a catchment, a form of the Antecedent Precipitation Index (API) was used. This serves as a covariate in the HMMs. Similar to the Standardized Precipitation Index (SPI), the API is an empirical index for indirectly estimating how much water is available in the catchment (soil) from precipitation. While SPI is calculated based on a fitted distribution of a moving average of the precipitation time series, API provides a current precipitation water availability indicator employing a constant rate of water depletion from the soil. API estimates the current water available in the soil by multiplying API at the previous time step by a depletion factor and adding the previous time step's precipitation. The definition of API as used in the present work is partly adapted from studies like Kohler and Linsley (1951); Crow et al. (2005); Y. Y. Liu et al. (2011); Holmes et al. (2017), where this index has been used for determining drought conditions and for other watershed analysis. API is a simplified water balance model built on the assumption that the amount of available water in a catchment is related to its antecedent precipitation conditions.

We computed the API at monthly time steps, multiplying the index from the previous month by the depletion rate (γ) and adding the current monthly precipitation as shown below:

$$API_t = min\left(\gamma_n API_{t-1} + 0.75P_t,\ API_{max,n}\right) \tag{17}$$

with the API at the first time step calculated as:

$$API_{(t=1)} = 0.75P_{(t=1)} \tag{18}$$

API_t and $API_{(t-1)}$ are the current and previous month's API, with γ modulating API_{t-1}, and P_t is the current month's precipitation depth. The multiplicative factor of 0.75 to P_t was used to account for the loss of precipitation water while reaching the soil (interception). Since API is representative of the amount of available water in the soil, it was capped to a maximum value ($API_{max,n}$) to indicate full saturation (Dharssi et al., 2017; Holmes et al., 2017) at a given catchment n. The value of $API_{max,n}$ was varied in proportion to the mean of all monthly precipitation values at that catchment, $\overline{P_n}$, as shown in Equation 19. The value of the multiplicative factor ϕ_n in Equation 19 indicates the proportion of maximum monthly water that the soil can hold to the average precipitation at the station.

$$API_{max,n} = \phi_n.\overline{P_n} \qquad \phi_n \in [4, 10] \tag{19}$$

The parameters γ and ϕ as used in Equations 17 and 19, respectively, are meant to simplify the complex mechanisms controlling water availability from precipitation at a catchment. They incorporate the dynamic range and variability of the actual daily API values that get reflected as monthly aggregated values. The values of ϕ and that of γ at a given catchment were chosen by running a simple optimization experiment for each catchment individually instead of assuming a single constant value for them uniformly across the study region. This was done as these parameters have a considerably large spatial variation due to several factors, including soil type, soil density, vegetation, exposure, hill slope, etc.

The optimization was aimed at yielding such values of these parameters that maximized the correlation between the low flow intensities at a catchment and the standardized time series of the catchment's API (sAPI). This allowed a maximum transfer of information in form of linear dependence from precipitation (through sAPI) to low flow intensity, assuming the latter was a response of the former. The range of the multiplicative factor ϕ was set to vary from 4 to 10 with increments of 1 while that of γ was varied from 0 to 0.99 with increments of 0.01. Since API as defined above is a measure of dryness or wetness of the soil in response to the monthly precipitation totals, the API is the soil water memory and is a proxy for the amount of water available from precipitation to contribute to flows. It takes into consideration the concurrent and lagged transfer of information from precipitation to flows (as represented by Equation 17). Further, it was also found that API as used here yielded a more direct relationship with low flow intensities than precipitation or SPI did with low flow intensities (Figure S3, Supporting Information S1). Since the API time series was derived with an inherent assumption that $API = 0$ at $t = 0$, the first twelve values of monthly sAPI were discarded considering those months to be the warming-up period of the API series. In the HMM models of intensity and duration, sAPI was used as a covariate, while for the annual frequency HMM, the mean of annual sAPI was used as the model covariate to be consistent with the timescales. Figure S5a shows the sAPI as obtained for a sample station through the process explained above. Figure S5b shows the established (inverse) relation between SDI and sAPI over time for a sample station. The sAPI closely mimics the SDI, thus supporting the use of sAPI as a predictor in the HMM.

2.3.3 Configurations of One-state and Two-state IDF Models

For modeling low flow intensity, a monthly HMM was built with gamma distribution as the error distribution model. The intensity data at a catchment was modeled using the corresponding value of the sAPI occurring at the same point in time. For any given catchment, two models were built — a one-state model and a two-state model. The mean and standard deviation of the two-state model were allowed to vary as shown in Table 1. While the mean was a function of the covariate as well as the state, the variance was varied only with the state and not with time. Similarly, for modeling duration, a monthly HMM was built with a log-normal distribution as the error distribution model. The duration data at a catchment was modeled using the corresponding value of the sAPI occurring at the same point of time as the intensity (peak) of the low flow spell. For modeling low flow frequency, the total count of all low flow events that took place in a streamflow water year was used. Annual HMMs were built with Poisson distribution as the error distribution model and the mean annual sAPI was used as a covariate.

Table 1 shows the model configurations for the one-state and two-state HMMs of the IDF. By employing such a framework, the cumulative probability of IDF was time-varying because of the non-stationary mean and standard deviation. Note that in the interests of parsimony, HMMs built here did not consider state changes for the parameter a_1 (Equations 4a and 4b).

Table 1: Configurations of the IDF HMMs

Low flow characteristic	Covariate used	Error distribution model (ε)	Model configuration
Intensity (I)	sAPI	Gamma	$\widehat{{}_tI_i} = a_{0,i} + a_1.(sAPI)_t$ ${}_tI_i \sim Gam(\widehat{{}_tI_i}, {\sigma_i}^2 \mid i)$
Duration (D)	sAPI	Log-normal	$\widehat{{}_tD_i} = a_{0,i} + a_1.(sAPI)_t$ ${}_tD_i \sim LogNorm(\widehat{{}_tD_i}, {\sigma_i}^2 \mid i)$
Frequency (F)	Mean Annual sAPI	Poisson	$\widehat{{}_tF_i} = a_{0,i} + a_1.(Mean\ Annual\ sAPI)_t$ ${}_tF_i \sim Pois(\widehat{{}_tF_i}, {\sigma_i}^2 \mid i)$

Ranges: $a_0 \in [-50,\ 50]$; $a_1 \in [-5,\ 5]$; $\sigma \in [1e-7,\ 35]$
The subscript i denotes the state index and can take values 1 or 2.
σ_i denotes the standard deviation of the error model in state i

2.3.4 Assigning of Viterbi States

Figure 4 depicts the possible Markov state transitions considered for the analysis here. As mentioned before in Section 2.3.1, it was assumed that the maximum number of states a given low flow characteristic's time series can take are only two, viz., normal and non-normal (Figure 4a). For illustration, Figure 4b shows the possible model outcomes of applying the framework on the intensities of low flows, where the three panels represent the time sequence of the Viterbi states taken under each of the outcomes. It may be noted that since we are modeling extreme characteristics of low flows, both states represent regimes of extremes. Thus, the normal state of the regime of an extreme implies a state when values of I/D/F of low flow droughts given the history of the region may be considered usual or not unexpected. In simple words, the normal state of low flow I/D/F as defined in the study here corresponds to low flow droughts that could be an outcome of a seasonal fluctuation resulting in flow conditions that, while still considered extreme, are within the statistical likelihood of an expected low flow drought condition for the region. The non-normal state, on the other hand, can either be less extreme than normal low flows or more extreme than normal low flows. However, both cannot co-occur for the time series of I/D/F for a given catchment, following the assumption that the maximum number of states allowed is 2. While modeling each of the IDF, we assigned states by assuming that the time stamp that had the value of the covariate (sAPI for intensity and duration; mean annual sAPI for frequency) closest to the median value of the covariate for a catchment was the time when the given I/D/F value was in a normal state. A two-state model of HMM would have either 'high' and 'normal' states or 'low' and 'normal' states (Figure 4a). The HMM built here classified an observation to be in a high state if the 50th percentile of the Viterbi I/D/F value simulated at a given point in time was more/higher than the 50th percentile of the normal state I/D/F value. An observation was classified to be in a low state if the 50th percentile of the Viterbi I/D/F value simulated at a given point in time was less than the 50th percentile of the normal state I/D/F value.

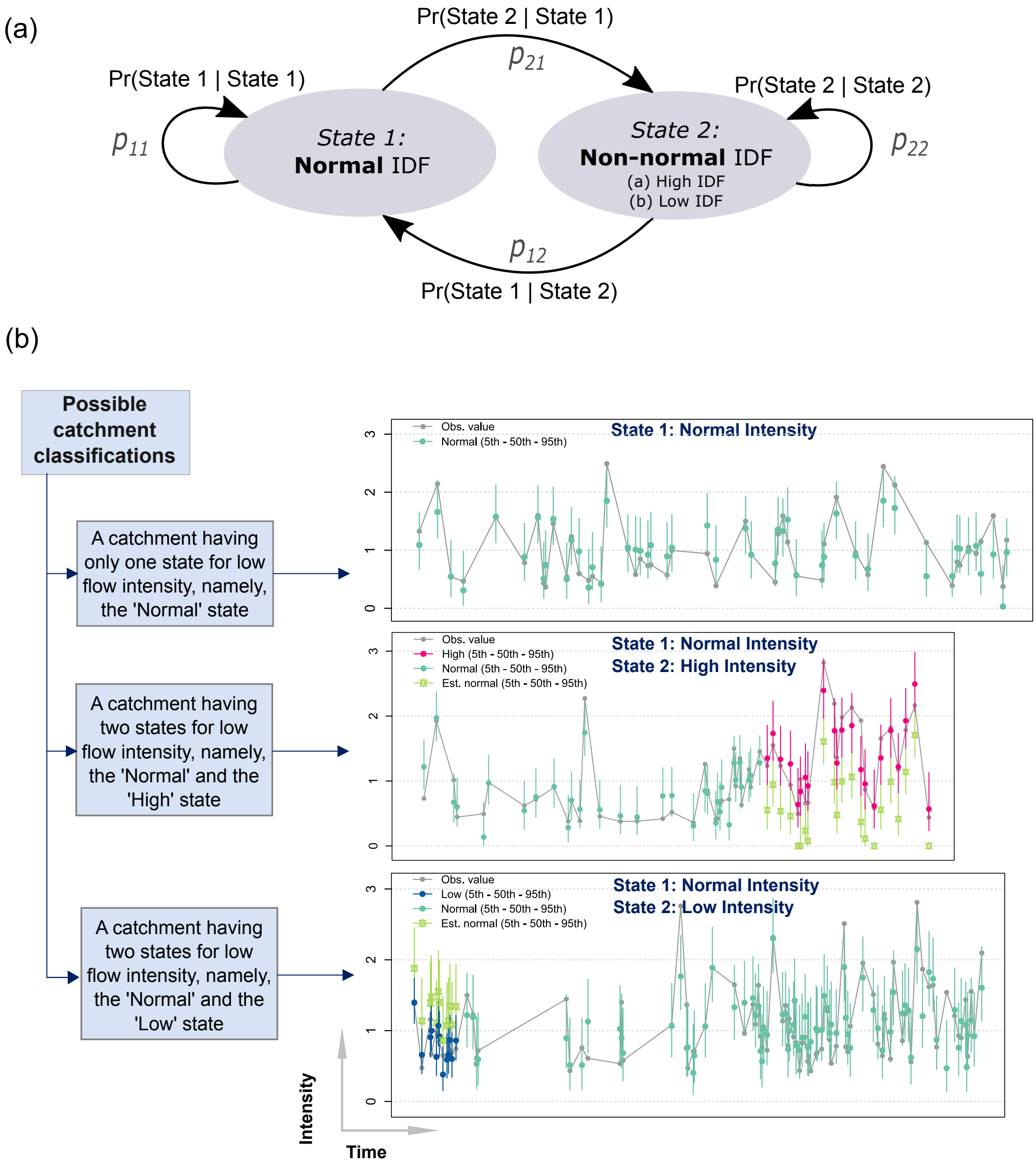

Figure 4: (a) Depiction of Markov state transitions in the applied HMM framework. Each state can either continue to sustain or switch to the other state. (b) The three possible outcomes from applying the proposed HMM to a low flow characteristic. For illustration, the time series of the intensity of low flows is used to demonstrate the possible results from applying the model. The top panel shows a catchment where the intensity only has one state. The middle panel shows a catchment where the intensity has two states, with the second state (the high state) representing more intense low flows. The bottom panel shows a catchment where the intensity has two states, with the second state (the low state) representing less intense low flows.

2.4 Identifying Catchments With Two States in IDF

The flowchart in Figure 5 summarizes the overall flow of the methodology pertaining to the analysis carried out. Following the steps as laid out in Figure 5, to decide the best model for a given characteristic at a catchment, the Akaike Information Criterion (AIC) was used. This is expressed as

$$AIC = -2ln(\mathscr{L}) + 2N \tag{20}$$

where N is the number of model parameters being estimated and $\mathscr{L}$ is the maximized likelihood of the model (expressed in Equation 3 in Supporting Information S1). Among the two models tested, i.e., the best one-state and the best two-state model, the one that had the lowest AIC was chosen for the catchment. Following the use of the AIC criterion, a catchment was identified as having two states in I/D/F if the best model at the catchment had: (a) observations belonging to a normal state and some to a low I/D/F state or (b) observations belonging to a normal state and some to a high I/D/F state as depicted in Figure 4b and as stated in the steps in Figure 5. In the present context of low flows, higher values of a low flow characteristic indicate a more extreme low flow event.

At catchments where, for a given low flow characteristic, the two-state model was the better model, the strength of simulation of the two-state model over the one-state model was established using the evidence ratio (ER) (Burnham & Anderson, 2002). The evidence ratio offers a way to quantify the strength of the evidence that the selected model (the two-state HMM in this case) is convincingly superior to the alternative model (the one-state HMM). It was computed by comparing the Akaike weights, w, of the two competing models, namely, the two-state model (2SM) and the one-state model (1SM), as expressed below:

$$ER = \frac{w_{2SM}}{w_{1SM}} \tag{21}$$

Here w_{1SM} and w_{2SM} are the Akaike weights for the one-state and two-state models, respectively, and are defined as:

$$w_{2SM} = \frac{1}{1 + exp(-\frac{1}{2}\Delta)} \tag{22}$$

$$w_{1SM} = \frac{exp(-\frac{1}{2}\Delta)}{1 + exp(-\frac{1}{2}\Delta)} \tag{23}$$

where Δ in this case is the AIC difference between the best one-state model and the best two-state model:

$$\Delta = AIC_{1SM} - AIC_{2SM} \tag{24}$$

The ER value serves to establish confidence in the two-state model relative to the one-state model, and hence the strength of evidence for the existence of two states. Any ER value > 10 suggests that the observations are more likely to be explained by the two-state model than the one-state model. The higher this value, the stronger the evidence. For the current work, we considered ER values greater than 10 (or its logarithmic values greater than 1) as denoting sufficient evidence to believe that a two-state model is convincingly better in performance over the one-state model, following Burnham and Anderson (2002); Goswami et al. (2022). The ER, however, only denotes how good the two-state model is relative to the one-state model and does not provide sufficient information on how qualified the two-state model is to represent the low flow characteristic being modeled. To address the later aspect, the model residuals were tested for their normality using the Shapiro-Wilk's test ($alpha = 0.05$) (Shapiro & Wilk, 1965) and were retained for further analysis only if their Shapiro-Wilk's test p-value was greater than 0.05. In addition, the aim was also to have a 2SM with at least a predefined minimum number of I/D/F values in each state to ensure that a meaningful state does indeed exists. For this, catchments that had less than five I/D/F data points in any state were removed for further analysis. To make sure the

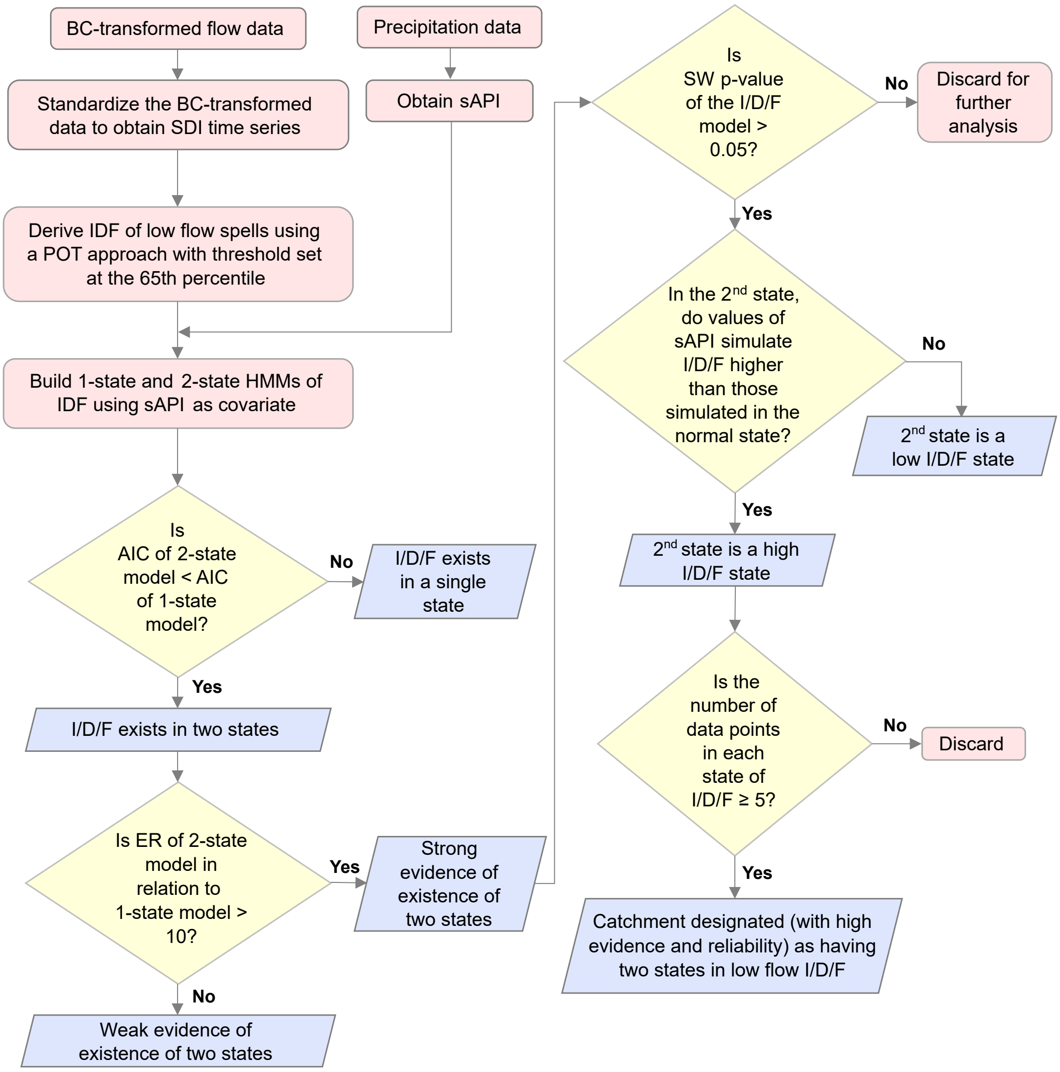

BC: Box-Cox; SDI: Streamflow Drought Index; I/D/F: Intensity/ Duration/ Frequency; POT: Peak Over Threshold; SW: Shapiro Wilk; sAPI: Standardized Antecedent Precipitation Index; HMMs: Hidden Markov Models; AIC: Akaike Information Criterion; ER: Evidence Ratio

Figure 5: Flowchart illustrating the main steps followed to identify if a catchment has two states in low flow I/D/F.

best model performed adequately, we also inspected the number of significant lags in the Auto-Correlation Function (ACF) of the normal pseudo-residuals, the histogram, and the Q-Q plot of the normal pseudo-residuals (Zucchini & MacDonald, 2009). The ACF serves as a visual check to confirm whether the model residuals are serially correlated or not. Serially correlated errors indicate that the model is not adequately built and there is loss of some information, thereby indicating that the model could be improved further.

3 Results and Discussion

3.1 States of Low Flow IDF

Figure 6 shows the low flow intensity Viterbi states over time for an example catchment, with Figure 6a showing the variation of the model covariate, i.e., sAPI. The results in Figure 6b shows that two states were identified, whereby the catchment was in a normal state until 1999, after which it switched to and persisted in a high intensity state. Furthermore, the conditional state probabilities (in Figure 6c) show that there is a very high probability of the aforementioned states. Practically, this indicates that low flow periods become more intense (i.e. drier) after 1999. This is illustrated in Figure 6b by the estimated normal values of intensity (points in lime green). These are the model-estimated values that indicate what would have been the intensity had the catchment been in the normal state at that epoch. These are the model-estimated values that indicate what would have been the intensity had the catchment been in the normal state at that epoch. These are determined using the relationship of intensity with the covariate as in the normal state (Equation 4a, with $i = 1$). For the epochs when the catchment is found to have switched into the second state, the results from Figure 6 suggest that the intensity for a given value of covariate is much higher than what it would have been expected had the catchment been in the normal state. Here the intensity HMM not only distinguishes the two states of low flow intensity but also informs the timing of the shifts in its states. Importantly, Figure 6 demonstrates that despite the inclusion of a covariate, the observed low flow intensity is best explained using more than one distribution. That is, the catchment not only displays non-stationarity arising from the precipitation (Figure 6a) but also from the state shifting. This provides preliminary evidence toward falsifying that one state is sufficient to explain low flow intensities.

Figure 6c shows the conditional probability of being in a given state at any given time for the catchment. It reflects the switching of the catchment between the two states. The catchment is believed to have switched to the other state when the state probability of the other state becomes greater than that of the state in which the catchment is currently in. Such a behavior as shown in Figure 6 suggests that hydrological droughts are becoming more extreme in the catchment, with the catchment continuing to be in an amplified extreme state until the end of the observation period. The two states as seen in Figure 6b are defined by two different distributions, supporting the notion of the need for state-dependent distributions. Thus, the observed intensity can lie in two states, shown by the green and pink color points. The second state represents more extreme low flow intensity than those represented by the normal low flow state. It must be noted here that the data represented by both states are extreme values, i.e. values pertaining to low flow droughts. The second state here refers to a more intensified extreme state, suggesting an amplification of extremes (low flow events here) in such catchments. The existence of mixture distribution as emerging from the outcomes in Figure 6 could mean that the observations in the two states are generated from separate flow processes or flow dynamics unique to the states and which are not explained by the variability in water availability from precipitation alone. These dynamics may be arising from real physical attributes, such as changes in baseflow. It is thus likely that the more intense low flows may be caused by less baseflow during such periods. Another factor that could be in play is systematic changes in groundwater levels. However, all these need further investigation.

For intensity data, it was found that the model satisfactorily simulates the values except for only a few instances in time where it misses estimating very high values of intensity accurately. However, most of the observations lie within the 95% confidence interval of the model. Considering this and the fact that modeling extreme values adequately is a challenge for any modeling framework, for the primary question being addressed in this work, the HMM framework proved to be a suitable technique for investigating changing regimes of extremes. Corresponding to Figure 6, Figure S4 in Supporting Information S1 provides an assessment of the model performance for the intensity HMM of the catchment in terms of the distribution of the normal pseudo-residuals and their autocorrelation. With the present ability of the HMM, the framework performs well in simulating low flow intensity data. The model residuals were found to be normally distributed along with the Shapiro-Wilk p-value being more than 0.05. This implies that the model residuals have very little information contained in them and they can be considered to be nearly random, suggesting a good match between the modeled values and the observations. A model having Shapiro-

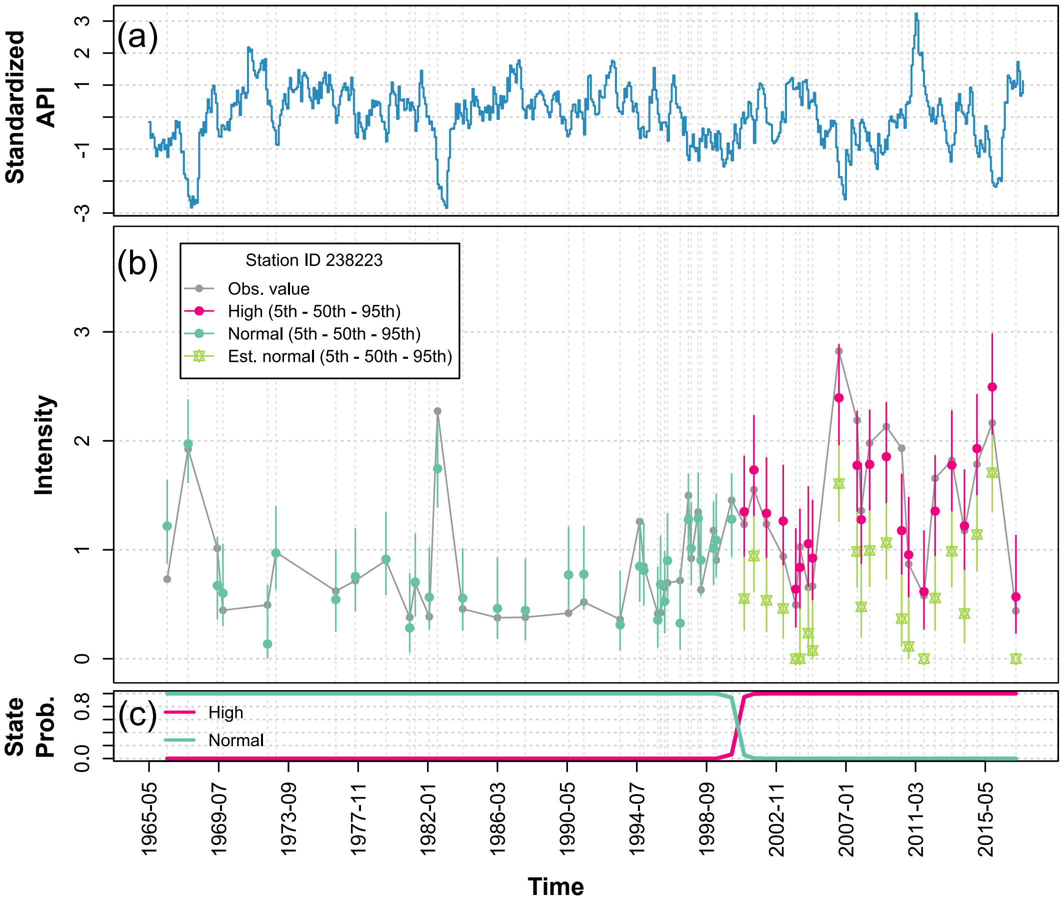

Figure 6: Viterbi states taken by the low flow intensity over time for station ID 238223. (a) The catchment's monthly variation of the sAPI, which is used as a covariate in the intensity model. (b) Time series of low flow intensity of the catchment. The green-colored circles indicate modeled values that belong to the normal state. Pink-colored circles indicate values belonging to the second state (more extreme than normal state). The lime green stars occurring in the same vertical spaces as that of the pink circles indicate the model-established value of intensity in the normal state at that time step. At any given time, the colored circles (or stars) represent the median value of the intensity. The colored vertical lines associated with each of these represent the error bar covering the 5th to the 95th percentile of the estimates. The gray-colored circles denote the observed intensities. (c) Variation of state conditional probability depicting the probability of intensity being in a given state at any given time. Clearly, a single state is not sufficient to describe the intensity data at this catchment.

Wilk's p-value greater than 0.05 suggests A similar inference holds for the ACF plot where there are not many lags that are significant, indicating that the model errors have very low predictive power.

Figure 7 shows the low flow duration results for a different example catchment. Although the outcomes from AIC showed that the duration data was better described by a 2SM than a 1SM, Figure 7b suggests that the duration modeling as undertaken in the current framework has a scope for improvement. As can be seen in Figure 7b, the median duration in a given state at each time point shows very little variability, which casts doubt on sAPI being an appropriate covariate for duration. Figure 8 shows the model simulation of annual frequency for a sample catchment. Figure 8a shows the corresponding time series of mean annual sAPI, which is the covariate to the frequency model. For the sample catchment, all the values lie in a single state (the normal state) as can be seen from Figure 8b. Hence a single state does a better job of explaining the frequency data than two states in this case. However, the simulated frequency values following the modeling as done here resulted in large error bars associated with the modeled values, implying that the frequency model too, like the duration model, may be further improved. Figures S5 and S6 in Supporting Information S1 provide assessments of model residual behavior corresponding to the duration and frequency HMM results discussed in Figures 7 and 8, respectively.

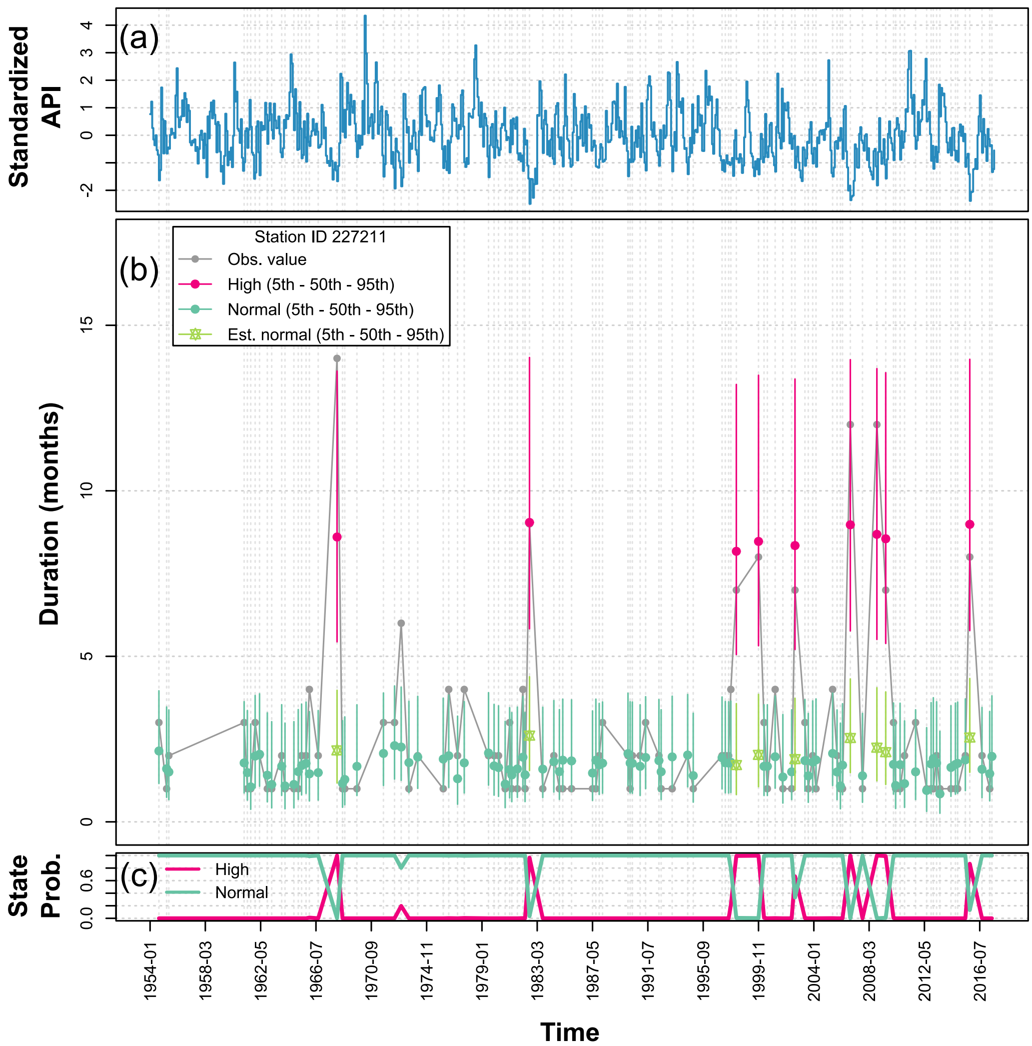

Figure 7: Viterbi states taken by the low flow duration over time for station ID 227211. See Figure 6 for a description of the figure elements.

As pointed out above, the current approach for modeling duration and frequency in the HMM framework needs improvement. Time series simulation of duration and frequency thus remains a challenge. The IDF HMMs as used here are built upon the linear dependence between sAPI and the low flow characteristic being modeled (Equation 4a and 4b). Thus, the results suggest that the sAPI's relation with duration and frequency is either non-linear, or an alternate covariate should be sought. For example, sAPI at a fortnightly or daily scale

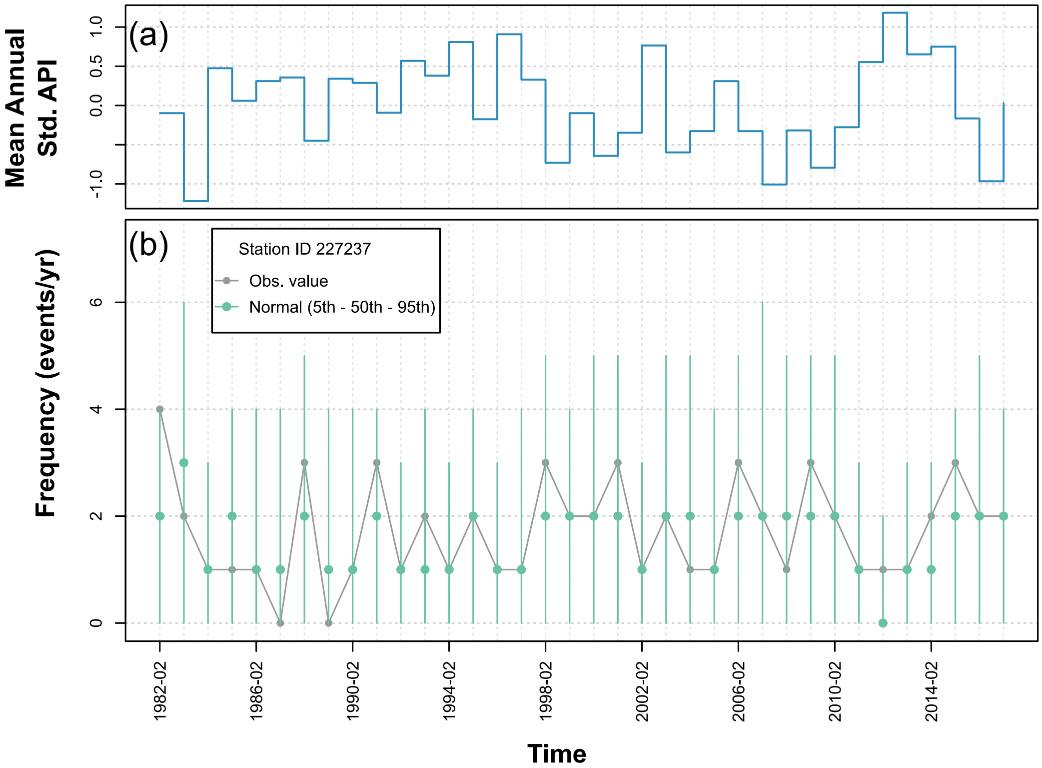

Figure 8: Variation of low flow annual frequency values with time for station ID 227237. (a) Catchment's mean annual sAPI which is used as a covariate in the frequency model. (b) Time series of the observed and simulated frequency. Only a single state was sufficient to describe the frequency data at this catchment.

than monthly may be a better predictor for duration, and seasonal mean sAPI instead of annual mean sAPI may work better for modeling low flow frequency. Another possibility could be understanding and establishing which physical covariate, if not sAPI, governs the variability in these characteristics and may potentially replace sAPI in these models.

For the reasons stated above, following this section, we focus primarily on presenting and discussing the results for low flow intensities, with only a brief discussion about duration and frequency.

3.2 Catchments with Two States in IDF

As depicted in the steps in Figure 5 and as discussed under Section 2.4, the candidate models at a catchment were screened for AIC and ER. Figure 9a shows the spatial distribution of catchments obtained after screening for AIC of 2SM < AIC of 1SM, and log(ER) > 1 for the intensity model over the study region. A total of 115 (71%) catchments (purple-colored) showed strong evidence of the existence of two states in the intensity of low flows. This suggests that low flow intensity extremes are a mixed process and hence warrant a mixture of distributions to represent them. Such results provide formal strength of evidence for the hypotheses that extremes can quantitatively shift to different states if perturbed and hence a single state cannot adequately explain them.

The 115 catchments as identified in Figure 9a were further screened for model performance based on the Shapiro-Wilk p-value for normality of the residuals. The number of catchments

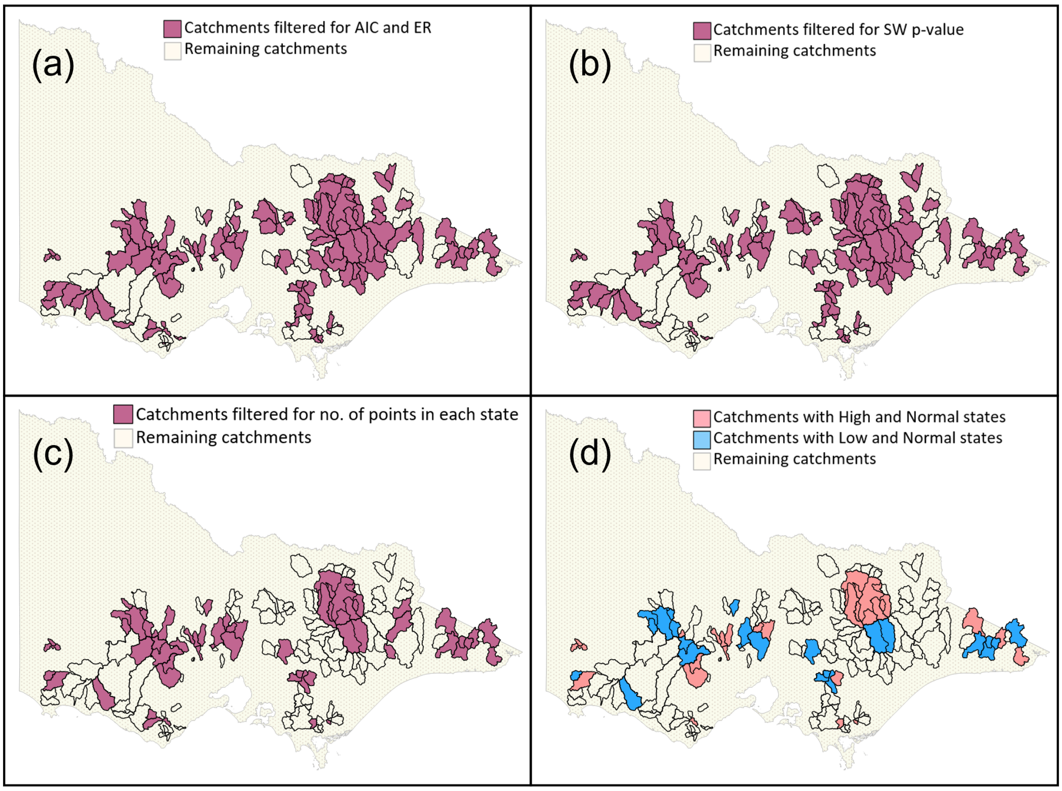

Figure 9: Spatial distribution of catchments having two states in low flow intensities. Figures a–d show the two-state catchments retained on subsequent steps of filtering. (a) The 115 catchments (colored in purple) having AIC of 2SM < AIC of 1SM and log(ER)>1 for 2SM over 1SM. (b) The 101 catchments (colored in purple) having Shapiro-Wilk p-value>0.05. (c) The 34 catchments (colored in purple) which had at least 5 intensity data points in each state (and hence at least 5 unique low flow spells in each regime). (d) Of the 34 catchments, the 21 catchments that have normal and high intensity states shown in a shade of red. For these catchments, the second state is a high intensity state. Of the 34 catchments, the 13 catchments that have normal and low intensity states shown in blue. The second state for these 13 catchments is a low intensity state.

that indicate high evidence for 2SM over 1SM provides provides support for the hypothesis that low flow extremes might switch states. 101 of these 115 satisfied the condition of Shapiro-Wilk p-value>0.05. These are shown further in Figure 9b (colored in purple). Further, to ensure a meaningful state exists, these 101 catchments were also checked for having the number of data points in each state more than or equal to 5. This condition ensured that such a catchment will have at least 5 unique low flow spells in both, normal and non-normal, regimes. Figure 9c shows the final 34 catchments meeting these criteria. Of these 34 catchments, there were catchments where the second state (the non-normal state) pointed to a low intensity state (shown in blue in Figure 9d) and catchments where the second state was a high intensity state (shown in a shade of red in Figure 9d).

The high spatial variability shown in Figure 9d is unexpected. It may be due to catchment-specific biophysical factors (combination of one or more of the slope, mean elevation, soil types, climate, vegetation, etc.) and hydrologic response to extremes emerging from the complex interactions of vegetation and soil hydraulics, making low flows, at least in the case of the SEA region, somewhat heterogeneous in space. The tendency to switch or to exhibit resilience against switching may thus possibly be controlled by a combination of topography, climatic factors, soils, and vegetation. Catchments having the second state as high state are likely to switch from a normal low flow state to a more extreme low flow state characterized by higher than usual values of low flow intensities, entailing a magnification of low flows. Further, since proxy information from precipitation and soil moisture was already provided in the form of sAPI for modeling the low flow intensities, the emergence of a two-state model with very high evidence and model reliability at as many as 34 catchments (Figure 9) suggests that not all observations can be explained by the precipitation data. Thus, extremes in low flows may not be sufficiently explained by changes in precipitation.

Figure 10 follows a similar basis as Figure 9, showing the catchments retained at every stage of filtering. Using AIC and ER values as the filtering criteria, a total of 112 (Figure 10a) out of 161 catchments showed a 2SM to be superior to 1SM in modeling low flow duration data. The 5 red shaded catchments in Figure 10d represent catchments as obtained after all the steps of performance filtering. For these, the second state of low flow duration was associated with higher values of duration. There is a good overlap of catchments having high evidence for exhibiting two states in intensity as well as in duration as can be seen from Figures 9a and 10a. The spatial differences, however, grow as one moves from subplots a–d in these figures. As per the AIC and ER criteria, of the 161 catchments, the number of catchments having two states in (1) only intensity (but not duration) were 30, (2) only duration (but not intensity) were 27, and (3) both intensity and duration were 85.

Unlike intensity and duration, annual frequency of the low flow events, on the other hand, did not exhibit switching of states for the way the framework models this characteristic. Of the catchments studied, only one catchment emerged where the 2SM was better than 1SM. Since for frequency of low flows, the number of catchments satisfying the AIC and ER criteria was not sufficient, the figure for the spatial distribution of 2SM catchments of frequency is not included here.

For several of the SEA catchments, the existence of multiple states of extremes is a recent phenomenon. The exact reasons that drive the switching of states of low flows still need to be explored. The answer may come with improved knowledge of the underlying systemic processes governing these and their complex feedbacks to one another. The results here provide evidence for low flow state transitions in these catchments and the changing regimes of hydrological extremes (low flow droughts). The intensities in the 'high' state represent unusual low flow droughts induced possibly from a hydrological disturbance which sets a positive feedback for the catchment's extreme characteristics to slip into the second state, as has been concluded to be the case for total flows by Peterson et al. (2021). Such a hydrological disturbance could be from catchment-wide changes, which control the runoff, changing the partitioning of the incoming precipitation at the surface between infiltration and surface runoff. This disturbance may be brought about by prolonged meteorological droughts and natural factors. Studies have also suggested groundwater storage (Fowler et al., 2020; Hughes et al., 2012; Kinal & Stoneman, 2012) and plant water use (Peterson et al., 2021; Ukkola et al., 2016) as causal factors, with the latter producing a positive feedback and hence persistent alternate states. Long hydrological memory linked with stored groundwater may also be an important facet (Alvarez-Garreton et al., 2021), which makes the current flow volumes to be governed more strongly by antecedent conditions. In such cases, the subsurface storages carried forward in time are often capable of equalizing the deficiencies in precipitation during the onset of a drought (Avanzi et al., 2020). Anomalously low streamflows have also been implicated in changes in the seasonality of climate conditions (both atmospheric and precipitation demands) (Williams et al., 2022). However, all this demands further research to draw more detailed conclusions around the drivers for the switch, including how feedbacks from the catchment's biophysical components may be affecting water partitioning (e.g., Peterson, Western, & Argent, 2014) and the triggers from global climate shifts.

Apart from natural controls on flows, low flows can vary as a response to human controls on flows as well (Gebremicael et al., 2013; Guzha et al., 2018). Studies have shown that

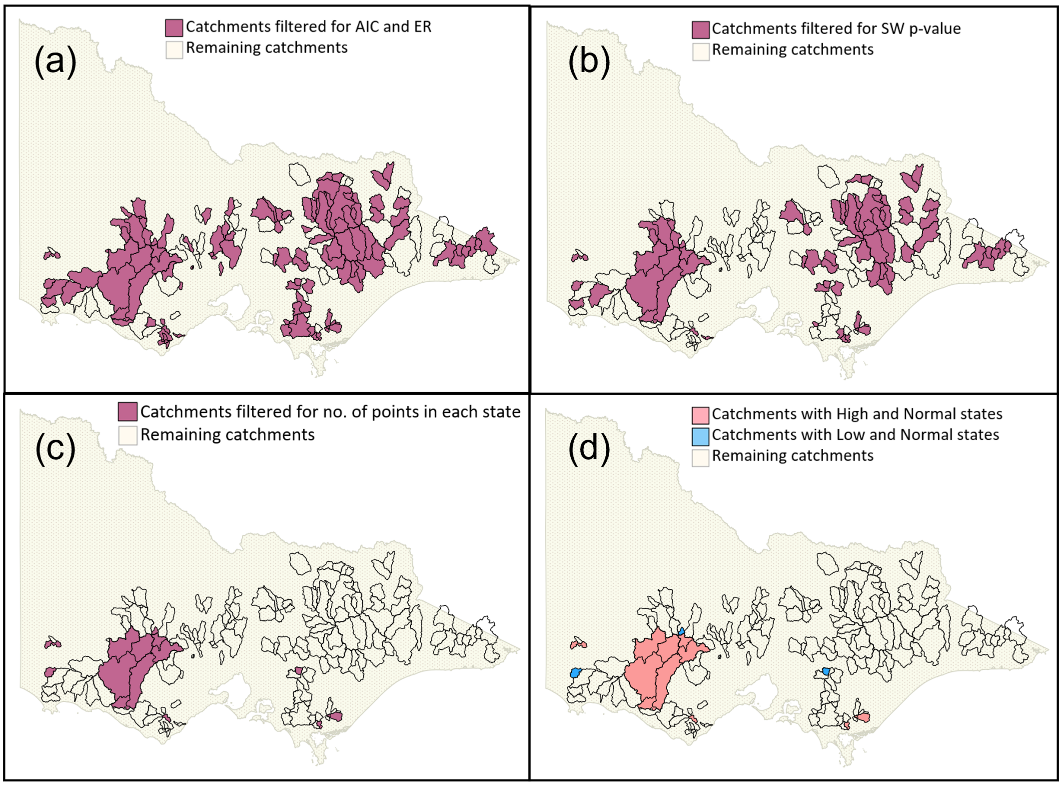

Figure 10: Same as Figure 9 but for duration of low flows. Figures a–d show the two-state catchments retained on subsequent steps of filtering. (a) The 112 catchments (colored in purple) having AIC of 2SM < AIC of 1SM and log(ER)>1 for 2SM over 1SM. (b) The 63 catchments (colored in purple) having Shapiro-Wilk p-value>0.05. (c) The 34 catchments (colored in purple) which had at least 5 duration data points in each state. (d) Of the 8 catchments, the 5 catchments that have normal and high duration states shown in a shade of red. For these catchments, the second state is a high duration state. Of the 34 catchments, the 3 catchments that have normal and low duration states shown in blue. The second state for these 3 catchments is a low duration state.

human activities such as water abstraction interventions and land use/cover change, such as fire/non-fire induced vegetation changes, can modify low flows in a catchment (Li et al., 2007; Chang et al., 2016; Gebremicael et al., 2020) as these activities may change the partitioning of the incoming precipitation on the land surface (Gates et al., 2011). In the case of the present study, the 161 SEA catchments were unregulated and had water extractions <10% of the mean annual runoff. Effects from land use change may be a driver responsible for switching of states of extremes. However, for these catchments, Peterson et al. (2021) (in their Supplementary Material) show that land use change (1985-2019) did not explain the observed runoff state shifts. The switching of states of low flows as found in this study is thus more likely an outcome of changes in the hydroclimate of the region or the response of a catchment to these or both.

3.3 Low Flow Intensity State Changes and Atmospheric Conditions

Extreme dry and warm conditions of the atmosphere may be one of the drivers of low flow switching. To examine this, a timeline of the 21 catchments identified to be switching between a normal intensity state and a high intensity state was studied. Figure 11a shows the number of catchments, of the 21 catchments, existing in their second state of low flow intensity for the time period 1950–2016. The height of the vertical black-colored bars indicates the number of catchments experiencing a low flow intensity lying in the second state at a given time. The gaps in between the bars represent a time instance when either none of those catchments had a low flow intensity (peak) occurrence or when there is a low flow intensity (peak) occurrence, but it belongs to the normal state. The height of the yellow bar at each month depicts the number of catchments that had gauge flow data available. The recent meteorological drought periods in the state of Victoria (Australian Bureau of Statistics, Year Book Australia 1998) were: (i) 1967–1968, (ii) 1972–1973, and (iii) 1982–1983. Combined with the Millennium Drought (1997-2009), these 4 periods denote abnormally dry periods over SEA on record. These are shown as gray-colored vertical strips in Figure 11a. These periods appear to coincide with peaks in the number of catchments in the second state of low flow intensity.

Also shown in Figure 11 are the periods of abnormally high sea surface temperature anomalies of the Niño3.4 region, characteristic of an El Niño event (orange vertical bars). These were derived from the Ocean Niño Index (ONI) obtained from the United States National Oceanic and Atmospheric Administration (NOAA) Climate Prediction Centre (CPC) (`www.cpc.ncep.noaa.gov`) (Refer Text S5 and Table S3 in Supporting Information S1 for details). It was also seen that many catchments switched to the second state during the warm episodes of the El Niño Southern Oscillation. However, the number of these catchments is comparable to those belonging to neither the meteorological drought nor the El Niño periods for the present study (Figure 11b and c). Figure 11 suggests that warm and dry atmospheric conditions such as those prevailing during sustained meteorological drought spells may create conditions conducive for catchments to switch states of low flows.

The boxplots in the lower panel of Figure 11 show the number of catchments in the second state for various periods, namely, periods of meteorological droughts (b), periods of warm ENSO (c), and periods that were neither meteorological droughts nor warm ENSO periods (d). The figure suggests that meteorological droughts have the potential to change low flow spells, adding to the existing literature on how severe and protracted meteorological droughts can potentially destabilize the hydrological behavior and resilience of catchments. With the projected increase (Xu et al., 2019) and changes in future meteorological droughts and the complex interactions between meteorological and hydrological droughts, low flow regimes are more likely to be dynamic and subject to modifications. Importantly, Figure 11 highlights the changing regimes of hydrological extremes in a changing climate. The results in the figure also suggest that the phenomenon of switching of low flow regimes can neither be considered exceptional nor rare any longer. With low flow droughts exhibiting regime-switching, the risks associated with them are also expected to vary in time. As the risk changes, water managers will have to understand how resilient are the catchments to changes in extremes.

4 Conclusions

Catchments can undergo complex changes in their behavior which can change how low flows respond to such changes. The study here examined whether low flow characteristics can exist in more than one state. This was done using HMMs with antecedent precipitation index as a covariate, applied to examine low flow IDF in 161 catchments in SEA. It was found that for the majority of the catchments ($\approx 70\%$), a two-state model explained the low flow intensity and duration data better than a one-state model, thereby suggesting that low flows exhibit multiple states. Very strong evidence of low flow intensity exhibiting two distinct states was found for at least 34 (21%) catchments in the region. For most catchments exhibiting switching of states of low flow intensity, the second state entailed an intensification of low flows. The regime-switching behavior can cause low flows to manifest in very different ways at two different epochs for the same catchment. Such a temporal behavior also points to changing risks associated with hydrological droughts. The two states are possibly governed

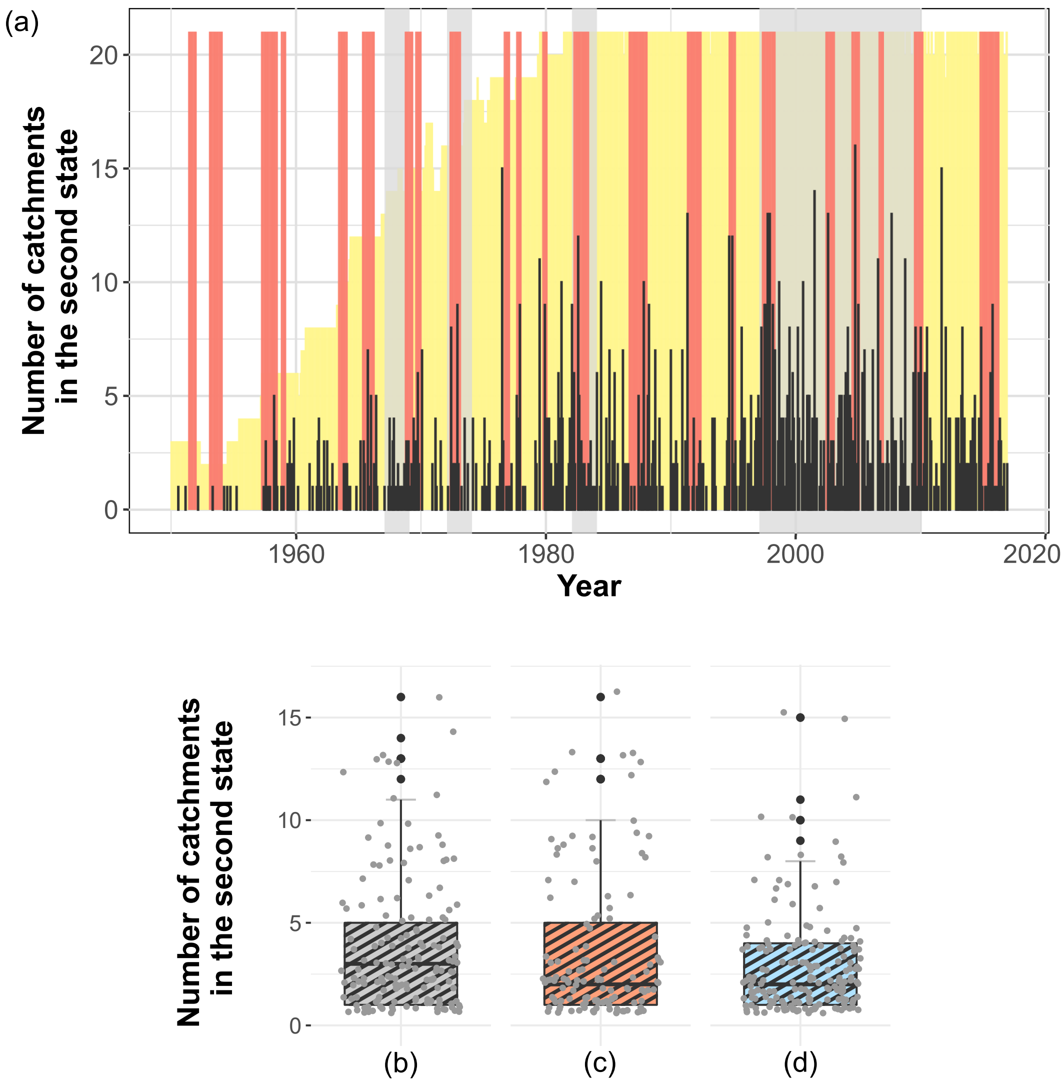

Figure 11: (a) Timeline (1950–2016) of the switching of states of low flow intensity for the 21 catchments. The height of the black-colored bars represents the number of catchments in the second state at a given time. The height of the yellow-colored bars at each month represents how many of these 21 catchments had flow data available for that month. The four gray-colored vertical strips shown in the background represent the four recent severe meteorological drought spells for the Victoria region, which are (i) 1967–1968, (ii) 1972–1973, (iii) 1982–1983, and (iv) 1997-2009, respectively, from left to right. The red-colored vertical strips represent time instances when the ONI indicates the occurrence of a warm ENSO episode. The three boxplots shown in the lower panel depict the number of catchments in the second state during (b) meteorological drought periods, (c) warm ENSO periods, (d) periods that were neither b nor c.

by unique processes generating the observations in the two states. Importantly this indicates that the use of one distribution is inadequate to explain the observed data, as is widely done. The work demonstrates the capability and reliability of HMMs to simulate extreme low flow intensities as well as the capability to capture temporal shifts in states.

Further, since the information from the catchment's antecedent conditions and precipitation was intrinsic to the model, the emergence of a two-state model at a catchment implies that information from precipitation, though useful in simulating low flow behavior, may not be sufficient to explain changes in low flow extremes. Low flow intensities in the second state are not explained by the corresponding variability in precipitation. The duration and frequency HMM have a scope for improvement in the current framework. For frequency of low flows, the current capability of the model framework was not satisfactory for establishing the strength of the 2SM over 1SM. These models may be improved by either incorporating non-linear relation with sAPI or by using covariates (for eg., climate indices) that may explain the variability in them better.

Switching of catchments into an intensified low flow state may be strongly influenced by sustained dry atmospheric conditions such as those during protracted meteorological droughts as well as the changes in them. The study also helps to understand how future extreme hydrological characteristics may behave in response to such meteo-climatological disturbances triggered naturally or due to climate change. This points to possible changes that catchments can undergo during and after a meteorological drought and how that impacts extreme hydrological behavior and response. As dry conditions and meteorological droughts change and become more frequent in a changing climate, their impact on hydrological cycle and on extreme flows can be very significant.

More research needs to be undertaken to understand the underlying physical processes and the driving mechanisms in play to explain the existence of more than one low flow regime, thereby reducing uncertainty about future low flow dynamics in watersheds. The results here demonstrate the potential of catchments to exhibit shifts in regimes of low flow extremes. A crucial aspect of enhancing future water security lies in understanding how these shifts might translate into impacts on streamflow services and how to manage these periods. Identification of shifts may enable system planners to consider solutions such as supply augmentation, demand management, inter-basin water transfers, managed groundwater aquifer recharge, conjunctive use, etc., thereby augmenting system resilience during low flow shifts in the future.

Conflict of Interest

The authors declare no conflicts of interest relevant to this study.

Acknowledgments

The authors acknowledge the IITB-Monash Research Academy for funding P. Goswami with a PhD scholarship to support this research. The authors are thankful to Christopher Pickett-Heaps from the Bureau of Meteorology, Australia, for his constructive comments on the manuscript, adding to its improvement. The authors also thank and acknowledge the developers and contributors of all the R packages that were used for this analysis.

Data Availability Statement

The implementation of the Hidden Markov modeling was carried out in the software environment R (R Core Team, 2021) using the R package "*HydroState*" available at `https://github.com/peterson-tim-j/HydroState`. The streamflow and precipitation data used for this study are available at `https://doi.org/10.5281/zenodo.6412694`. The ONI data was sourced from `https://origin.cpc.ncep.noaa.gov/products/analysis_monitoring/ensostuff/ONI_v5.php`. To aid in the analysis of the current work, R packages such as DEoptim, MASS, extRemes, ggplot2, ggpattern, ggpubr, zoo, dplyr, rgdal, sf, RColorBrewer, ggsn, cowplot, and ggspatial were also used. Developers and contributors of all these packages are acknowledged.

References

Alvarez-Garreton, C., Boisier, J. P., Garreaud, R., Seibert, J., & Vis, M. (2021). Progressive water deficits during multiyear droughts in basins with long hydrological memory in Chile. *Hydrology and Earth System Sciences*, *25*(1), 429–446.

Australian Bureau of Statistics. (Year Book Australia 1998). Canberra, Australia: Australian Government Publishing Service, 1998. *Australia*.

Avanzi, F., Rungee, J., Maurer, T., Bales, R., Ma, Q., Glaser, S., & Conklin, M. (2020). Climate elasticity of evapotranspiration shifts the water balance of Mediterranean climates during multi-year droughts. *Hydrology and Earth System Sciences*, *24*(9), 4317–4337.

Baum, L. E., & Petrie, T. (1966). Statistical inference for probabilistic functions of finite state Markov chains. *The annals of mathematical statistics*, *37*(6), 1554–1563.

Bennett, K. E., Cannon, A. J., & Hinzman, L. (2015). Historical trends and extremes in boreal Alaska river basins. *Journal of Hydrology*, *527*, 590–607.

Box, G. E. P., & Cox, D. R. (1964). An Analysis of Transformations. *Journal of the Royal Statistical Society: Series B (Methodological)*, *26*(2), 211–243. doi: 10.1111/j.2517-6161.1964.tb00553.x

Bracken, C., Rajagopalan, B., & Zagona, E. (2014). A hidden Markov model combined with climate indices for multidecadal streamflow simulation. *Water Resources Research*, *50*(10), 7836–7846.

Burn, D. H., Sharif, M., & Zhang, K. (2010). Detection of trends in hydrological extremes for Canadian watersheds. *Hydrological Processes*, *24*(13), 1781–1790.

Burnham, K. P., & Anderson, D. R. (2002). *A practical information-theoretic approach* (Vol. 2). Springer New York.

Chang, J., Zhang, H., Wang, Y., & Zhu, Y. (2016). Assessing the impact of climate variability and human activities on streamflow variation. *Hydrology and Earth System Sciences*, *20*(4), 1547–1560.

Chiew, F. H. S., Potter, N., Vaze, J., Petheram, C., Zhang, L., Teng, J., & Post, D. (2014). Observed hydrologic non-stationarity in far south-eastern Australia: implications for modelling and prediction. *Stochastic Environmental Research and Risk Assessment*, *28*(1), 3–15.

Coles, S., Bawa, J., Trenner, L., & Dorazio, P. (2001). *An introduction to statistical modeling of extreme values* (Vol. 208). Springer.

Crow, W. T., Bindlish, R., & Jackson, T. J. (2005). The added value of spaceborne passive microwave soil moisture retrievals for forecasting rainfall-runoff partitioning. *Geophysical Research Letters*, *32*(18).

Dharssi, I., Bally, J., Steinle, P., McJannet, D., & Walker, J. (2017). Comparison of soil wetness from multiple models over Australia with observations. *Water Resources Research*, *53*(1), 633–646.

Forney, G. D. (1973). The viterbi algorithm. *Proceedings of the IEEE*, *61*(3), 268–278.

Fowler, K., Knoben, W., Peel, M., Peterson, T. J., Ryu, D., Saft, M., . . . Western, A. (2020). Many commonly used rainfall-runoff models lack long, slow dynamics: Implications for runoff projections. *Water Resources Research*, e2019WR025286.

Fowler, K., Peel, M., Saft, M., Nathan, R., Horne, A., Wilby, R., . . . Peterson, T. (2022). Hydrological shifts threaten water resources. *Water Resources Research*, e2021WR031210.

Gates, J. B., Scanlon, B. R., Mu, X., & Zhang, L. (2011). Impacts of soil conservation on groundwater recharge in the semi-arid Loess Plateau, China. *Hydrogeology Journal*, *19*(4), 865–875.

Gebremicael, T. G., Mohamed, Y., Betrie, G., Van der Zaag, P., & Teferi, E. (2013). Trend analysis of runoff and sediment fluxes in the Upper Blue Nile basin: A combined analysis of statistical tests, physically-based models and landuse maps. *Journal of Hydrology*, *482*, 57–68.

Gebremicael, T. G., Mohamed, Y. A., van der Zaag, P., Hassaballah, K., & Hagos, E. Y. (2020). Change in low flows due to catchment management dynamics—Application of a comparative modelling approach. *Hydrological Processes*, *34*(9), 2101–2116.

Goswami, P., Peterson, T. J., Mondal, A., & Rüdiger, C. (2022). Non-stationary Influences of Large-scale Climate Drivers on Low Flow Extremes in Southeast Australia. *Water Resources Research*, e2021WR031508.

Guzha, A., Rufino, M. C., Okoth, S., Jacobs, S., & Nóbrega, R. (2018). Impacts of land use and land cover change on surface runoff, discharge and low flows: Evidence from East Africa. *Journal of Hydrology: Regional Studies*, *15*, 49–67.

Holmes, A., Rüdiger, C., Mueller, B., Hirschi, M., & Tapper, N. (2017). Variability of soil moisture proxies and hot days across the climate regimes of Australia. *Geophysical Research Letters*, *44*(14), 7265–7275.

Hughes, J., Petrone, K., & Silberstein, R. (2012). Drought, groundwater storage and stream flow decline in southwestern Australia. *Geophysical Research Letters*, *39*(3).

Katz, R. W. (2013). Statistical methods for nonstationary extremes. In *Extremes in a changing climate* (pp. 15–37). Springer.

Kendall, M. G. (1975). *Rank correlation methods.* (4th ed. 2d impression). Griffin.

Kiem, A. S., & Verdon-Kidd, D. C. (2010). Towards understanding hydroclimatic change in Victoria, Australia–preliminary insights into the “Big Dry”. *Hydrology and Earth System Sciences*, *14*(3), 433–445. doi: 10.5194/hess-14-433-2010

Kinal, J., & Stoneman, G. (2012). Disconnection of groundwater from surface water causes a fundamental change in hydrology in a forested catchment in south-western Australia. *Journal of Hydrology*, *472*, 14–24.

Kohler, M. A., & Linsley, R. K. (1951). *Predicting the runoff from storm rainfall* (Vol. 30). US Department of Commerce, Weather Bureau.

Li, L.-J., Zhang, L., Wang, H., Wang, J., Yang, J.-W., Jiang, D.-J., . . . Qin, D.-Y. (2007). Assessing the impact of climate variability and human activities on streamflow from the Wuding River basin in China. *Hydrological Processes: An International Journal*, *21*(25), 3485–3491.

Liu, X., Liu, C., & Brutsaert, W. (2018). Investigation of a generalized nonlinear form of the complementary principle for evaporation estimation. *Journal of Geophysical Research: Atmospheres*, *123*(8), 3933–3942.

Liu, Y. Y., Parinussa, R., Dorigo, W. A., De Jeu, R. A., Wagner, W., Van Dijk, A., . . . Evans, J. (2011). Developing an improved soil moisture dataset by blending passive and active microwave satellite-based retrievals. *Hydrology and Earth System Sciences*, *15*(2), 425–436.

Mallya, G., Tripathi, S., Kirshner, S., & Govindaraju, R. S. (2013). Probabilistic Assessment of Drought Characteristics Using Hidden Markov Model. *Journal of Hydrologic Engineering*, *18*(7), 834–845. doi: 10.1061/(asce)he.1943-5584.0000699

Mann, H. B. (1945). Nonparametric tests against trend. *Econometrica: Journal of the econometric society*, 245–259.

Miao, C., Ashouri, H., Hsu, K.-L., Sorooshian, S., & Duan, Q. (2015). Evaluation of the PERSIANN-CDR daily rainfall estimates in capturing the behavior of extreme precipitation events over China. *Journal of Hydrometeorology*, *16*(3), 1387–1396.

Miller, W. P., & Piechota, T. C. (2008). Regional analysis of trend and step changes observed in hydroclimatic variables around the Colorado River Basin. *Journal of Hydrometeorology*, *9*(5), 1020–1034.

Peel, M. C., McMahon, T. A., & Finlayson, B. L. (2004). Continental differences in the variability of annual runoff-update and reassessment. *Journal of Hydrology*, *295*(1-4), 185–197.

Peterson, T. J., Saft, M., Peel, M. C., & John, A. (2021). Watersheds may not recover from drought. *Science*, *372*(6543), 745–749. doi: 10.1126/science.abd5085

Peterson, T. J., & Western, A. (2014). Multiple hydrological attractors under stochastic daily forcing: 1. Can multiple attractors exist? *Water Resources Research*, *50*(4), 2993–3009.

Peterson, T. J., Western, A., & Argent, R. (2014). Multiple hydrological attractors under stochastic daily forcing: 2. Can multiple attractors emerge? *Water Resources Research*, *50*(4), 3010–3029.

Pushpalatha, R., Perrin, C., Le Moine, N., & Andréassian, V. (2012). A review of efficiency criteria suitable for evaluating low-flow simulations. *Journal of Hydrology*, *420*, 171–182.

R Core Team. (2021). R: A Language and Environment for Statistical Computing [Computer software manual]. R Foundation for Statistical Computing, Vienna, Austria. Retrieved from `https://www.R-project.org/`

Robertson, A. W., Kirshner, S., & Smyth, P. (2003). Hidden Markov models for modeling daily rainfall occurrence over Brazil. *Information and Computer Science, University of California*.

Robertson, A. W., Kirshner, S., & Smyth, P. (2004). Downscaling of daily rainfall occurrence over northeast Brazil using a hidden Markov model. *Journal of climate*, *17*(22), 4407–4424.

Rolim, L. Z. R., & de Souza Filho, F. d. A. (2020). Shift detection in hydrological regimes and pluriannual low-frequency streamflow forecasting using the hidden markov model. *Water*, *12*(7), 2058.

Saft, M., Western, A. W., Zhang, L., Peel, M. C., & Potter, N. J. (2015). The influence of multiyear drought on the annual rainfall-runoff relationship: An Australian perspective. *Water Resources Research*, *51*(4), 2444–2463. doi: 10.1002/2014WR015348

Sagarika, S., Kalra, A., & Ahmad, S. (2014). Evaluating the effect of persistence on long-term trends and analyzing step changes in streamflows of the continental United States. *Journal of Hydrology*, *517*, 36–53.

Shapiro, S. S., & Wilk, M. B. (1965). An analysis of variance test for normality (complete samples). *Biometrika*, *52*(3/4), 591–611.

Solander, K. C., Bennett, K. E., & Middleton, R. S. (2017). Shifts in historical streamflow extremes in the Colorado River Basin. *Journal of Hydrology: Regional Studies*, *12*, 363–377.

Tauro, F. (2021). River basins on the edge of change. *Science*, *372*(6543), 680–681.

Thyer, M., & Kuczera, G. (2000). Modeling long-term persistence in hydroclimatic time series using a hidden state Markov model. *Water resources research*, *36*(11), 3301–3310.

Thyer, M., & Kuczera, G. (2003). A hidden Markov model for modelling long-term persistence in multi-site rainfall time series 1. Model calibration using a Bayesian approach. *Journal of Hydrology*, *275*(1-2), 12–26.

Tian, W., Bai, P., Wang, K., Liang, K., & Liu, C. (2020). Simulating the change of precipitation-runoff relationship during drought years in the eastern monsoon region of China. *Science of the Total Environment*, *723*, 138172.

Turner, S., & Galelli, S. (2016). Regime-shifting streamflow processes: Implications for water supply reservoir operations. *Water Resources Research*, *52*(5), 3984–4002.

Ukkola, A. M., Prentice, I. C., Keenan, T. F., Van Dijk, A. I., Viney, N. R., Myneni, R. B., & Bi, J. (2016). Reduced streamflow in water-stressed climates consistent with CO2 effects on vegetation. *Nature Climate Change*, *6*(1), 75–78.

Van Dijk, A. I., Beck, H. E., Crosbie, R. S., De Jeu, R. A., Liu, Y. Y., Podger, G. M., ... Viney, N. R. (2013). The Millennium Drought in southeast Australia (2001-2009): Natural and human causes and implications for water resources, ecosystems, economy, and society. *Water Resources Research*, *49*(2), 1040–1057. doi: 10.1002/wrcr.20123

Wasko, C., Shao, Y., Vogel, E., Wilson, L., Wang, Q. J., Frost, A., & Donnelly, C. (2021). Understanding trends in hydrologic extremes across Australia. *Journal of Hydrology*, *593*, 125877. doi: 10.1016/j.jhydrol.2020.125877

Wilhite, D. A., & Glantz, M. H. (1985). Understanding: the drought phenomenon: the role of definitions. *Water international*, *10*(3), 111–120.

Williams, A. P., Cook, B. I., & Smerdon, J. E. (2022). Rapid intensification of the emerging southwestern North American megadrought in 2020–2021. *Nature Climate Change*, *12*(3), 232–234.

Xu, L., Chen, N., & Zhang, X. (2019). Global drought trends under 1.5 and 2 C warming. *International Journal of Climatology*, *39*(4), 2375–2385. doi: 10.1002/joc.5958

Zhang, X., Harvey, K. D., Hogg, W., & Yuzyk, T. R. (2001). Trends in Canadian streamflow. *Water Resources Research*, *37*(4), 987–998.

Zhang, X. S., Amirthanathan, G. E., Bari, M. A., Laugesen, R. M., Shin, D., Kent, D. M., ... Tuteja, N. K. (2016). How streamflow has changed across Australia since the 1950s: evidence from the network of hydrologic reference stations. *Hydrology and Earth System Sciences*, *20*(9), 3947–3965.

Zipper, S., Popescu, I., Compare, K., Zhang, C., & Seybold, E. C. (2022). Alternative stable states and hydrological regime shifts in a large intermittent river. *Environmental Research Letters*, *17*(7), 074005.

Zucchini, W., & MacDonald, I. L. (2009). *Hidden Markov models for time series: an introduction using R*. Chapman and Hall/CRC.

Supporting Information for "On the existence of multiple states of low flow regimes in catchments in southeast Australia"

Pallavi Goswami[1], Tim J. Peterson[2,3], Arpita Mondal[4,5], Christoph Rüdiger[2,6]

[1]IITB-Monash Research Academy, IIT Bombay, Mumbai, India
[2]Department of Civil Engineering, Monash University, Clayton, Victoria, Australia
[3]Department of Infrastructure Engineering, University of Melbourne, Parkville, Victoria, Australia
[4]Department of Civil Engineering, Indian Institute of Technology Bombay, Mumbai, India
[5]Interdisciplinary Program in Climate Studies, Indian Institute of Technology Bombay, Mumbai, India
[6]Bureau of Meteorology, Melbourne, Victoria, Australia

Introduction

This document contains text, figures, and tables that are meant to provide additional details that supplements some of the information provided in the Methods and Results & Discussion sections of the paper to which this SI is associated.

Contents of this file:

1. Text S1–S5
2. Tables S1–S3
3. Figures S1–S6

Corresponding author: Pallavi Goswami, IITB-Monash Research Academy, IIT Bombay, Mumbai, Maharashtra 400076, India. (Pallavi.Goswami@monash.edu)

Text S1. Details of the streamflow gauge stations

Table S1, adopted from Supplementary Information of Goswami et al. (2022), details information on the gauges used for the study. The streamflow data was taken from Peterson et al. (2021), wherein all the gauges used were quality controlled. Monthly streamflow data as flow depth (in mm) are available for these catchments, obtained by aggregating daily data. The area of these catchments ranges from 5.5 to 8463.6 km^2, with a median catchment area of 295.6 km^2. For more details, the reader is referred to the Supplementary Material of Peterson et al. (2021). The streamflow data used for this study, along with the catchment shapefiles, are available at `https://zenodo.org/record/6659706#.Y52tpHZBxdg`. Table S1 is followed by Table S2, displaying the overall mean and median values of flow depth for all these catchments taken together.

Table S1: Details of the streamflow gauge stations used in the study

Sr. No.	Gauge ID	Gauge name	Catchment area (km^2)	Latitude (°S)	Longitude (°E)	Data starting from	Data up to	No. of months for which data was unavailable	Years of available data
1	221201	CANN RIVER (WEST BRANCH) WEERAGUA	323.30	37.37	149.2	May 1922	Jul 2017	271	72.67
2	221207	ERRINUNDRA RIVER ERRINUNDRA	160.88	37.45	148.92	Apr 1968	Jul 2017	7	48.83
3	221208	WINGAN RIVER WINGAN INLET NATIONAL PARK	419.83	37.69	149.49	Sep 1979	Jul 2017	0	38.08
4	221209	CANN RIVER (EAST BRANCH) WEERAGUA	148.09	37.36	149.21	Feb 1973	Jul 2017	3	44.5
5	221210	GENOA RIVER THE GORGE	836.84	37.42	149.52	Jan 1973	Jul 2017	0	44.92
6	221211	COMBIENBAR RIVER COMBIENBAR	178.54	37.44	148.98	Feb 1975	Jul 2017	0	42.92
7	221212	BEMM RIVER PRINCES HIGHWAY	730.62	37.61	148.9	Nov 1975	Jul 2017	4	41.92
8	222202	BRODRIBB RIVER SARDINE CREEK	650.16	37.51	148.55	Dec 1922	Aug 2017	198	78.83
9	222206	BUCHAN RIVER BUCHAN	847.74	37.5	148.17	Dec 1926	Aug 2017	206	74.25
10	222210	DEDDICK RIVER DEDDICK (CASEYS)	847.70	37.09	148.42	Jan 1965	Aug 2017	47	49.5
11	222217	RODGER RIVER JACKSONS CROSSING	433.18	37.41	148.36	Apr 1977	Aug 2017	0	41.25
12	223202	TAMBO RIVER SWIFTS CREEK	896.08	37.27	147.73	May 1948	Jul 2017	1	70.08
13	223204	NICHOLSON RIVER DEPTFORD	289.37	37.59	147.7	Jun 1962	Jul 2017	7	55.58
14	223205	TAMBO RIVER D/S OF RAMROD CREEK	2676.68	37.67	147.87	Aug 1966	Jul 2017	0	52.08
15	224201	WONNANGATTA RIVER WATERFORD	1974.27	37.49	147.17	Jun 1923	Jul 2017	292	71
16	224203	MITCHELL RIVER GLENALADALE	3920.57	37.76	147.37	Dec 1938	Jul 2017	0	79.92
17	224206	WONNANGATTA RIVER CROOKED RIVER	1103.33	37.41	147.09	Oct 1954	Jul 2017	4	63.83
18	224213	DARGO RIVER LOWER DARGO ROAD	668.17	37.5	147.27	Nov 1974	Jul 2017	2	44
19	224214	WENTWORTH RIVER TABBERABBERA	440.75	37.5	147.39	Feb 1976	Jul 2017	3	42.75
20	225201	AVON RIVER STRATFORD	1467.28	37.97	147.08	Jul 1978	Jul 2017	0	40.67
21	225209	MACALISTER RIVER LICOLA	1237.60	37.63	146.62	Apr 1954	Jul 2017	9	64.25
22	225213	ABERFELDY RIVER BEARDMORE	312.39	37.85	146.43	Apr 1965	Aug 2017	1	54.08
23	225218	FREESTONE CREEK BRIAGALONG	304.99	37.81	147.1	Mar 1969	Aug 2017	0	50.33
24	225219	MACALISTER RIVER GLENCAIRN	572.36	37.52	146.57	Apr 1969	Jul 2017	2	50.08
25	225221	MACALISTER RIVER STRINGYBARK CREEK	1542.29	37.77	146.67	Apr 1970	Aug 2017	54	44.92
26	225223	VALENCIA CREEK GILLIO ROAD	203.19	37.74	146.99	Nov 1973	Aug 2017	19	44.33
27	225224	AVON RIVER THE CHANNEL	557.42	37.8	146.88	Oct 1974	Aug 2017	1	45
28	226023	TRARALGON CREEK TRARALGON	172.40	38.19	146.54	Feb 1963	Jul 2017	72	50.75
29	226204	LATROBE RIVER WILLOW GROVE	560.91	38.09	146.16	Mar 1927	Aug 2017	0	92.83
30	226205	LATROBE RIVER NOOJEE	295.57	37.91	146.02	Sep 1959	Jul 2017	3	60.08
31	226209	MOE RIVER DARNUM	230.59	38.21	146	Feb 1964	Aug 2017	0	56.08
32	226218	NARRACAN CREEK THORPDALE	65.73	38.27	146.19	Feb 1958	Aug 2017	0	62.17
33	226220	LOCH RIVER NOOJEE	106.01	37.87	146.01	Dec 1959	Jul 2017	37	57.25
34	226226	TANJIL RIVER TANJIL JUNCTION	297.73	37.98	146.19	Mar 1963	Aug 2017	1	57.17
35	226402	MOE DRAIN TRAFALGAR EAST	610.47	38.18	146.21	May 1960	Aug 2017	0	60.17
36	226407	MORWELL RIVER BOOLARRA	116.51	38.41	146.31	Oct 1961	Aug 2017	120	48.83
37	227200	TARRA RIVER YARRAM	217.08	38.54	146.67	Mar 1949	Jul 2017	18	69.92
38	227202	TARWIN RIVER MEENIYAN	1072.24	38.58	145.99	Aug 1958	Aug 2017	0	62.17
39	227205	MERRIMAN CREEK CALIGNEE SOUTH	39.48	38.35	146.65	Mar 1950	Aug 2017	189	54.92
40	227210	BRUTHEN CREEK CARRAJUNG LOWER	17.91	38.4	146.74	Dec 1955	Jul 2017	0	64.92
41	227211	AGNES RIVER TOORA	66.09	38.64	146.37	May 1956	Aug 2017	45	60.92
42	227213	JACK RIVER JACK RIVER	34.88	38.53	146.54	Mar 1964	Jul 2017	0	56.83
43	227219	BASS RIVER LOCH	53.31	38.36	145.73	Oct 1969	Jul 2017	2	51.17
44	227225	TARRA RIVER FISCHERS	19.00	38.47	146.56	Dec 1971	Jul 2017	2	49.08
45	227226	TARWIN RIVER EAST BRANCH DUMBALK NORTH	125.64	38.5	146.16	Jan 1974	Aug 2017	0	47.33
46	227227	WILKUR CREEK LEONGATHA	105.28	38.39	145.96	May 1974	Jul 2017	0	47
47	227236	POWLETT RIVER D/S FOSTER CREEK JUNCTION	233.33	38.56	145.71	Apr 1983	Jul 2017	1	38.08
48	227237	FRANKLIN RIVER TOORA	75.23	38.63	146.31	Jun 1983	Aug 2017	0	38.17
49	230205	DEEP CREEK BULLA (D/S OF EMU CREEK JUNCT.)	865.25	37.63	144.8	Jul 1959	Aug 2017	5	61.75
50	230209	BARRINGO CREEK BARRINGO (U/S OF DIVERSION)	5.53	37.41	144.63	Aug 1970	Aug 2017	1	51.08

Sr. No.	Gauge ID	Gauge name	Catchment area (km^2)	Latitude (°S)	Longitude (°E)	Data starting from	Data up to	No. of months for which data was unavailable	Years of available data
51	230210	SALTWATER CREEK BULLENGAROOK	38.91	37.47	144.52	Aug 1972	Aug 2017	2	49.08
52	231225	WERRIBEE RIVER BALLAN (U/S OLD WESTERN HWY)	107.49	37.6	144.25	Sep 1977	Aug 2017	1	44.17
53	231231	TOOLERN CREEK MELTON SOUTH	94.53	37.73	144.58	Sep 1983	Dec 2015	0	36.67
54	232214	BLACK CREEK U/S OF BUNGAL DAM	12.78	37.63	144.06	Dec 1981	Aug 2017	2	40
55	232215	WOOLLEN CREEK U/S OF BUNGAL DAM	8.62	37.63	144.08	Jan 1982	Aug 2017	0	40.17
56	233211	BIRREGURRA CREEK RICKETTS MARSH	114.29	38.3	143.84	Feb 1958	Aug 2017	14	63
57	233214	BARWON RIVER EAST BRANCH FORREST	16.59	38.53	143.73	Feb 1960	Aug 2017	0	62.25
58	233223	WARRAMBINE CREEK WARRAMBINE	53.87	37.93	143.87	Mar 1975	Aug 2017	1	47.17
59	234200	WOADY YALOAK RIVER PITFIELD	315.32	37.81	143.59	Jun 1922	Aug 2017	355	70.5
60	234201	WOADY YALOAK RIVER CRESSY (YARIMA)	1155.17	38.01	143.64	May 1960	Aug 2017	7	61.67
61	234203	PIRRON YALLOCK CREEK PIRRON YALLOCK (ABOVE H'WY BR.)	169.11	38.35	143.42	May 1969	Jul 2017	0	53.25
62	234209	DEAN CREEK LAKE COLAC	53.12	38.34	143.56	Jan 1981	Aug 2017	0	41.75
63	235203	CURDIES RIVER CURDIE	781.68	38.44	142.96	Jan 1961	Jul 2017	3	61.5
64	235204	LITTLE AIRE CREEK BEECH FOREST	11.17	38.65	143.53	Aug 1960	Aug 2017	70	56.5
65	235209	AIRE RIVER BEECH FOREST	25.22	38.67	143.58	Aug 1969	Aug 2017	0	53.42
66	235210	LARDNER CREEK GELLIBRAND	51.74	38.53	143.54	Dec 1969	Aug 2017	4	52.83
67	235211	KENNEDYS CREEK KENNEDYS CREEK	269.42	38.59	143.26	Jan 1970	Aug 2017	7	52.58
68	235216	CUMBERLAND RIVER LORNE	38.19	38.57	143.95	Dec 1971	Aug 2017	0	51.33
69	235219	AIRE RIVER WYELANGTA	91.16	38.7	143.48	Dec 1972	Aug 2017	3	50.17
70	235227	GELLIBRAND RIVER BUNKERS HILL	313.65	38.52	143.48	Jan 1976	Aug 2017	8	46.75
71	235233	BARHAM RIVER EAST BRANCH APOLLO BAY PARADISE	43.45	38.76	143.62	Sep 1983	Aug 2017	1	39.75
72	235234	LOVE CREEK GELLIBRAND	76.66	38.48	143.57	Apr 1985	Aug 2017	0	38.33
73	236202	HOPKINS RIVER WICKLIFFE	1358.79	37.7	142.72	Jun 1970	Aug 2017	4	52.92
74	236203	MOUNT EMU CREEK SKIPTON	1230.00	37.69	143.36	Aug 1926	Aug 2017	142	85.33
75	236204	FIERY CREEK STREATHAM	1001.32	37.68	143.06	Sep 1926	Aug 2017	123	86.92
76	236205	MERRI RIVER WOODFORD	888.01	38.32	142.48	Nov 1954	Jul 2017	3	68.75
77	236209	HOPKINS RIVER HOPKINS FALLS	8463.59	38.34	142.63	Oct 1961	Jul 2017	3	61.92
78	236210	HOPKINS RIVER FRAMLINGHAM	5143.99	38.24	142.7	Dec 1961	Jul 2017	0	62.08
79	236212	BRUCKNELL CREEK CUDGEE	230.51	38.35	142.65	Jan 1972	Jul 2017	0	52.08
80	236213	MOUNT EMU CREEK MENA PARK	313.91	37.53	143.46	Aug 1973	Aug 2017	2	50.5
81	236216	MOUNT EMU CREEK TAROON (AYRFORD ROAD BRIDGE)	2946.43	38.31	142.88	Jul 1984	Jul 2017	5	39.33
82	237200	MOYNE RIVER TOOLONG	568.69	38.32	142.23	Mar 1955	Jul 2017	0	69.17
83	237202	FITZROY RIVER HEYWOOD	264.11	38.13	141.62	Jun 1955	Aug 2017	0	69.08
84	237205	DARLOT CREEK HOMERTON BRIDGE	748.34	38.15	141.77	Jan 1970	Aug 2017	0	54.58
85	237206	EUMERALLA RIVER CODRINGTON	458.01	38.26	141.94	Mar 1971	Aug 2017	0	53.5
86	237207	SURRY RIVER HEATHMERE	296.06	38.24	141.66	Jun 1977	Aug 2017	0	47.33
87	238208	JIMMY CREEK JIMMY CREEK	22.24	37.37	142.51	Apr 1957	Aug 2017	0	67.58
88	238219	GRANGE BURN MORGIANA	1110.91	37.71	141.83	Nov 1970	Jul 2017	55	49.42
89	238223	WANDO RIVER WANDO VALE	173.58	37.5	141.43	Sep 1971	Aug 2017	2	53.17
90	238229	CHETWYND RIVER CHETWYND	69.75	37.32	141.48	Sep 1974	Jun 2017	7	49.67
91	238230	STOKES RIVER TEAKETTLE	191.46	37.87	141.41	Jan 1974	Aug 2017	3	50.92
92	238235	CRAWFORD RIVER LOWER CRAWFORD	613.62	37.98	141.45	Jan 1978	Aug 2017	0	47.25
93	401203	MITTA MITTA RIVER HINNOMUNJIE	1531.39	36.95	147.61	Mar 1933	Jul 2017	2	91.92
94	401208	CUDGEWA CREEK BERRINGAMA	357.52	36.21	147.68	Feb 1961	Aug 2017	0	64.33
95	401210	SNOWY CREEK BELOW GRANITE FLAT	413.32	36.57	147.41	Sep 1940	Aug 2017	0	84.83
96	401212	NARIEL CREEK UPPER NARIEL	255.72	36.45	147.83	Apr 1962	Aug 2017	0	63.33
97	401215	MORASS CREEK UPLANDS	536.17	36.87	147.7	Nov 1937	Jul 2017	1	87.67
98	401216	BIG RIVER JOKERS CREEK	357.48	36.93	147.47	Oct 1942	Jul 2017	3	82.67
99	401217	GIBBO RIVER GIBBO PARK	389.34	36.76	147.71	Oct 1979	Jul 2017	0	46
100	401220	TALLANGATTA CREEK McCALLUMS	454.44	36.21	147.34	Nov 1985	Aug 2017	2	39.92
101	402204	YACKANDANDAH CREEK OSBORNES FLAT	275.16	36.3	146.91	Mar 1973	Aug 2017	3	52.58
102	402206	RUNNING CREEK RUNNING CREEK	127.52	36.54	147.04	Oct 1974	Aug 2017	5	50.92
103	402213	KINCHINGTON CREEK OSBORNES FLAT	120.28	36.32	146.89	Nov 1977	Jul 2017	8	47.58
104	403200	OVENS RIVER WANGARATTA	5119.74	36.35	146.32	Feb 1894	Aug 2017	14	131
105	403205	OVENS RIVERS BRIGHT	493.67	36.73	146.95	Sep 1933	Aug 2017	128	82
106	403209	REEDY CREEK WANGARATTA NORTH	389.38	36.33	146.34	Mar 1949	Aug 2017	1	77.17
107	403213	FIFTEEN MILE CREEK GRETA SOUTH	226.77	36.62	146.24	Nov 1967	Aug 2017	6	58.17
108	403214	HAPPY VALLEY CREEK ROSEWHITE	139.81	36.58	146.82	Jun 1970	Aug 2017	2	56
109	403217	ROSE RIVER MATONG NORTH	178.61	36.82	146.58	Sep 1971	Aug 2017	7	54.42
110	403221	REEDY CREEK WOOLSHED	211.47	36.31	146.6	Jan 1974	Aug 2017	2	52.58
111	403222	BUFFALO RIVER ABBEYARD	415.09	36.91	146.7	Sep 1974	Aug 2017	3	51.92
112	403223	KING RIVER DOCKER ROAD BRIDGE	1085.31	36.52	146.39	May 1975	Aug 2017	3	51.33
113	403224	HURDLE CREEK BOBINAWARRAH	156.03	36.51	146.45	Sep 1975	Aug 2017	0	51.33
114	403226	BOGGY CREEK ANGLESIDE	109.19	36.61	146.36	Aug 1976	Aug 2017	18	49
115	403230	OVENS RIVER ROCKY POINT	2970.15	36.53	146.67	Jan 1975	Aug 2017	4	51.83
116	403232	MORSES CREEK WANDILIGONG	126.02	36.75	146.98	Jul 1982	Aug 2017	10	43.92
117	403233	BUCKLAND RIVER HARRIS LANE	457.07	36.72	146.88	Feb 1982	Aug 2017	6	44.75
118	404204	BOOSEY CREEK TUNGAMAH	830.67	36.12	145.83	Sep 1976	Aug 2017	0	50.75
119	404207	HOLLAND CREEK KELFEERA	460.78	36.61	146.06	Apr 1970	Aug 2017	1	57.17
120	405205	MURRINDINDI RIVER MURRINDINDI ABOVE COLWELLS	107.70	37.41	145.56	Jun 1949	Jul 2017	3	77.83
121	405209	ACHERON RIVER TAGGERTY	626.25	37.32	145.71	Jan 1956	Jul 2017	1	71.5
122	405214	DELATITE RIVER TONGA BRIDGE	358.12	37.16	146.11	Apr 1957	Aug 2017	0	70.5
123	405215	HOWQUA RIVER GLAN ESK	368.65	37.23	146.21	May 1957	Aug 2017	224	51.83
124	405217	YEA RIVER DEVLINS BRIDGE	361.53	37.38	145.47	Jul 1964	Jul 2017	4	63
125	405218	JAMIESON RIVER GERRANG BRIDGE	367.23	37.29	146.19	Nov 1964	Aug 2017	0	63.17
126	405219	GOULBURN RIVER DOHERTYS	701.64	37.33	146.13	Feb 1965	Aug 2017	8	62.33
127	405226	PRANJIP CREEK MOORILIM	791.16	36.62	145.31	Jul 1968	Jul 2017	0	59.58
128	405227	BIG RIVER JAMIESON	626.51	37.37	146.06	Oct 1968	Aug 2017	0	59.5
129	405228	HUGHES CREEK TARCOMBE ROAD	483.80	36.94	145.29	Jun 1969	Jul 2017	1	58.75
130	405229	WANALTA CREEK WANALTA	106.16	36.63	144.87	Mar 1971	Aug 2017	1	57.17
131	405230	CORNELLA CREEK COLBINABBIN	253.08	36.6	144.8	Apr 1971	Aug 2017	4	56.92
132	405234	SEVEN CREEKS D/S OF POLLY MCQUINN WEIR	154.62	36.89	145.68	Jun 1976	Jul 2017	14	50.92
133	405237	SEVEN CREEKS EUROA TOWNSHIP	347.86	36.73	145.57	Jun 1974	Jul 2017	10	53.33
134	405238	MOLLISON CREEK PYALONG	163.47	37.12	144.86	Jul 1977	Sep 2016	6	49.83
135	405240	SUGARLOAF CREEK ASH BRIDGE	609.80	37.06	145.06	Mar 1984	Aug 2017	15	43.42
136	405245	FORD CREEK MANSFIELD	115.73	37.04	146.05	Sep 1981	Aug 2017	1	47.17
137	405246	CASTLE CREEK ARCADIA	202.72	36.59	145.35	Oct 1981	Jun 2017	32	44.42
138	405248	MAJOR CREEK GRAYTOWN	284.69	36.85	144.91	Oct 1982	Aug 2017	1	46.25
139	405251	BRANKEET CREEK ANCONA	118.78	36.97	145.79	Dec 1982	Aug 2017	2	46.08
140	405264	BIG RIVER D/S OF FRENCHMAN CREEK JUNCTION	331.66	37.52	146.08	Nov 1986	Jun 2017	0	42.25
141	405274	HOME CREEK YARCK	180.80	37.11	145.61	Mar 1989	Jul 2017	0	40.08
142	406208	CAMPASPE RIVER ASHBOURNE	39.05	37.39	144.45	Feb 1945	Aug 2017	0	84.33
143	406213	CAMPASPE RIVER REDESDALE	637.64	37.02	144.54	Sep 1965	Jul 2017	60	58.75
144	406214	AXE CREEK LONGLEA	235.63	36.77	144.43	Mar 1977	Jul 2017	0	52.33
145	406226	MOUNT IDA CREEK DERRINAL	175.63	36.88	144.65	Jul 1990	Jul 2017	2	38.92
146	406235	WILD DUCK CREEK U/S OF HEATHCOTE-MIA MIA ROAD	211.92	36.95	144.66	Jan 1993	Jul 2017	10	35.83
147	407211	BET BET CREEK BET BET	628.62	36.92	143.75	Dec 1955	Jul 2017	350	44.67
148	407214	CRESWICK CREEK CLUNES	310.46	37.3	143.79	Dec 1955	Aug 2017	0	74
149	407217	LODDON RIVER VAUGHAN D/S FRYERS CREEK	295.45	37.16	144.21	Oct 1959	Jul 2017	3	69.92
150	407221	JIM CROW CREEK YANDOIT	166.79	37.21	144.1	Dec 1966	Jul 2017	3	62.83
151	407230	JOYCES CREEK STRATHLEA	149.01	37.16	143.96	Dec 1975	Jul 2017	0	54.17
152	407239	MIDDLE CREEK RODBOROUGH	148.06	37.14	143.91	Jan 1983	Jul 2017	144	35.17
153	407246	BULLOCK CREEK MARONG	188.61	36.73	144.14	Nov 1985	Jul 2017	3	44.17
154	408202	AVOCA RIVER AMPHITHEATRE	76.54	37.18	143.41	Aug 1979	Aug 2017	7	50.25
155	415201	WIMMERA RIVER GLENORCHY WEIR TAIL GAUGE	1967.83	36.91	142.64	Nov 1962	Aug 2017	4	67.33
156	415206	WIMMERA RIVER GLYNWYLLN	1377.05	36.95	142.86	Sep 1915	Aug 2017	504	72.92
157	415207	WIMMERA RIVER EVERSLEY	305.00	37.19	143.18	Nov 1915	Aug 2017	708	55.83
158	415220	AVON RIVER WIMMERA HIGHWAY	519.88	36.64	142.98	Mar 1976	Aug 2017	22	52.75
159	415226	RICHARDSON RIVER CARRS PLAINS	129.91	36.74	142.79	Jul 1984	Aug 2017	7	45.75
160	415237	CONCONGELLA CREEK STAWELL	241.27	37.03	142.82	Apr 1990	Aug 2017	1	40.58
161	415238	WATTLE CREEK NAVARRE	138.75	36.9	143.11	Jul 1989	Aug 2017	11	40.58

Table S2: Median and mean flow depths for the study region taking all catchments into account

	Jan	Feb	Mar	Apr	May	Jun	Jul	Aug	Sep	Oct	Nov	Dec
Median of flow depth (mm)	2.26	1.37	1.36	1.96	3.52	7.95	16.96	24.93	22.79	15.23	7.74	4.27
Mean of flow depth (mm)	6.55	4.90	4.83	6.70	10.77	20.36	32.11	40.24	37.35	29.93	17.86	11.35

Text S2. Box-Cox transformation of streamflows

The flow data for most of the studied catchments was highly skewed towards lower flow values. Since the analysis required deriving a standardized streamflow index, it is important that the series of this standardized streamflow index is as close to a normal distribution as possible. However, with skewed flow data, such an outcome could not be achieved. A Box-cox transformation was thus used to normalize the flow data. The Box-Cox transformation is a power transformation that eliminates non-linearity between variables, differing variances, and variable asymmetry. It is commonly used to transform a series into a new series with an almost normal distribution. Although it is not always possible for a power transformation to bring the distribution to exactly normal, the usual estimates of λ will lead to a distribution that satisfies certain restrictions on the first 4 moments which thus will usually be symmetric. For the present study, a one-parameter Box-Cox transformation of the original streamflow depth data (for $Q_i > 0$) was done, as expressed below.

$$\widehat{Q_i} = (Q_i + 1)^{\lambda} - 1 for \lambda \neq 0 \quad (1)$$

$$\widehat{Q_i} = \ln(Q_i + 1) for \lambda = 0 \quad (2)$$

In the above equation, a value of 1 was added to the original value of Q_i to ensure that the quantity being transformed was always greater than 1 for the transformation to be feasible. Here, λ is the transformation parameter of the transformation and was estimated using the

MASS package available in R, through maximum likelihood estimation. Figure S1 shows the plot of log-likelihood vs lambda for station ID 235204 with the dotted lines indicating the 95% confidence interval for the optimum lambda value. Initially, the optimum value of λ was arrived at by trying values from the set (0.1, 5] at increments of 0.1. However, while using this range it was later realized that allowing λ to take negative values improves the transformation for many catchments. Additionally, positive values beyond 2 were hardly selected. The range was thus revised to be [-2,2].

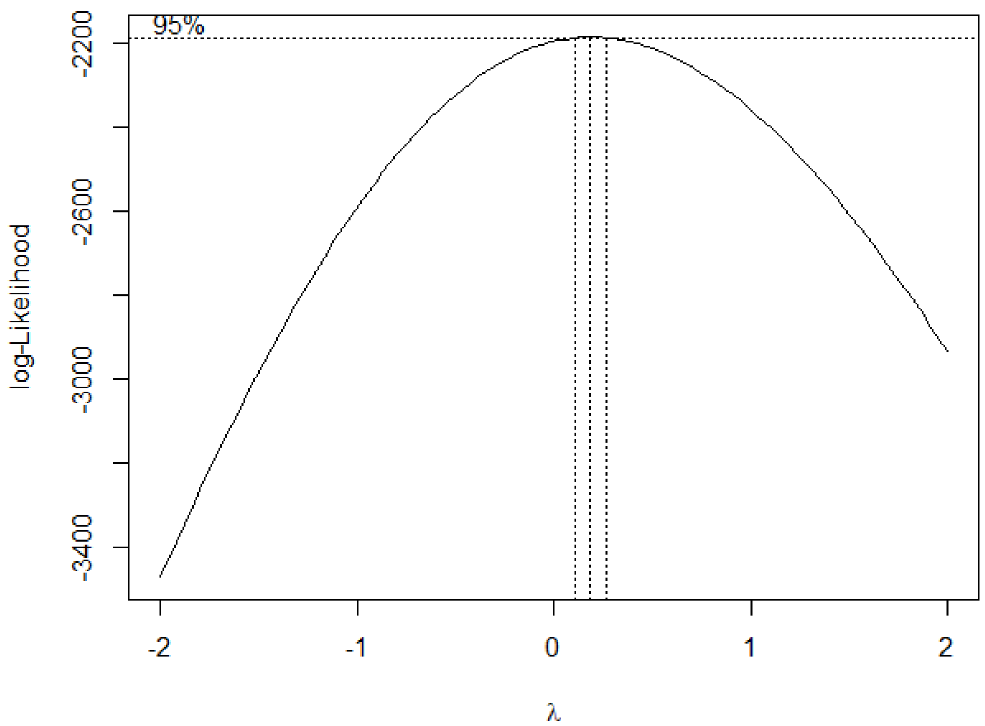

Figure S1: Log-likelihood vs λ for the identification of the optimum value of λ for station ID 235204. The optimization yields a value of $\lambda = 0.18$ as the optimum lambda for the BC transform for this station. The vertical dotted lines around the vertical line at 0.18 indicate the 95% confidence interval for the optimum lambda value.

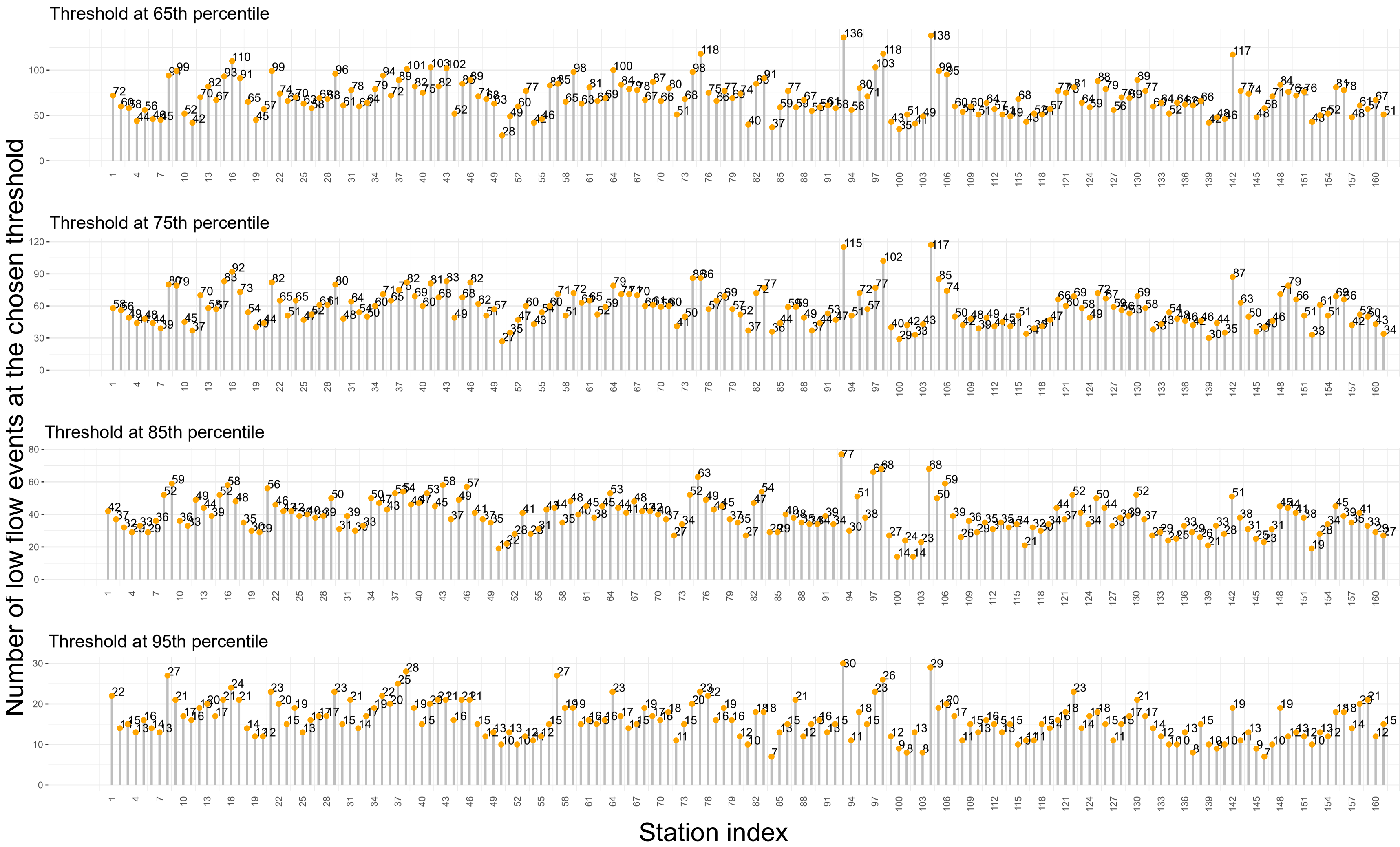

Figure S2: Number of low flow events for each catchment for a chosen value of threshold. From top to bottom, the sub-figures correspond to the 65th, 75th, 85th, and 95th percentiles of the SDI series, respectively, in the adopted POT approach. For the HMM to simulate satisfactorily, it was considered necessary that most of the catchments should have at least 40 observations for low flow IDF. This was achieved for a threshold of 65th percentile which was consequently chosen for the study.

Text S3. Calibration of the HMMs

The parameters of the HMM were arrived at using a constrained maximum likelihood estimation, where the likelihood function $\mathscr{L}_T$ is expressed as:

$$\mathscr{L}_T = \boldsymbol{\delta P}(x_1)\boldsymbol{\Gamma P}(x_2)....\boldsymbol{\Gamma P}(x_T)1' \quad (3)$$

Here $\boldsymbol{\delta}$ is the initial state distribution (Equation 8 in the paper), $\boldsymbol{\Gamma}$ (as $\boldsymbol{\Gamma}_1$ or $\boldsymbol{\Gamma}_2$) is the transition matrix for the relevant model and T is the number of time steps. $\boldsymbol{P}(x)$ is the $m \times m$ diagonal emissions matrix of probabilities for an m-state HMM, obtained from the error distribution model having the ith diagonal element equal to the probability of being in state i at a given point in time (Equation 9,12, or 15 in the paper). The emission probabilities $\boldsymbol{P}$ were obtained from the corresponding error distribution model used to model the variable x.

The likelihood was estimated recursively as $\mathscr{L}_T = \alpha_T 1'$, where

$$\alpha_1 = \boldsymbol{\delta P}(x_1) \quad (4)$$

and

$$\alpha_t = \alpha_{t-1}\boldsymbol{\Gamma P}(x_t) \qquad for\ t = 2, 3, 4, ...T$$

Numerically, $\mathscr{L}_T$ was maximized by rearrangement to a negative log-likelihood and minimized using global optimization.

The optimization response surface of a multi-state HMM often tends to have multiple local optima (Supplementary Material of Peterson et al., 2021). To reliably identify the global optima, a Differential Evolution-based global optimization scheme (Storn & Price, 1997) was adopted. This scheme involves transforming a set of parameter vectors, termed as population, into a new parameter vector set at each generation of evolution. The evolution is brought about by perturbing an old parameter vector with the scaled difference of two arbitrarily selected parameter vectors. The new set members thus obtained are more likely to optimize the objective function. To ensure a robust optimization, the population size per parameter was set as 10 as it has been noted that convergence to the global optimum is facilitated if this value is 10 or greater (Price et al., 2006). Higher values in this case incurred undesirably larger computational time without significant improvement in the model fit. Further, the maximum number of generations was set to 550 as nearly all the models were seen to converge at either far less than or near to 550 generations. Model calibration at each catchment was performed 10 times for each state model for the given low flow characteristic. Each calibration was run with a different random seed and a randomly selected differential evolution strategy. To arrive at the most probable sequence of states from all possible combinations of sequences for the given observation sequence of intensity/duration/frequency (I/D/F), an efficient dynamic programming method, called the Viterbi algorithm (Forney, 1973; Zucchini & MacDonald, 2009) was used. This algorithm identifies the most probable sequence of states from the Markov chain of probabilities. The states of I/D/F obtained through this were also referred to as the Viterbi states (named after the algorithm). The algorithm was applied over the entire observation record to identify the most probable sequence of I/D/F states, thereby also identifying any switching, if at all, in the states of the I/D/F.

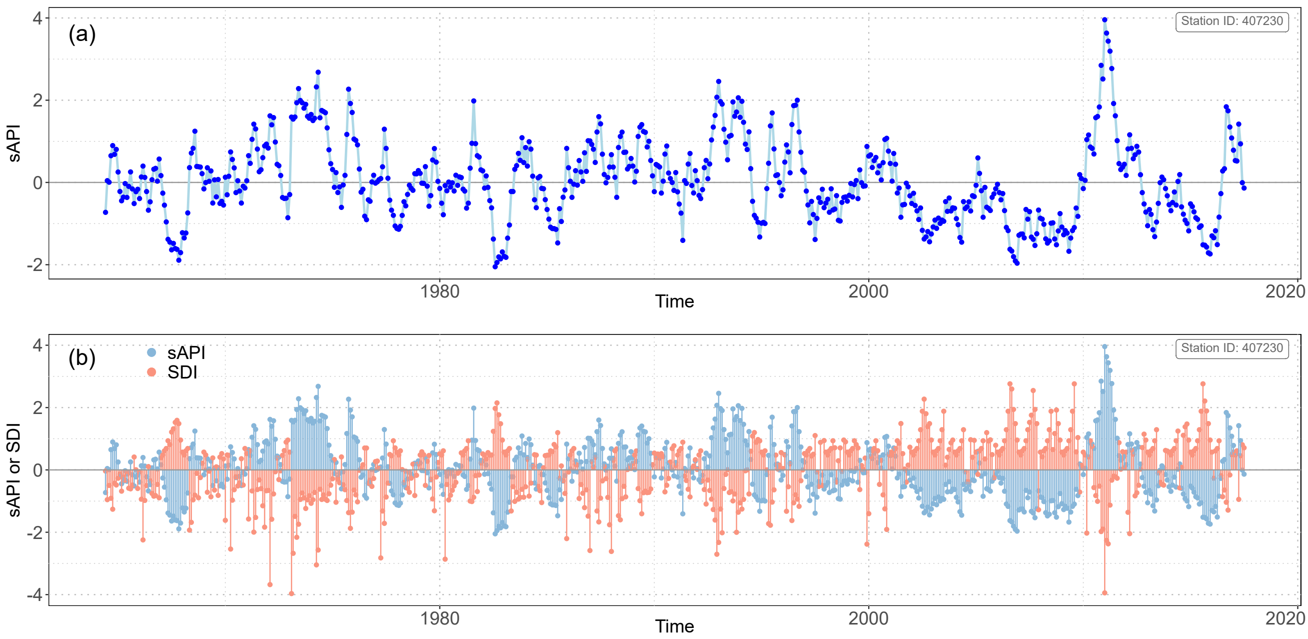

Figure S3: (a) Time series of standardized Antecedent Precipitation Index (sAPI) obtained for station ID 407230. (b) Variation of SDI and sAPI over time for the catchment. The sAPI mirrors the variability in the SDI series of the catchment, making it a suitable choice for a predictor in the HMMs of the low flow characteristics.

Text S4. Assessing model reliability of IDF HMMs through diagnostic plots of residuals

The validity and reliability of the IDF HMMs emerging from the application as discussed in the paper were assessed by inspecting whether the pseudo-residuals were normally distributed or not (Zucchini & MacDonald, 2009). This was carried out by visual inspection of pseudo-residual plots and through the Shapiro-Wilk test (alpha = 0.05) as discussed in the paper under Section 3.1. For models to be accurate, the pseudo-residuals must be normally distributed. The autocorrelation plots of the pseudo-residuals help determine if the model has performed sufficiently well. If minimal autocorrelation is seen to carry into subsequent time steps, it indicates that errors do not accumulate over time and that no information is 'leftover' and not incorporated in the model.

The next three figures represent the assessment of the behavior of residuals of the HMMs of the three low flow characteristic for selected sample stations. Figure S4 gives an example of an acceptable model performance as per the pseudo-residual analysis where the residuals may be considered to be very close to being normally distributed. The auto-correlation of the pseudo-residuals is almost always within the acceptable bounds for many consecutive time steps, indicating that significant information from the data has been included in the model. No or minimal serial correlation of the pseudo-residuals implies that inaccuracies in the model at a given time step have very little effect on future time steps. The Shapiro-Wilk p-value is greater than 0.05 for the pseudo-residuals in Figure S4 which confirms that the residuals are normal and that the model is performing adequately.

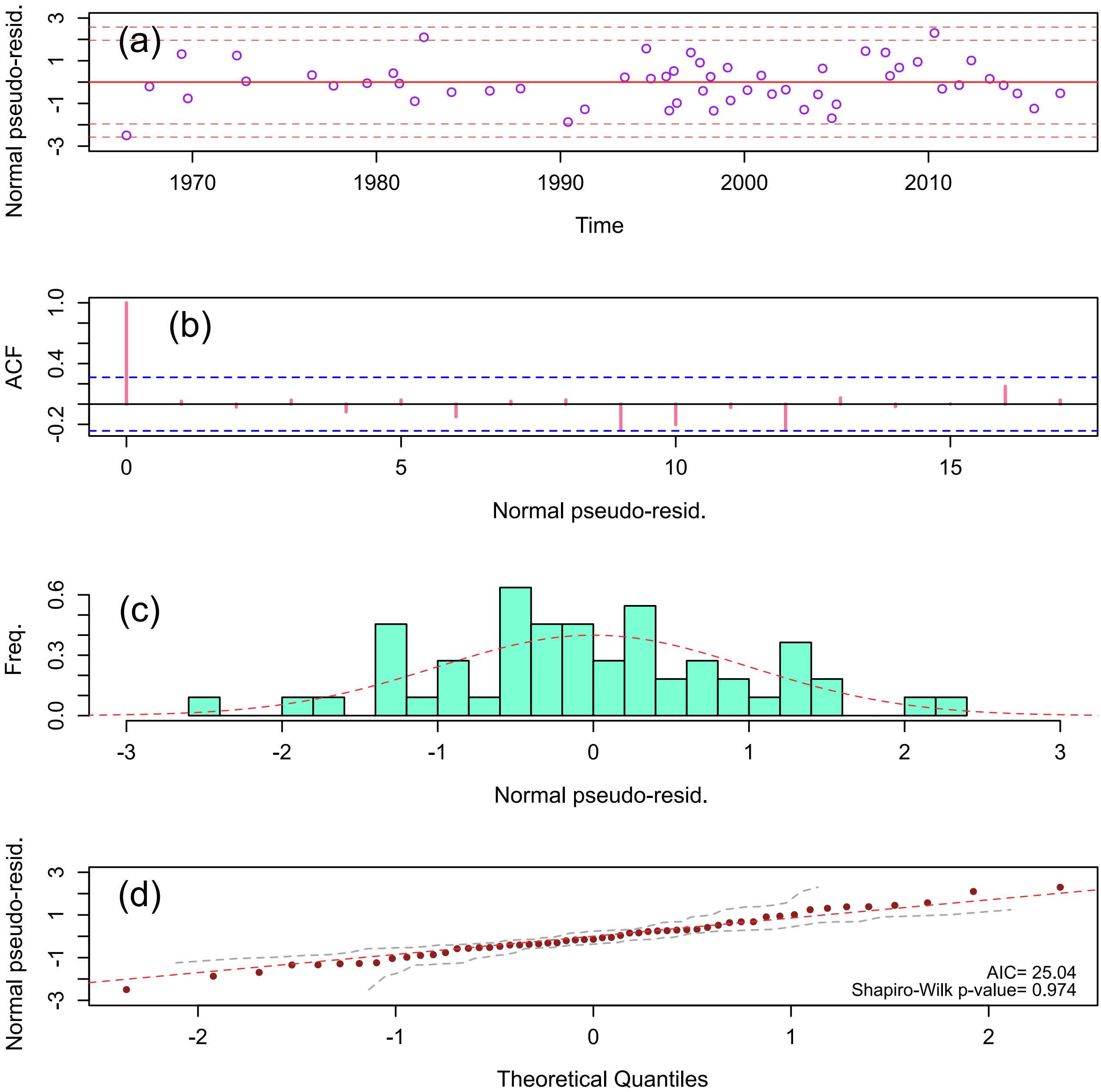

Figure S4: Diagnostic plots of the model residuals corresponding to the intensity HMM output as discussed in Figure 6 for station ID 238223. (a) Time series of the normal pseudo-residuals corresponding to the low flow peaks occurring over time (red lines at 0, ±1.96, ±2.58). (b) Auto-correlation of the normal pseudo-residuals, with the blue dotted lines indicating the 95th percentile confidence intervals for uncorrelated series. (c) Histogram of the normal pseudo-residuals, with the red dotted line indicating a standard normal distribution. (d) Quantile-Quantile (Q-Q) plot of the normal pseudo-residuals in relation to the theoretical quantiles.

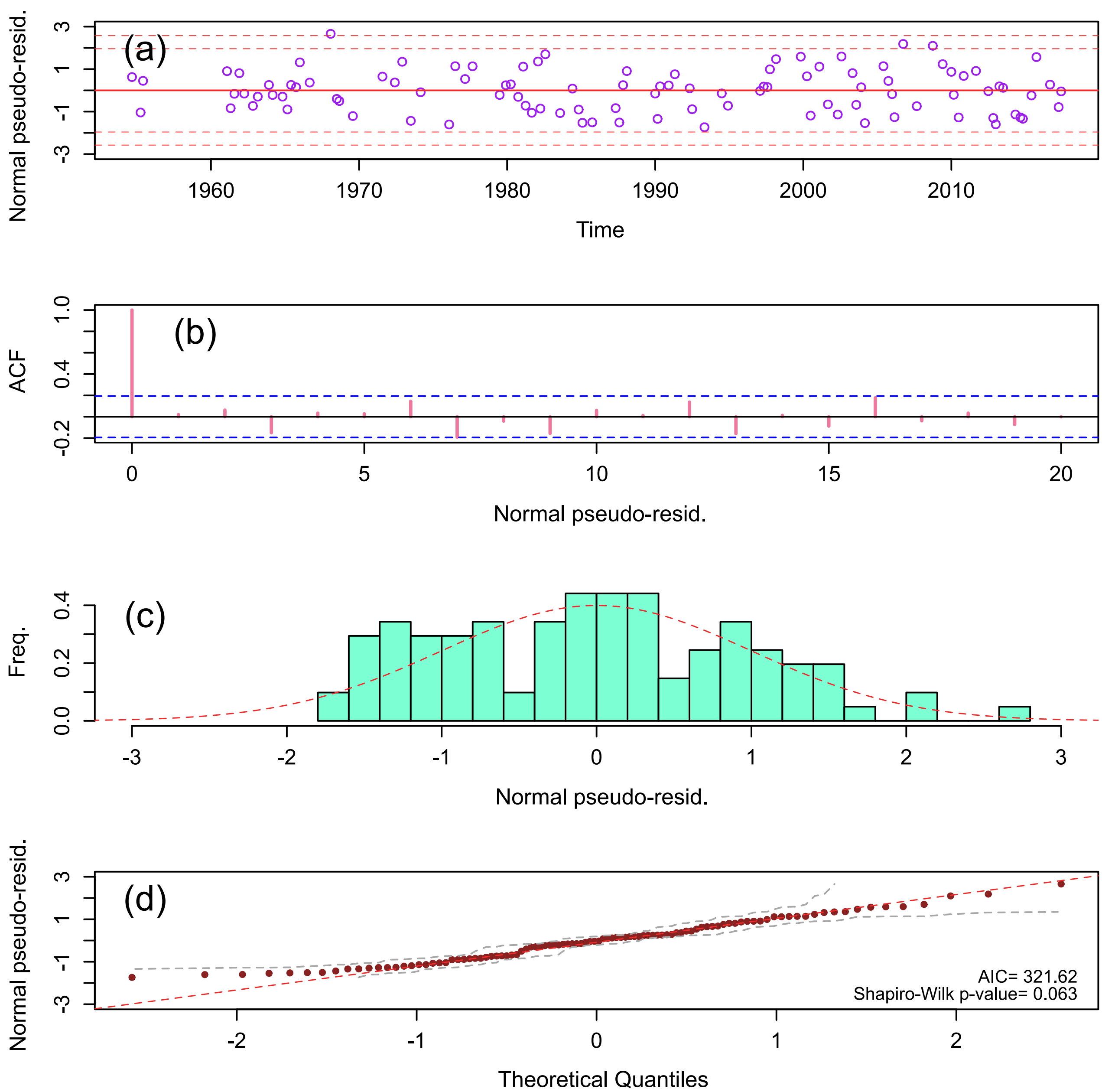

Figure S5: Diagnostic plots of the model residuals corresponding to the duration HMM output as discussed in Figure 7 for station ID 227211. (a) Time series of the normal pseudo-residuals corresponding to the low flow peaks occurring over time (red lines at 0, ±1.96, ±2.58). (b) Auto-correlation of the normal pseudo-residuals, with the blue dotted lines indicating the 95th percentile confidence intervals for uncorrelated series. (c) Histogram of the normal pseudo-residuals, with the red dotted line indicating a standard normal distribution. (d) Quantile-Quantile (Q-Q) plot of the normal pseudo-residuals in relation to the theoretical quantiles.

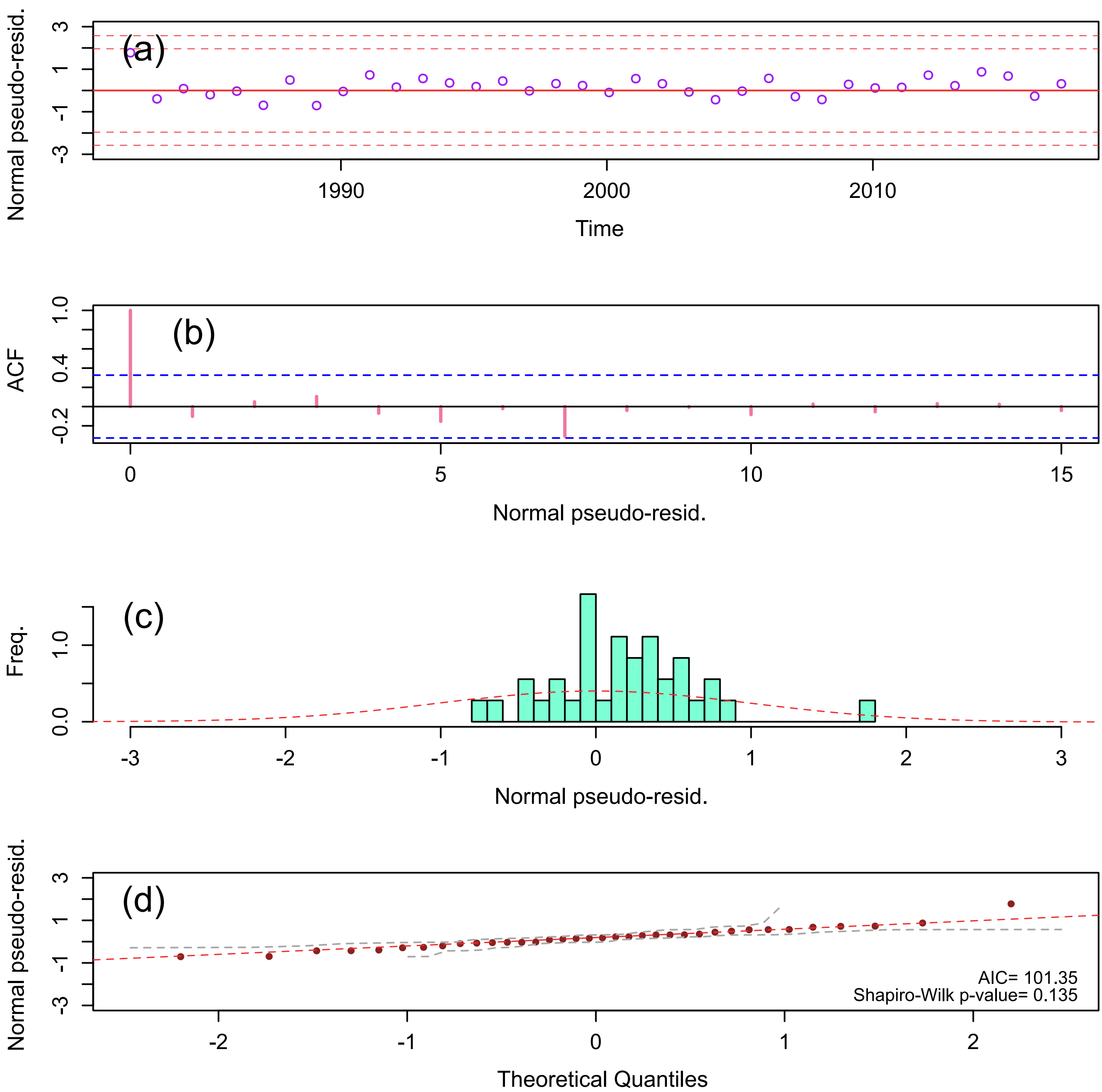

Figure S6: Diagnostics of the model residuals corresponding to the frequency HMM output as discussed in Figure 8 for station ID 227237. Residual (a) Annual time series of the normal pseudo-residuals (red lines at 0, ±1.96, ±2.58). (b) Auto-correlation of the normal pseudo-residuals, with the blue dotted lines indicating the 95th percentile confidence intervals for uncorrelated series. (c) Histogram of the normal pseudo-residuals, with the red dotted line indicating a standard normal distribution. (d) Quantile-Quantile (Q-Q) plot of the normal pseudo-residuals in relation to the theoretical quantiles.

Text S5. Warm periods of ENSO as used in the study

The ONI value at a given month is obtained from a 3-month running mean of the sea surface temperature anomalies of the Niño3.4 region (5°N-5°S, 120-170°W) in the equatorial Pacific Ocean that are above a threshold of 0.5°C. Warm (positive) SST anomalies are associated with El Niño events while La Niña events are typically associated with cold (negative) SST anomalies. Any given value would be considered to be indicating the occurrence of a warm ENSO episode when at least 5 consecutive values in the ONI series lie above the threshold of 0.5°C. The warm periods identified in this way are shown below and are displayed as red vertical strips in Figure 10 of the paper. These were sourced from the United States National Oceanic and Atmospheric Administration (NOAA) Climate Prediction Centre (CPC) (`www.cpc.ncep.noaa.gov`).

Table S3: List of the warm periods of the ONI as used in Figure 10 of the paper.

MJJ 1951	MJJ 1958	AMJ 1969	AMJ 1982	JAS 1991	SON 2002	MJJ 2015
JJA 1951	JJA 1958	JAS 1969	MJJ 1982	ASO 1991	OND 2002	JJA 2015
JAS 1951	OND 1958	ASO 1969	JJA 1982	SON 1991	NDJ 2002	JAS 2015
ASO 1951	NDJ 1958	SON 1969	JAS 1982	OND 1991	DJF 2003	ASO 2015
SON 1951	DJF 1959	OND 1969	ASO 1982	NDJ 1991	JFM 2003	SON 2015
OND 1951	JFM 1959	NDJ 1969	SON 1982	DJF 1992	JJA 2004	OND 2015
NDJ 1951	FMA 1959	DJF 1970	OND 1982	JFM 1992	JAS 2004	NDJ 2015
DJF 1952	MJJ 1963	AMJ 1972	NDJ 1982	FMA 1992	ASO 2004	DJF 2016
JFM 1953	JJA 1963	MJJ 1972	DJF 1983	MAM 1992	SON 2004	JFM 2016
FMA 1953	JAS 1963	JJA 1972	JFM 1983	AMJ 1992	OND 2004	FMA 2016
MAM 1953	ASO 1963	JAS 1972	FMA 1983	MJJ 1992	NDJ 2004	MAM 2016
AMJ 1953	SON 1963	ASO 1972	MAM 1983	ASO 1994	DJF 2005	
MJJ 1953	OND 1963	SON 1972	AMJ 1983	SON 1994	JFM 2005	
JJA 1953	NDJ 1963	OND 1972	MJJ 1983	OND 1994	ASO 2006	
JAS 1953	DJF 1964	NDJ 1972	ASO 1986	NDJ 1994	SON 2006	
ASO 1953	JFM 1964	DJF 1973	SON 1986	DJF 1995	OND 2006	
SON 1953	AMJ 1965	JFM 1973	OND 1986	JFM 1995	NDJ 2006	
OND 1953	MJJ 1965	FMA 1973	NDJ 1986	FMA 1995	DJF 2007	
NDJ 1953	JJA 1965	ASO 1976	DJF 1987	AMJ 1997	JJA 2009	
DJF 1954	JAS 1965	SON 1976	JFM 1987	MJJ 1997	JAS 2009	
JFM 1954	ASO 1965	OND 1976	FMA 1987	JJA 1997	ASO 2009	
MAM 1957	SON 1965	NDJ 1976	MAM 1987	JAS 1997	SON 2009	
AMJ 1957	OND 1965	DJF 1977	AMJ 1987	ASO 1997	OND 2009	
MJJ 1957	NDJ 1965	JFM 1977	MJJ 1987	SON 1997	NDJ 2009	
JJA 1957	DJF 1966	ASO 1977	JJA 1987	OND 1997	DJF 2010	
JAS 1957	JFM 1966	SON 1977	JAS 1987	NDJ 1997	JFM 2010	
ASO 1957	FMA 1966	OND 1977	ASO 1987	DJF 1998	FMA 2010	
SON 1957	MAM 1966	NDJ 1977	SON 1987	JFM 1998	SON 2014	
OND 1957	SON 1968	DJF 1978	OND 1987	FMA 1998	OND 2014	
NDJ 1957	OND 1968	SON 1979	NDJ 1987	MAM 1998	NDJ 2014	
DJF 1958	NDJ 1968	OND 1979	DJF 1988	AMJ 1998	DJF 2015	
JFM 1958	DJF 1969	NDJ 1979	JFM 1988	MJJ 2002	JFM 2015	
FMA 1958	JFM 1969	DJF 1980	AMJ 1991	JJA 2002	FMA 2015	
MAM 1958	FMA 1969	JFM 1980	MJJ 1991	JAS 2002	MAM 2015	
AMJ 1958	MAM 1969	MAM 1982	JJA 1991	ASO 2002	AMJ 2015	

References

Forney, G. D. (1973). The viterbi algorithm. *Proceedings of the IEEE*, *61*(3), 268–278.

Goswami, P., Peterson, T. J., Mondal, A., & Rüdiger, C. (2022). Non-stationary Influences of Large-scale Climate Drivers on Low Flow Extremes in Southeast Australia. *Water Resources Research*, e2021WR031508.

Peterson, T. J., Saft, M., Peel, M. C., & John, A. (2021). Watersheds may not recover from drought. *Science*, *372*(6543), 745–749. doi: 10.1126/science.abd5085

Price, K., Storn, R. M., & Lampinen, J. A. (2006). *Differential evolution: a practical approach to global optimization.* Springer Science & Business Media.

Storn, R., & Price, K. (1997). Differential Evolution - A Simple and Efficient Heuristic for Global Optimization over Continuous Spaces. *Journal of Global Optimization*, *11*(4), 341–359. doi: 10.1023/A:1008202821328

Zucchini, W., & MacDonald, I. L. (2009). *Hidden Markov models for time series: an introduction using R*. Chapman and Hall/CRC.